20095

NATIONAL LIBRARY
OTTAWA

CANADA

BIBLIOTHÈQUE NATIONALE
OTTAWA

NAME OF AUTHOR.....SERGIO DE PAOLI.....

TITLE OF THESIS...INTERACTION OF Hg 6($^3P_1$) AND Hg.....

.....

UNIVERSITY.....UNIVERSITY OF ALBERTA.....

DEGREE FOR WHICH THESIS WAS PRESENTED...Ph. D.....

YEAR THIS DEGREE GRANTED.....1974.....

Permission is hereby granted to THE NATIONAL LIBRARY OF CANADA to microfilm this thesis and to lend or sell copies of the film.

The author reserves other publication rights, and neither the thesis nor extensive extracts from it may be printed or otherwise reproduced without the author's written permission.

(Signed)...Sergio De Paoli...

PERMANENT ADDRESS:

...R.R. 1 CAYLEY.....

...ALTA.....

.....

DATED...May 14.....1974

NL-91 (10-68)

THE UNIVERSITY OF ALBERTA

INTERACTION OF Hg6($^3P_0$) and 6($^3P_1$) WITH FOREIGN GASES

BY

© SERGIO DE PAOLI

A THESIS

SUBMITTED TO THE FACULTY OF GRADUATE STUDIES AND RESEARCH

IN THE PARTIAL FULFILMENT OF THE REQUIREMENTS FOR THE

DEGREE OF DOCTOR OF PHILOSOPHY

DEPARTMENT OF CHEMISTRY

UNIVERSITY OF ALBERTA

EDMONTON, ALBERTA

SPRING, 1974

THE UNIVERSITY OF ALBERTA

FACULTY OF GRADUATE STUDIES AND RESEARCH

The undersigned certify that they have read, and recommend to the Faculty of Graduate Studies and Research, for acceptance, a thesis entitled

INTERACTION OF $Hg6(^3P_0)$ and $6(^3P_1)$ WITH FOREIGN GASES

submitted by Sergio De Paoli in partial fulfilment of the requirements for the degree of Doctor of Philiosophy.

.....
Supervisor

.....

.....

.....

.....

.....
External Examiner

Date May 10, 1974

ABSTRACT

The quenching mechanism of Hg $6(^3P_0)$ and $6(^3P_1)$ atoms and the relative importance of $Hg(^3P_0)$ atom participation in $Hg(^3P_1)$ photosensitization of various foreign gases have been studied in detail.

Collisionally induced transitions to the $^3P_1$ state is the major process by which $Hg(^3P_0)$ atoms are removed in the presence of nitrogen under conditions of low imprisonment of resonance radiation. The presence of $Hg(^3P_1)$ atoms is evidenced by the persistence of a weak 2537Å emission (delayed fluorescence) after the exciting light has been extinguished. The rate of formation of Hg_2 $A(^3\Sigma_u^+)$ molecules may be enhanced relative to delayed fluorescence by increasing the imprisonment of the 2537Å radiation which results in an increase in the 4850Å and 3350Å emission band intensities.

Absolute quenching rate constants for Hg $6(^3P_0)$ atoms by various light and deuterated alkanes have been obtained by monitoring the delayed fluorescence intensity in flashed mixtures of these substrates with nitrogen. The presence of the low population of $Hg(^3P_1)$ atoms in the $Hg(^3P_0)$-nitrogen system has a significant effect on the determination of $Hg(^3P_0)$ atom quenching cross-section values for weak quenchers. Increasing the temperature has little effect on the

$Hg(^3P_0)$ quenching rate of ethane, neopentane and propane but decreases those of cyclopentane and cyclohexane. These results are explained in terms of a simplified potential energy diagram compatible with the processes known to occur in these systems.

Absolute quenching rate constants for $Hg(^3P_0)$ atoms by hydrogen, deuterium, ethylene, deuterated ethylene, benzene, deuterated benzene and hexafluorobenzene have been measured at room temperature.

Delayed fluorescence decay measurements demonstrate that an increase in temperature decreases the rate constant values for $Hg(^3P_0)$ atom quenching by oxygen- and sulphur-containing organic compounds. The formation of a $(Hg(^3P_0)$-substrate) complex is implicated in the quenching mechanism from observation of diffuse bands due to its decay via radiative transitions. The detection of these bands, centered around 3000Å, implies that $^3P_0$ atoms play an important role in the $Hg(^3P_1)$ sensitization of these substrates. Based on the effects of deuterium substitution, it is proposed that decomposition occurs when the complex assumes a configuration appropriate for the abstraction of an α-hydrogen.

Data obtained from measurements of the $(Hg(^3P_0)$-$NH_3)$ complex emission intensity at 3600Å indicates that ammonia quenches $Hg(^3P_0)$ atoms according to second and third order

kinetics at 28°C, but by second order kinetics only at 70°C. A three-fold increase in the second order rate constant over this temperarure range may be attributed to an increase in the rate of decomposition.

Spectroscopic studies of the band emission in the sensitization of nitrogen-xenon mixtures shows that $Hg(^3P_0)$ atoms are insignificant in the $Hg(^3P_1)$ sensitization of xenon.

The appearance of two or more intensity maxima at 2537Å with time in flashed mixtures of mercury and low pressures of the rare gases, methane, ethane, tetrafluoromethane, nitrogen and dimethylether has been observed. The intensity and the delay time between peaks depends on the temperature, flash intensity and the nature and pressure of the foreign gas. The result suggests the possiblity of a laser process in these systems. Only one intensity maximum was observed with added hydrogen or ethylene.

ACKNOWLEDGMENTS

The author wishes to express his sincere gratitude to Dr. O.P. Strausz for his guidance and assistance throughout the course of this investigation.

The efforts of Dr. E. M. Lown in reading the manuscript are gratefully acknowledged.

Special thanks goes to A. Clement for his help with some of the experimental work.

Dr. H.S. Sandhu, Dr. J.M. Campbell, Dr. R.S. McDaniel and Dr. S. Penzes offered much constructive advice and many stimulating discussions for which the author is greatly appreciative.

The assistance from the members of the photochemistry group and the co-operation of the electronic and glass-blowing shops is appreciated.

The author wishes to thank his fiancée, O.S. Herasymowych, for her understanding, patience, and encouragement during the preparation of the manuscript.

The financial assistance provided by the University of Alberta and the National Research Council of Canada during the course of this work is gratefully acknowledged.

TABLE OF CONTENTS

	Page
ABSTRACT	v
ACKNOWLEDGEMENTS	vii
LIST OF TABLES	xiii
LIST OF FIGURES	xv
CHAPTER I. INTRODUCTION	1
1. Mercury as a Sensitizer	2
2. Relaxation Processes in Mercury Sensitization	6
a. Imprisonment of Resonance Radiation	
b. Excimer Formation	8
c. Quenching of $Hg(^3P_1)$ Atoms	9
i. The Physical Method	10
ii. The Chemical Method	12
iii. Real Time Method	14
d. Production and Detection of $Hg(^3P_0)$ Atoms	7
i. 4047Å Absorption	18
ii. 4047Å, 4358Å and 5461Å Emission	20
iii. Ejection of Electrons	20
iv. 2537Å Delayed Fluorescence	23
v. 2656Å Emission Intensity	23
e. Relaxation of $Hg(^3P_0)$ Atoms by Processes Other Than Quenching	24

TABLE OF CONTENTS

	Page
f. Quenching of $Hg(^3P_1)$ Atoms by Foreign Gases	25
3. Interaction of Excited Mercury Atoms With Various Substances	26
a. Ground State Mercury Atoms	28
b. Nitrogen	30
c. Paraffins	33
d. Hydrogen	40
e. Unsaturated Hydrocarbons	41
f. Nitrogen-Containing Compounds	41
i. Ammonia	42
ii. Aliphatic Amines	44
g. Oxygen-Containing Compounds	45
i. Water	45
ii. Alcohols	45
iii. Ethers	47
h. Rare Gases	49
4. Aims of the Present Research	51
CHAPTER II. EXPERIMENTAL	53
1. Apparatus	53
a. The Circulating System	53
i. Cell-Lamp Assembly	56
ii. The Filter Solution	58

TABLE OF CONTENTS

	Page
iii. The Spectrograph	58
iv. The Light Detection and Recording Instruments	59
v. Data Processing	59
vi. Operating Procedure	60
b. The Flow System	60
i. Emission Cell	61
ii. Light Source	61
iii. Photographic Plates	61
iv. Operating Procedure	62
2. Materials	62
CHAPTER III. INTERACTION OF EXCITED MERCURY ATOMS WITH NITROGEN	64
1. Results	64
2. Discussion	73
CHAPTER IV. INTERACTION OF $Hg(^3P_0)$ ATOMS WITH FOREIGN GASES	78
1. Isotopic Hydrogen and Hydrocarbon Compounds	80
a. Results	80
b. Discussion	93

TABLE OF CONTENTS

	Page
2. Oxygen- and Sulphur-Containing Compounds	103
a. Results	103
b. Discussion	116
3. Aromatic Compounds	126
a. Results and Discussion	127
4. Ammonia	130
a. Results and Discussion	130
CHAPTER V. EMISSION FROM EXCITED MERCURY + SUBSTRATE SYSTEMS	137
1. Results and Discussion	137
a. Hg + Ether Systems	137
b. Hg + N_2 + X and Hg + N_2 + C_3H_8 Systems	143
c. Hg + Various Substrate Gases	146
CHAPTER VI. COMPLEX TIME DEPENDENCE OF 2537Å EMISSION IN Hg($^3P_1$) + SUBSTRATE MIXTURES	148
1. Results	148
2. Discussion	168
CHAPTER VII. SUMMARY AND CONCLUSIONS	175
BIBLIOGRAPHY	182
APPENDIX A	198

TABLE OF CONTENTS

Page

APPENDIX B 198

APPENDIX C 201

APPENDIX D 204

LIST OF TABLES

TABLE		Page
I	Quenching Cross-Sections for $Hg(^3P_1)$ Atoms by the Physical and Chemical Methods	15
II	Quantum Yields for Spin-Orbit Relaxation of $Hg(^3P_1)$ Atoms	21
III	Quenching Cross-Sections for $Hg(^3P_0)$ Atoms	27
IV	Rate Constants for Reactions of Ammonia, Water and Alcohols With $Hg(^3P_0)$ Atoms	48
V	Rate Constant Values Employed in the Kinetic Calculations in the $Hg(^3P_1) + N_2$ System	68
VI	Quenching Data for $Hg(^3P_0)$ Atoms by Isotopic Hydrogen and Hydrocarbon Molecules	82
VII	Quenching Data for $Hg(^3P_0)$ Atoms by Oxygen- and Sulphur-Containing Compounds	114
VIII	Arrhenius Parameters for the Quenching of $Hg(^3P_0)$ Atoms by Oxygen- and Sulphur-Containing Compounds	119
IX	Quenching Data for $Hg(^3P_0)$ Atoms by Aromatic Compounds	129
X	Relative Intensity and Separation of the Emission Band Maxima From the 2537Å (39,424 cm^{-1}) Resonance Line for Various Ethers	141

LIST OF TABLES

TABLE		Page
XI	Collected Data From Time Dependence of 2537Å Intensity Measurements in Several $Hg(^3P_1)$ + Foreign Gas Systems	167
XII	Effect of Wall Material and Surface Treatment on the Relative Intensity of Triboluminescence from Ampules Containing Mercury and Neon	207
XIII	Variation of Triboluminescence Intensity With Pressure of Several Foreign Gases	209
XIV	Comparison of Maximum Emission Intensities of Various Foreign Gases	210
XV	Emission Characteristics from Sodium Amalgam ...	212
XVI	Product Yields from the Triboelectrical Discharge Decomposition of Hydrocarbons and Acetone	215

LIST OF FIGURES

FIGURE		Page
1	Lower excited states of the mercury atom	4
2	The circulating system vacuum apparatus	54
3	The flow system vacuum apparatus and cell used in band emission studies	55
4	Flash lamp - cell assembly	57
5	$1/\tau$ vs nitrogen pressure at 290C	65
6	$1/\tau$ nitrogen concentration at 290C and 750C .	66
7	Time dependence of 4858Å band intensity with 800 torr N_2 at 810C	71
8	$1/\tau$ vs C_3H_8 concentration	83
9	$1/\tau$ vs neo-C_5H_{12} concentration	84
10	$1/\tau$ vs CH_4 and C_2H_6 concentration	85
11	$1/\tau$ vs c-C_5D_{10} and c-C_5H_{10} concentration	86
12	$1/\tau$ vs c-C_6D_{12} and c-C_6H_{12} concentration	87
13	$1/\tau$ vs H_2 and D_2 concentration	88
14	$1/\tau$ vs $CH_3CD_2CH_3$ concentration	89
15	$1/\tau$ vs i-C_4H_{10} and n-C_4H_{10} concentration	90
16	$1/\tau$ vs C_2H_4 and C_2D_4 concentration	91
17	Schematic potential energy diagram for the interaction of $Hg(^3P_0)$ and $Hg(^3P_1)$ atoms with alkanes	97
18	$1/\tau$ vs C_2H_5CH concentration in different nitrogen bath pressures	104

LIST OF FIGURES

FIGURE		Page
19	$1/\tau$ vs CH_3CD_2OH and CH_3CH_2OH concentration	106
20	$1/\tau$ vs $(CH_3)_2CO$ concentration	107
21	$1/\tau$ vs $(C_2H_5)_2O$ concentration	108
22	$1/\tau$ vs $(CH_3CD_2)_2O$ concentration	109
23	$1/\tau$ vs $(CD_3CD_2)_2O$ concentration	110
24	$1/\tau$ vs CH_3SH concentration	111
25	$1/\tau$ vs C_2H_5SH concentration	112
26	$1/\tau$ vs $(CH_3)_2S$ concentration	113
27	Arrhenius plots for $(C_2H_5)_2O$, $(CH_3CD_2)_2O$ and $(C_2D_5)_2O$ substrates	117
28	Arrhenius plots for $(CH_3)_2S$, C_2H_5SH and CH_3SH substrates	118
29	Schematic configurations in $Hg(^3P_0)$ quenching by oxygen-containing organic compounds	123
30	$1/\tau$ vs C_6D_6, C_6F_6 and C_6H_6 concentration	128
31	Rate data plots for the relaxation of $Hg(^3P_0)$ atoms by ammonia. top: $1/\tau \div [NH_3]$ vs ammonia concentration bottom: $1/\tau$ vs ammonia concentration	133
32	Schematic potential energy diagram for the interaction of $Hg(^3P_0)$ and $Hg(^3P_1)$ atoms with ammonia	135

LIST OF FIGURES

FIGURE		Page
33	Microdensitometer traces of $(CH_3)_2O$ and $(C_2H_5)_2O$ band emission spectra	138
34	Microdensitometer traces of $C_2H_5OC(CH_3)_3$ and tetrahydrofuran band emission spectra	139
35	Microdensitometer traces of band emission spectra of $N_2 + C_3H_8$ mixtures	144
36	Microdensitometer traces of band emission spectra of $N_2 + Xe$ mixtures	145
37	Typical time dependence of the 2537Å intensity. A: flash profile, B and C: distorted flash curves, D and E: partially resolved shoulders, F: two separate peaks	149
38	t" vs neon, argon and xenon pressure	151
39	t" vs helium pressure	152
40	t" vs krypton pressure	153
41	ln(t") vs neon, argon and xenon pressure	155
42	ln(t") vs helium and krypton pressure	156
43	(t"-t')/substrate pressure for argon and xenon	157
44	Time dependence of 2537Å intensity in the $Hg(^3P_1)$+He system at various temperatures	158
45	Time dependence of 2537Å intensity in the $Hg(^3P_1)$+Ar system at various temperatures	159

LIST OF FIGURES

FIGURE		Page
46	t" vs temperature for helium and argon	160
47	t" vs nitrogen pressure	162
48	t" vs dimethylether pressure	163
49	ln(t") vs nitrogen pressure	165
50	ln(t") vs dimethylether pressure	166
51	Slopes of ln(t") curves as a function of the ionization potential of the noble gases	170

CHAPTER I

INTRODUCTION

The processes by which an energy-rich atom or molecule becomes thermalized are of fundamental importance in chemical kinetics. In photochemistry, energy is introduced into a system by absorption of electromagnetic radiation, usually between 10,000Å and 1000Å, which provides energy in the range 23 to 230 kcal per mole. The excess energy is dissipated through physical processes such as luminescence or through chemical processes such as the decomposition or isomerization of a molecule (1).

Electronic excitation can be brought about indirectly by the transference of the electronic energy of a photosensitizer atom or molecule. In a photosensitization system three consecutive events occur:

(i) absorption of radiation by the sensitizer
(ii) transfer of energy (in whole or in part) from the sensitizer to the acceptor and
(iii) the processes by which the acceptor is relaxed as a consequence of (ii).

An understanding of such a photochemical system requires the elucidation of all three steps. The information required to describe step (i), such as the lifetimes and energy content

of the various excited states of the sensitizer, can be determined from spectroscopic properties. Steps (ii) and (iii) may be elucidated by consideration of the physical and chemical properties of both the sensitizer and acceptor and the effects produced by their interaction under different experimental conditions.

The extensive amount of work which has been reported on metal atom sensitized reactions in the gas phase is due principally to the conceptual simplicity of such systems and the availability of pertinent information necessary to interpret the results.

1. Mercury as a Sensitizer.

The essential requirements of a good gas phase sensitizer are:

(i) a chemically inert ground state with a comparatively high vapour pressure,

(ii) well defined energy levels which may be populated by absorption of radiation with high extinction coefficients and

(iii) upper states that exist long enough for extensive energy transfer to occur.

These properties are exhibited by mercury without recourse to elaborate experimental procedures. For this reason, it is

not surprising that the first example of energy transfer (2) involved mercury as sensitizer. Mercury sensitization has been used extensively as a model photochemical system, which is reflected by the large number of papers and several reviews (1,3,4) on the subject.

The ground state of the mercury atom, $Hg(^1S_0)$, hereafter denoted simply as Hg, has a $6s^2$ electronic configuration which is converted to a 6s6p configuration by the absorption of resonance radiation. Depending on the spin orientation of the two electrons, a singlet or a triplet term may result (Figure 1). The singlet level, $Hg(^1P_1)$ (Hg'), which lies 154 kcal above the ground state, is populated by absorption of the 1849Å resonance line. Absorption at 2537Å induces transition to the $Hg(^3P_1)$ (Hg*) state which is one member of the triplet manifold that includes the $Hg(^3P_2)$ and $Hg(^3P_0)$ (Hg^0) states. Strong spin-orbit coupling gives rise to large energy splitting between the three levels. The $(^3P_2)$ state lies 13 kcal above and the $(^3P_0)$ level 5 kcals below the Hg* state which is 112 kcal above the ground state.

The spin-orbit interaction in heavy atoms such as mercury is described by j-j coupling. Accordingly, only the J quantum number has physical significance and the probability of radiative transitions is governed primarily by the J selection rules. Transitions which violate these rules,

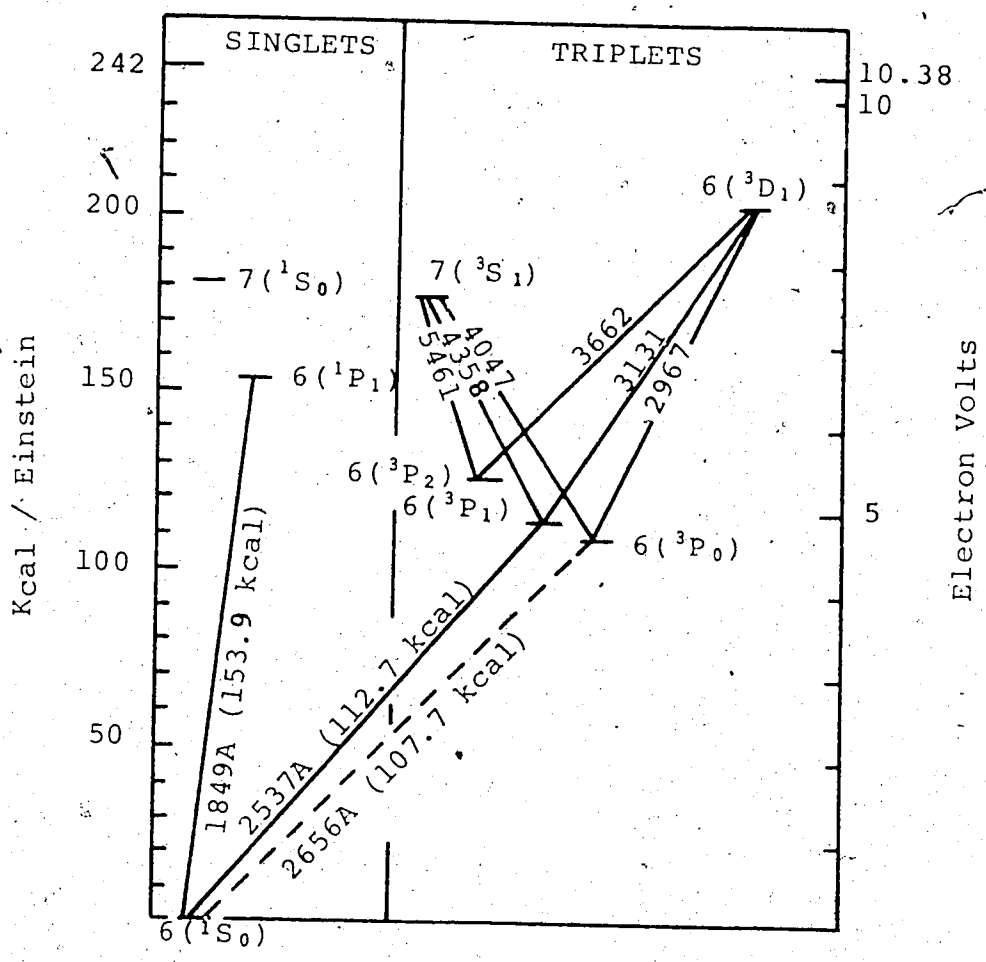

FIGURE 1: Lower excited states of the mercury atom.

such as $Hg(^3P_2) \rightarrow Hg$ ($\Delta J \neq 2$) or $Hg^0 \rightarrow Hg$ ($J=0 \not\leftrightarrow J=0$), are forbidden and appear weakly in the mercury spectrum. The $\Delta S = 0$ selection rule is relaxed to the extent that several intercombination lines, such as the 2537Å resonance line, appear with high intensity. Of the two resonance transitions at 1849Å and 2537Å, only the $Hg' \rightarrow Hg$ is fully allowed.

Einstein's formula for radiative transition probability shows that the greater the probability of absorption and emission the shorter the radiative lifetime of the upper state. For example, the $Hg' \rightarrow Hg^0$ transition, which is completely allowed, has a radiative lifetime of 1.31×10^{-9} seconds (5), while the forbidden transition $Hg^0 \rightarrow Hg$ has a natural lifetime of 2.0 seconds (6). The $Hg^* \rightarrow Hg$ transition, which is intermediate between a fully allowed and a fully forbidden transition has a lifetime of 1.141×10^{-7} seconds (7).

Absorption of radiation by an atom is governed by the Beer-Lambert law,

$$I = I_0 \exp(-\epsilon l c)$$

where I_0 is the intensity of incident radiation, I is the intensity of the radiation after passing through a distance l of the absorbing species, ϵ is the extinction coefficient and c is the concentration of the absorber. Both of mercury's resonance transitions have high extinction coef-

ficients so that even at very low mercury concentrations or short path lengths, a comparatively high concentration of excited atoms may be readily obtained, An experimental difficulty resulting from this fact is the phenomenon of imprisonment, the repeated absorption and emission of photons at the resonance wavelength before they escape from the cell. This has the effect of lengthening the apparent radiative lifetime and must be taken into account in kinetic studies based on the lifetime of the excited state.

2. Relaxation Processes in Mercury Sensitization.

A general mechanism for the relaxation of Hg* atoms in the presence of a substrate A is listed below:

$$Hg + h\nu(2537\text{Å}) \rightarrow Hg^* \quad [1]$$

$$Hg^* \rightarrow Hg + h\nu(2537\text{Å}) \quad [2]$$

$$Hg^* + A \rightarrow (HgA)^* \quad [3]$$

$$(HgA)^* \rightarrow Hg^* + A \quad [-3]$$

$$(HgA)^* \rightarrow Hg + A^* \text{ (or products)} \quad [4]$$

$$(HgA)^* \rightarrow Hg^0 + A \quad [5]$$

$$(HgA)^* \rightarrow Hg + A + h\nu' \quad [6]$$

$$Hg^0 + A \rightarrow (HgA)^0 \quad [7]$$

$$(HgA)^0 \rightarrow Hg^0 + A \quad [-7]$$

$$(HgA)^0 \rightarrow Hg + A^* \text{ (or products)} \quad [8]$$

$$(HgA)^0 \rightarrow Hg + A + h\nu''. \quad [9]$$

The principal modes by which Hg* and Hg^0 atoms are relaxed will depend on the nature of the substrate and the experimental conditions. The important features of each process are described below.

(a) Imprisonment of Resonance Radiation.

In the absence of a quencher, Hg* atoms relax almost exclusively via reaction [2]. However, the rate of this process is greatly influenced by imprisonment of the radiation.

In theoretical treatments of imprisonment, the ratio of the imprisonment lifetime, τ, to the natural lifetime, τ_0, is expressed in terms of the opacity, kl, where k is the absorption coefficient at the center of the 2537Å line and is directly proportional to the mercury concentration. Certain idealizations of the cell geometry, namely the "infinite slab" and "infinite cylinder" are assumed to minimize computational difficulties involving l. The earliest study (8) treated the problem as a diffusion phenomenon. This was later modified by Samson (9) who used an equivalent opacity, $\bar{k}l$, which allowed for the possibility that the frequency of the scattered radiation may be different from that of absorbed radiation due to Doppler broadening. Holstein has derived a formula for the "infinite slab" and "infinite cylinder" (10) geometries, after consideration

of both Doppler and dispersion broadening, which agrees well with experiment (11) for mercury concentrations less than 10^{16} atoms/cc. An expression for mercury concentrations greater than this has also been obtained (12). Holstein solved the Boltzmann-type integrodifferential transport equation by variational techniques while Biberman (13) solved the equation by numerical methods. Refinements of Holstein's calculations to include the effects of pressure broadening and the hyperfine structure of the 2537Å line have been reported by Walsh (14). Yang (15) has determined an empirical relationship to define the imprisonment at low mercury concentrations.

(b) Excimer Formation.

The existence of an excited mercury-substrate complex as an intermediate in the quenching of Hg* and Hg^0 atoms (reactions [3] and [7]) has been inferred from the detection of band emission (reactions [6] and [9]) in irradiated mixtures of mercury with several substrates. Complexes of an excited state species and its ground state are usually called excimers while those formed with a different ground state species are referred to as exciplexes. Both types are found in mercury sensitization. The 4850Å and the 3350Å emission bands which appear in the spectra of mercury vapour originate from the $Hg_2A(^3\Sigma_u^-)$ (Hg_2**) and $Hg_2A(^1\Sigma_u)$ (Hg_2*) excimers which correlate with a ground state mercury atom

and a Hg and Hg* atom respectively (16). Evidence for exciplex formation in the interaction between an excited mercury atom and rare gas atoms (17,18), water (19,20) ammonia (20) and methane (21) has been reported in early studies. More recently, band emission has been observed in mixtures of Hg with several paraffins (22) and medium resolution spectra of mercury exciplexes with CO, N_2, H_2O, NH_3, SF_6, ethanol, the rare gases, fluorinated methanes and paraffins have been described (23).

Studies of the band emission from complexes of mercury and the noble gases (24,25), ammonia (26-30), water (31,32), alcohols (32,33), amines (34,35) and other substrates (36) have produced useful kinetic and spectroscopic information. These investigations have provided ample evidence that relaxation of Hg* and Hg^0 atoms involves the formation of an excited mercury-substrate complex as a precursor, at least for those substrates for which exciplex emission has been observed.

(c) Quenching of $Hg(^3P_1)$ Atoms.

The formation of a Hg*-foreign gas complex, whether it exists for one or many vibrations, results in a decrease in the Hg* population which is evidenced by a decrease in the intensity of the 2537Å fluorescence. A substrate gas is thus said to quench the resonance radiation. This phenomenon was

first noted by Wood (37) with hydrogen as the foreign gas, and was later associated (2) with an energy transfer process, i.e. quenching, since hydrogen atoms were produced.

In the gas phase, energy transfer occurs as a result of a bimolecular collision between the Hg* atom and the substrate, A. For this reason, the quenching rate constant, k_q, is usually compared to the gas kinetic collision frequency, Z, by the relationship

$$Z = k_q[A] = \sigma^2 \left\{ 8\pi RT \frac{M_{Hg} + M_A}{M_{Hg} M_A} \right\}^{1/2} [A] \qquad [10]$$

where M_{Hg} is the atomic weight of mercury and M_A is the atomic (or molecular) weight of the substrate. σ^2, the quenching cross-section, expresses the relative efficiency of the quenching process with respect to the gas kinetic collision diameter and is independent of the relative velocities of the colliding particles.

Two techniques are commonly used to determine the quenching rate constant of reaction [3]. Only a general outline of the theory and procedures involved will be given here since these are well documented (1,3).

(i) The Physical Method.

Under conditions of continuous irradiation, k_q is obtained by measuring the difference in the fluorescence

intensity in the presence and absence of a substrate and attributing this difference to the competition from the quenching reaction. This can be illustrated by reference to a simple Stern-Volmer mechanism:

$$Hg + h\nu(2537\text{Å}) \rightarrow Hg^*$$

$$Hg^* \rightarrow Hg + h\nu(2537\text{Å}) \qquad k = 1/\tau$$

$$Hg^* + A \rightarrow Hg + \text{products.} \qquad k_q$$

A steady-state treatment of the above scheme offers the expression

$$I/I_0 - 1 = \tau k_q[A]$$

where I and I_0 represent the 2537Å intensity measured in the presence and absence of quencher gas respectively. If τ is known, k_q is obtained from the slopes of I/I_0 vs. $[A]$ plots. The quenching cross-section is then derived using equation [10]. If the more detailed scheme (see page 6) is considered, k_q is replaced by

$$(k_3 + k_4 + k_5)/(k_{-3} + k_3 + k_4 + k_5) = k_q.$$

This method accounts for the total quenching of Hg^* irrespective of the the number of channels by which they are deactivated.

The early investigations using this technique were handicapped by the inability to accurately determine the extent of imprisonment, and, therefore, the value of τ.

Yarwocd, Strausz and Gunning (38) showed that their values for Hg* quenching obtained using Holstein's equation (10) were 23% higher than Zemansky's data (39) calculated on the basis of Samson's theory of equivalent opacity (9). They also showed that their data varied by a factor of 1.75 from Zemansky's original results (40) which were calculated using Milne's formula.

The relative cross-sections within a particular set, however, are independent of the imprisonment correction used since the ratio of the slopes, S, obtained from Stern-Volmer plots for two quenchers 1 and 2 is given by

$$\frac{S_1}{S_2} = \frac{\tau k_{q,1}}{\tau k_{q,2}} = \frac{\sigma_1^2}{\sigma_2^2}\left\{\frac{M_2(M_{Hg}+M_1)}{M_1(M_{Hg}+M_2)}\right\}^{1/2}$$

and does not contain τ. An accurate comparison of the relative values reported from the different laboratories can thus be made.

(ii) The Chemical Method.

The details of this method, which utilizes the competitive quenching between N_2O and a substrate A, has been worked out by Cvetanovic (4) on the basis of the following mechanism:

$$Hg^* + N_2O \rightarrow Hg + N_2 + O \qquad k_{N_2O}$$

$$Hg^* + A \rightarrow Hg + \text{products} \qquad k_d$$

$$Hg^* + A \rightarrow Hg^0 + A. \qquad k_s$$

The quantum yield of N_2 in the complete quenching region is given by

$$\phi^{-1} = a\ (1.0 + b\ [A]/[N_2O])$$

where a is the intercept and b is the slope to intercept ratio of ϕ^{-1} vs $[A]/[N_2O]$ plots. Relative quenching cross-sections are calculated from the expression

$$\frac{\sigma_A^2}{\sigma_{N_2O}^2} = b \left\{ \frac{1.0 + M_{Hg}/M_{N_2O}}{1.0 + M_{Hg}/M_A} \right\}^{1/2}$$

It is important that there be no other source of N_2 other than the $Hg^* + N_2O$ reaction. Yang (41) demonstrated that in studying the quenching of Hg* atoms by hydrogen, complications from the reaction

$$N_2O + H \rightarrow N_2 + \text{[illegible]}$$

must be suppressed by the addition of a hydrogen atom scavenger in order to obtain reproducible results.

The discrepancy between the quenching cross-sections measured by the physical method and those obtained by Bellas and co-workers (42) using the chemical method for some alcohols, ethers and ethylmercaptan were attributed to the

participation of Hg^0 atoms in the production of N_2 by the reaction

$$Hg^0 + N_2O \rightarrow Hg + N_2 + O.$$

The chemical method may yield erroneous results since, in certain instances (43), the σ^2 values seem to be dependent on the light intensity. Table I compares quenching cross-sections determined by the physical and chemical methods for a number of substrates.

(iii) Real Time Method.

Quenching cross-sections for Hg^* atoms may also be obtained by measuring the relaxation of the 2537Å fluorescence intensity following cessation of excitation. Matland (44) measured the decay rate in the presence of nitrogen, $1/T$, and related this to the decay rate in pure mercury vapour, $1/T_i$, by the expression

$$1/T = 1/T_i + 1/T_q$$

where $1/T_q$ is the decay rate due to the quenching by nitrogen. The quenching cross-section was then calculated using the equation

$$1/T_q = N \sigma_q v$$

where v is the average relative velocity and N is the concentration of quencher.

TABLE I

Quenching Cross-Sections for $Hg(^3P_1)$ Atoms by the Physical and Chemical Methods (a).

Compound	σ^2, Å^2 (phys) (45)	(38)	(1)	σ^2, Å^2 (chem) (42)	(1)
H_2		9.8	8.6		
D_2			11.9		
N_2			0.274		
O_2		23	19.9		
NO			35.3		33
CO			5.82		
N_2O		25			18.0
CO_2			3.54		
CH_4			0.085		
C_2H_6	0.21		0.16		0.14
C_3H_8	2.86	2.6	2.3		1.7
$CH_3CD_2CH_3$	0.99				0.24
C_3D_8	0.82				0.13
$n\text{-}C_4H_{10}$		8.9	5.7	5.4 (b)	5.1
$i\text{-}C_4H_{10}$			7.3		6.9
$C(CH_3)_4$			2.1	1.8	

cont'd

TABLE I (cont'd)

Quenching Cross-Sections for $Hg(^3P_1)$ Atoms by the Physical and Chemical Methods.

Compound	σ^2, Å^2 (phys) (45)	(38)	(1)	σ^2, Å^2 (chem) (42)	(1)
$c\text{-}C_3H_6$	1.85		1.6	0.38	
$c\text{-}C_5H_{10}$	19.0		19	10.1	
$c\text{-}C_5D_{10}$	7.3				
$c\text{-}C_6H_{12}$	21.9		20	11.7	
$c\text{-}C_6D_{12}$	7.9			0.36	
C_2H_4		42	37		31
C_2D_4	43				
CH_3CH_2CH		32		5.4	
CH_3CD_2CH	31.1				
$(CH_3)_2O$	17.3		12	4.2	
$(CH_3CH_2)_2O$	48.8			22.7	
$(CH_3CD_2)_2O$	48.4				
CH_3SH	67.5				
CH_3CH_2SH	62.3			67.5	
$(CH_3)_2S$	67.5				

a. References given in parenthesis above each column.

b. Reference standard.

(d) Production and Detection of Hg($^3P_0$) Atoms.

The optical metastability of the $^3P_0$ state restricts the direct production or detection of this level using the "forbidden" 2656Å line. This state is more readily attained by collisional spin-orbit relaxation of Hg* atoms (reaction [5]).

There is no particular physical or chemical property of a foreign gas which will allow prediction of the efficiency of this process. Bykhovskii and Nikitin (46) have carried out a quantum mechanical treatment of the quenching of $^3P_1$ atoms by homonuclear diatomic molecules. They concluded that $^3P_0$ atoms would be formed, accompanied by vibrational excitation of the quencher, when the electronic-vibrational terms of the $(HgX_2)^*$ complex intersect, particularly when the energy discrepancy of the reaction

$$Hg^* + X_2(v=0) \rightarrow Hg^0 + X_2(v=1) - \Delta E$$

is small. Vibrational excitation of CO ($v \leq 9$) (47) and NO ($v \leq 17$) (48) has been demonstrated in Hg* sensitization of these gases by observing the infrared emission.

Metastable mercury atoms may also be produced in pure mercury vapour. Quenching of Hg* atoms to the ($^3P_0$) level by a ground state atom has a cross-section of 0.03-0.1 Å^2 (12). At sufficiently high mercury concentrations, the presence of

Hg^0 atoms can be inferred from the appearance of the broad emission bands (49) due to the mercury excimers.

Several methods, which involve observation of the following quantities, have been used to detect and study the reactivity of Hg^0 atoms.

(1) 4047Å Absorption.

This technique, which monitors the $7^3S_1 \leftarrow 6^3P_0$ transition, was initially used to demonstrate the presence of Hg^0 atoms in Hg-N_2 mixtures (19,50). By this method, Pool (51) showed that the quenching probably produced vibrationally excited nitrogen

$$Hg^* + N_2 \rightarrow Hg^0 + N_2(v=1) - 1.6 \text{ kcal/mole.}$$

Penzes and co-workers (52) were able to detect metastable atoms in eight deuterated paraffins and light neopentane using this method. This study represented a major expansion of the number of compounds known to produce Hg^0 atoms. They suggested that the discrepancy between the quenching cross-sections measured by the physical and chemical methods could be due to the presence of Hg^0 atoms in these systems.

Qualitative studies employing this method have been carried out by several workers (50,53-55) on the assumption that the absorption is proportional to the Hg^0 concentra-

tion. Horiguchi and Tsuchiya (56) have shown that this assumption is not valid and that the absorption intensity is a function of the ratio of the spectral half-widths of the incident and absorption profiles.

Flash photolysis techniques were used by Callear and Norrish (57) and later Callear and Williams (58) to generate Hg^0 atoms in the presence of 780 torr of nitrogen. The rate of removal of these atoms in nitrogen-foreign gas mixtures was studied by kinetic absorption spectroscopy at 4047Å and 2967Å. By using argon in the cell to pressure broaden the 2537Å absorption line, metastable atoms were detected upon addition of N_2, CO, H_2O and D_2O. They were not able to detect Hg^0 atoms in NO, H_2, O_2, N_2O, CH_4, C_2H_6, C_3H_8, C_2H_4, NH_3 or BF_3. A severe drawback of their apparatus was the low concentration of Hg* atoms (and consequently Hg^0 atoms) attainable with the conventional flash lamp. This problem was overcome by using a microwave pulse generator (59-61) or a flash lamp with a large number of closely spaced electrodes (62-64) which provide monochromatic excitation. With the multi-electrode flash lamp, (resonance flash lamp), most of the useful energy output is in the form of 2537Å radiation (64). Callear and McGurk (63) showed that N_2 $A^3\Sigma^+$, (N_2^*), is produced when "black body" and microwave pulsed excitation sources are used to irradiate Hg-nitrogen mixtures which invalidated the earlier quantum yields of Hg^0 formation reported by Callear and Hedges (59). The quantum

yields of spin-orbit relaxation were remeasured using the multi-electrode flash lamp (62).

Data on Hg^0 atom formation has been obtained by Vikis, Torrie and Le Roy (65,66) using a technique based on the decomposition of C_2H_4 by Hg^0 atoms and by Horiguchi and Tsuchiya (67) using 4358Å, and 4047Å absorption techniques. The data on spin-orbit relaxation quantum yields reported by the various workers has been complied in Table II.

(ii) 4047Å, 4358Å, and 5461Å Emission.

Absorption of 4047Å radiation results in an increase in the Hg $7(^3S_1)$ population. The intensity of the resulting emissions from this level at 4047Å, 4358Å ($7^3S_1 \rightarrow 6^3P_1$) and 5461Å ($7^3S_1 \rightarrow 6^3P_2$), observed at right angles to the exciting beam, have also been used to measure Hg^0 atom concentrations (53,68,69).

(iii) Ejection of Electrons.

The ability of Hg^0 atoms to eject electrons from a metal surface has been described (70) and used by several workers to study metastable atom reactions (53,71-73). Darwent and Hurturbise (71) noted an increase in the electric current from an nickel surface with C_2H_4, C_2H_6, N_2 and H_2 but not with O_2 or CO_2 in the cell. Scheer and Fine, using a silver cathode, made a careful study of the quenching processes of Hg^* by nitrogen and CO (72). They demonstrated

TABLE II

Quantum Yield for Spin-Orbit Relaxation of $Hg(^3P_1)$ Atoms (a).

Compound	Quantum Yield (ϕ^o)				
	(62)	(66)	(67)	(26)	(74)
N_2	1.0 (b)	1.0 (b)	>0.92		>0.99
H_2	<0.03		<0.01		
D_2			<0.01		
O_2	<0.1				
N_2O	<0.1				
NO	<0.1		0.20		
CO	0.95	0.99	0.78		
CO_2	0.02	<0.01	0.0008		
NH_3	0.62	1.0		0.70	
ND_3		1.0		1.0	
H_2C	0.38	0.76			
D_2C		1.0			

cont'd

Table II (cont'd)

Quantum Yields for Spin-Orbit Relaxation of $Hg(^3P_1)$ Atoms.

Compound	Quantum Yield (ϕ^0)				
	(62)	(66)	(67)	(26)	(74)
CH_4	0.15		0.43		
C_2H_6	0.80	0.64			
C_3H_8	0.30	0.14			
$CH_3CD_2CH_3$		0.51			
C_3D_8		0.47			
$n\text{-}C_4H_{10}$		0.11			
$i\text{-}C_4H_{10}$		0.05			
$C(CH_3)_4$		0.38			
$c\text{-}C_3H_6$		0.56			
C_2H_4	<0.1				

a. References given in parenthesis at top of each column.

b. ϕ^0 assumed equal to 1.0 for nitrogen.

that both gases were equally efficient at quenching to the $^3P_0$ level and attributed carbon monoxide's 20-fold larger quenching cross-section to a greater ability to quench Hg* atoms directly to the ground state. This technique has been criticized by Callear (75) on the grounds that the effect is not specific to Hg^0 atoms and that any electronically excited species having an energy greater than the work function of the metal can produce an electron upon impact. The observation that Hg_2^+ ions appear to be generated in mixtures of Hg^0, Hg* and N_2 (53) add further doubt to the accuracy of this method.

(iv) 2537Å Delayed Fluorescence.

The 5 kcal/mole energy required to promote a metastable atom to the $^3P_1$ level can be provided by a collision with a nitrogen molecule. Thus, Hg* atoms will be produced from the Hg^0 level and yield a weak 2537Å delayed fluorescence that persists for some time after the exciting light has been shut off. The intensity of the emission has been correlated with the Hg^0 concentration (9,62,74,76).

(v) 2656Å Intensity.

The presence of Hg^0 atoms produced in irradiated $Hg-N_2$ mixtures has been demonstrated by photographically recording an increase in the 2656Å line intensity (77). Only a single study (54) has used this method to obtain kinetic data.

Although $^3P_0 \rightarrow {}^1S_0$ transition is forbidden by optical selection rules, the weak intensity of the 2656Å line can be explained by coupling of the nuclear and electronic spins. Mercury has 7 stable isotopes two of which possess odd mass numbers, 199 and 201, and have finite nuclear spin. Since the total angular momentum is different from zero, there is a small transition moment for these two isotopes. Thus only ^{199}Hg and ^{201}Hg exhibit spontaneous emission at 2656Å (78). Even mass isotopes in the $^3P_0$ state may be relaxed by this route by first undergoing the energy exchange reaction

$$Hg^0_{even} + Hg_{odd} \rightarrow Hg_{even} + Hg^0_{odd}$$

which occurs readily (79).

(e) Relaxation of $Hg(^3P_0)$ Atoms by Processes Other Than Quenching by Foreign Gases.

The methods described above to detect Hg^0 atoms perforce reduce the population of this species. However, the amount of Hg^0 removed by these various routes can, by selecting appropriate experimental conditions, be made very small. For instance, promotion to higher energy states by 4047Å or 2967Å absorption may be eliminated by preventing radiation of these wavelengths from entering the reaction cell. No control can be exercized over the spontaneous emission of the 2656Å line, but the long radiative lifetime of Hg^0 atoms makes this process insignificant and it is

usually omitted from reaction mechanisms which involve quenching of this level.

The metastability of Hg^0 atoms allows the possibility of a first order deactivation process at the wall of the reaction vessel

$$Hg^0 \rightarrow Hg \text{ (at the wall)}.$$

The diffusion rate was studied by Kimbell and Le Roy (54) in a nitrogen filled, uniformly irradiated cylindrical reaction cell. The rate constant is given by

$$K = 4D[N_2]/R^2$$

where D is the diffusion coefficient, assumed to be equal to that measured by Spier (80) for Hg atoms, and R is the radius of the cell. The rate of diffusion is inversely proportional to the concentration of a foreign gas in the reaction vessel. Therefore, by making the cell radius large or by increasing the gas pressure, the rate of removal of Hg^0 atoms by diffusion can be made negligibly slow.

(f) Quenching of $Hg(^3P_1)$ Atoms by Foreign Gases.

In recent years, several workers have studied the quenching of Hg^0 atoms by foreign gases using various techniques. Quenching rates were obtained by Callear and McGurk using the delayed fluorescence method (62,63). These workers employed a multi-electroded flash lamp to avoid the inter-

ference from N_2^* molecules that invalidated earlier measurements (57,58) obtained with conventional flash sources. Absorption at 4047Å (55) and emission at 3350Å and 4850Å (81) have been related to the quenching by a foreign gas in Hg-N_2 mixtures. Quenching cross-sections have been obtained (67) from measurements of 4047Å absorption in in mixtures of Hg and the substrate only. Vikis and Moser (73) have employed the ethylene decomposition technique as well as electron emission from a silver metal to measure Hg^0 quenching. Upper limits for quenching cross-sections have been reported by Phillips and co-workers (36) from phase shift measurements. The results of these studies are listed in Table III. It can be seen that although there is good agreement between the relative quenching rates, the absolute values may differ by two orders of magnitude.

3. Interaction of Hg($^3P_1$) and ($^3P_0$) Atoms with Various Substrates.

From a comparison of cross-sections for the quenching of Hg* atoms by different gases, it was soon recognized that the excited mercury atom displayed a marked selectivity in the energy transfer process. A framework for the understanding of the interactions between an excited mercury atom and a quencher gas has been based on consideration of Hg* atoms as both an energy carrier and a chemically active species.

TABLE III

Quenching Cross-Sections for $Hg(^3P_0)$ Atoms (a).

Compound	$(\sigma^0)^2$, Å^2					
	(62)	(73)	(36)	(81)	(55)	(67)
H_2	0.98	0.123	1.			2.1
D_2		0.118				2.9
N_2						8x10^{-6}
O_2	12.1		18.0			
NO	1.63		13.0			8.0
CO	0.65		2			0.21
N_2O	8.34		4.4	0.42	0.43	
CO_2	0.034					0.035
CH_4	2.9x10^{-4}	2.5x10^{-5}				1.4x10^{-4}
C_2H_6	0.0058	0.0010	0.03	0.087	0.07	
C_3H_8	0.034	0.0097		0.29	0.50	
$CH_3CD_2CH_3$		7.7x10^{-4}			0.069	
C_3D_8					0.037	
$n\text{-}C_4H_{10}$		0.017				
$i\text{-}C_4H_{10}$		0.055				
$C(CH_3)_4$		0.0011				
$c\text{-}C_3H_6$		4.5x10^{-4}				
C_2H_4	26.4	2.5				
C_2D_4		2.3				

a. References given in parenthesis at top of each column.

Rousseau and co-workers (82) have shown that the Hg* atom behaves as an electrophilic reagent in which the transfer of energy occurs through a (Hg-substrate)* complex of specific configuration. On the basis of their results, they proposed the following primary interaction modes:

$$\overset{Hg^*}{\underset{\uparrow}{R_2C{=}CR_2}}$$ olefins

$H_3N: \rightarrow Hg^*$ NH_3, PH_3, AsH_3 and their alkyl derivatives

$H_2C: \rightarrow Hg^*$ H_2O, H_2S and their alkyl derivatives

$R\text{-}X: \rightarrow Hg^*$ for alkyl halides (except fluorides)

$$\overset{Hg^*}{\underset{\uparrow}{R\text{-}H}}$$ for paraffinic hydrocarbons, and

$$\overset{Hg^*}{\underset{\uparrow}{R_2C{=}O}}$$ for carbonyl compounds.

This high specificity for the point of attack by Hg* atoms together with the large number of mercury sensitization studies in the literature make it desirable to discuss the various interactions according to the class of quencher.

(a) Ground State Mercury Atoms.

Two broad emission bands centered at 4850Å and 3350Å appear in the spectrum of mercury vapour at high concentration when illuminated by 2537Å radiation. Fine structure on the long wavelength tail of the 4850Å band has recently been detected (83). These bands were shown to be linked to the presence of Hg^0 atoms in the system (84). Mrozowsky (16) assigned these bands to $A(^3O_u^-) \rightarrow X(^1\Sigma^+)$ and $A(^1{}_u) \rightarrow X(^1\Sigma^+)$ transitions from excited diatomic mercury molecules to the unstable ground state Hg_2 molecule. The $A(^3O_u^-)$ and $A(^1{}_u)$ states collapse into a common $(^3\Sigma^+)$ state at short internuclear distances. This allows spin-orbit relaxation of Hg* atoms to the $^3P_0$ level and a much greater probability for radiative relaxation by the (Hg^0Hg) complex at short internuclear distances. McCoubrey (85), on the other hand, suggested that both bands arise from the $A(^3O_u^-)$ state, the 3350Å band by spontaneous emission and the 4850Å band by a pressure induced radiative transition. He demonstrated third order kinetics for the formation of the excited diatomic molecule by the reaction

$$Hg^0 + 2Hg \rightarrow Hg_2^* + Hg$$

as well as a pressure dependence of the relative intensity of the two bands.

Ladd and co-workers (86) employed phase shift techniques to show that the 4850Å band arose from a pressure induced transition from the $A(^3O_u^-)$ excimer and that the 3350Å

band resulted from a spontaneous transition from the $A(^3\Sigma_u^+)$ excimer.

(b) Nitrogen.

The quenching of Hg* atoms by nitrogen has attracted interest for several decades, partly because no decomposition of the nitrogen can occur and also because of the early observations that metastable atoms are formed in large quantities in the presence of this substrate (87). Recent work has shown the quantum yield for spin-orbit relaxation is almost unity (56,74).

Samson (9) has shown that slow collisional reactivation of the metastable atoms back to the Hg* level,

$$Hg^0 + N_2 \rightarrow Hg^* + N_2,$$

which results in 2537Å delayed fluorescence, is an important process removing Hg^0 atoms in this system. The rate was found to increase rapidly with temperature, as expected for an endothermic reaction. Quenching to the ground state from either of the upper levels was found to be negligible, although accurate absolute σ^2 values were not obtained because of the uncertainty in the imprisonment correction. Since a large population of Hg^0 atoms can be produced in the $Hg-N_2$ system, almost all of the studies concerned with the reactivity of Hg^0 atoms have been carried out with $Hg-N_2$ gas

mixtures.

Matland (44) observed a two-fold increase in the quenching cross-section of Hg* atoms as the temperature was increased from 52 to 252°C and postulated that only collisions having kinetic energies greater than 1.6 kcal/mole could result in quenching, since this is required to promote the nitrogen into its first vibrational level. The temperature dependence was described by the equation

$$\sigma^2 = f\sigma_T^2$$

where $\sigma_T^2 = 1.7$ Å^2 and represents the quenching cross-section for molecules colliding with energy greater than 1.6 kcal/mole and

$f = (1 + E/kT)\exp(-E/kT)$ and represents the fraction of molecules possessing an energy greater than the threshold energy, E. k is Boltzmann's constant and T is the absolute temperature.

Berberet and Clark (53) made a detailed study of this system using various techniques and showed that Hg^0 atoms decayed by a third order process involving a mercury excimer,

$$Hg^0 + Hg + N_2 \rightarrow Hg_2^* + N_2$$

analogous to that postulated by McCoubrey in pure mercury vapour.

Callear and Williams (58) on the other hand, concluded from their experiments using flash techniques that deactivation of Hg^0 atoms proceeded according to the second order reactions

$$Hg^0 + N_2 \rightarrow Hg + N_2 \qquad k = 8.7 \times 10^7 \text{ cc mole}^{-1}\text{sec}^{-1}$$

$$Hg^0 + Hg \rightarrow 2\,Hg \qquad k = 3.4 \times 10^{13} \text{ cc mole}^{-1}\text{sec}^{-1}.$$

However, the effect of N_2^* molecules arising from "double pumping" was not realized at the time of this investigation and the kinetics are undoubtedly more complicated than these workers assumed.

Using the technique of 4047Å absorption (88) and measurements on the 3350Å and 4850Å band intensities (89), Le Roy and co-workers found that the metastable atoms were removed by a third order process involving Hg^0, Hg and N_2. They proposed a mechanism comprised of a series of second order reactions in order to reconcile their low pressure data with the results of Callear and Williams, which were obtained at high pressures.

Penzes and co-workers (90) measured the 3350Å and 4850Å emission intensity to determine a third order rate constant of 1.1×10^{18} $cc^2 moles^{-2} sec^{-1}$ for the removal of Hg^0 atoms. From the effect of foreign gases on the ratio of the band intensities in irradiated Hg-nitrogen mixtures, they showed that two emitting excited states must be incorporated into

the reaction mechanism:

$$Hg^0 + Hg + N_2 \rightarrow Hg_2^*(^3\Sigma_u) + N_2$$

$$Hg_2^* \rightarrow 2Hg + h\nu(3350\text{Å})$$

$$Hg_2^* + N_2 \rightarrow Hg_2^{**}(^3\Sigma_u^-) + N_2$$

$$Hg_2^{**} \rightarrow 2Hg + h\nu(4850\text{Å}).$$

A more detailed investigation of the two emission band intensities (81) showed that both of the excited Hg_2 molecules can be collisionally quenched by nitrogen and other foreign gases. A quenching rate constant of 3 x 10^{12} cc [illegible] was obtained for the quenching of the $A(^3\Sigma_u)$ state and 2 x 10^7 cc $mole^{-1}sec^{-1}$ for the $A(^3\Sigma_u^-)$ excimer by nitrogen molecules.

Campbell and co-workers (55) redetermined the third order rate constant for the disappearance of Hg^0 atoms to be (3.8 to 5.8) x 10^{18} $cc^2mole^{-2}sec^{-1}$ using 4047Å absorption. Since absorption of this line does not obey the Beer-Lambert law (56), somewhat more weight should be placed on the earlier value (90).

(c) Paraffins.

Several features characterize the interaction of triplet mercury with paraffins. The quenching cross-sections are smaller than the gas kinetic collision cross-sections,

particularly for the first few members of the series (1). Darwent (91) showed that the quenching diameter for Hg* atoms, σ, is approximately a linear function of the carbon number within a homologous series, with methyl, methylene and methine groups contributing 0.15-0.30, 1.0 and 1.3 Å to the total quenching diameter, respectively. Rousseau and co-workers (82) pointed out the relationship between the specific σ increments and the electron donating power of these groups and suggested interaction of the electrophilic Hg* atom with the C-H bond.

Evidence for direct interaction with specific H atoms in the paraffin was presented by Gunning and co-workers (82,92-94) from Hg* quenching cross-sections obtained by the chemical method for various light and deuterated alkanes. Large k_H/k_D values found for secondary and tertiary C-H bonds were interpreted as primary isotope effects and the much lower k_H/k_D values found for H_2O, NH_3, PH_3 and C_2H_4 were attributed to secondary isotope effects.

Decomposition of paraffins is exclusively via C-H bond cleavage (95). If the alkane possesses more than one type of C-H bond, i.e. 1°, 2° or 3°, products arising from all the possible C-H bond ruptures are formed (95,96). Using ethylene-C^{14} as a hydrogen radical trap and internal scavenger for alkyl radicals to study the product distribution in Hg* sensitization of propane, Holroyd and Klein (97) and

Chesick (98) determined the primary i-propyl to n-propyl radical yield ratio to be approximately 1:9. Jakubowski and co-workers (99) also studied the primary product yield in the reaction of Hg* with propane and deuterated propanes using methyl radicals, produced from the decomposition of dimethylmercury, as a radical trap and a mass spectrometer to analyze the resulting addition products. The value obtained for the i-propyl to n-propyl ratio for light propane was virtually identical to the earlier result of Holroyd and Klein. In addition, the radical ratios of >30.0, 0.6 and 7.0 were determined for $CD_3CH_2CD_3$, $CH_3CD_2CH_3$ and $CD_3CD_2CD_3$, respectively. The data obtained in the quenching and primary decomposition yield studies clearly indicate that the primary yields of the various possible alkyl radicals are in the ratio of the quenching efficiencies of the respective C-H bonds in the molecule, in decreasing order from $3^0 > 2^0 > 1^0$.

Band emission for several light and deuterated alkanes has been reported by Penzes and co-workers (22) who conclusively demonstrated the existence of an excited mercury-substrate complex in the primary quenching act by paraffins. The band intensity was in the reverse order of the decomposition quantum yields, i.e. $CH_4 > C_2H_6 > C_2H_8$. An upper limit of 10^{-9} seconds was estimated for the emission lifetime of the complex, based on the observation that no deactivation was apparent up to 500 torr of propane. More

recently, the band emission, which is in the vicinity of the 2537Å line, has been photographed for several alkanes (23) and attributed to van der Waals molecules formed between Hg* atoms and the substrate.

The intermediacy of Hg^0 atoms in the quenching reactions of Hg* atoms by several light and deuterated alkanes was demonstrated by Penzes and co-workers (52). The measurements of the quantum yields for this process (63,66) have emphasized the importance of this mode of relaxation in all of the alkanes which were investigated.

Relatively few papers dealing with the effect of temperature on the triplet mercury sensitization of paraffins are found in the literature. Back and van der Auwera (100) noted that the quantum yield for decomposition of CH_4 increased as the temperature was increased. From a study of Hg* and ammonia and ammonia-propane mixtures, Takamuku and Back (101) concluded that the rates of the reactions

$$NH_3 + (Hg^* \text{ or } Hg^0) \rightarrow Hg + NH_2 + H$$

$$(HgRH)^* \rightarrow R + H + Hg$$

$$Hg^0 + RH \rightarrow Hg + R + H$$

could increase with an increase in temperature.

A detailed temperature study of Hg* (102) and Hg^0 (103) reactions with propane has recently been carried out. It was

shown that both of the excited mercury atoms decompose the substrate by C-H bond cleavage and the quantum yield of decomposition by Hg* atoms decreases, while that for Hg^0 atoms increases with an increase in temperature. Vikis and co-workers demonstrated that HgH is produced along with an alkyl radical in the Hg^0 sensitization of this system (104). The n-propyl to i-propyl ratio was also temperature dependent for the Hg* and Hg^0 initiated reactions. Although the quantum yields vary with temperature, the quenching cross-sections measured by the chemical method for Hg* atoms by C_3H_8 and $CH_3CD_2CH_3$ are invariant (105) over the temperature range of 30 to 150°C.

Several theories have been advanced to account for the experimental results as they were being accumulated. Rousseau, Strausz and Gunning (82) used absolute reaction rate theory (106) to calculate quenching cross-sections for comparison with their experimentally observed σ^2 values of light and deuterated alkanes (42,82). They assumed a linear transition complex, C•••H•••Hg*, in the rate determining step. Good agreement was found when the differences in the stretching and bending frequencies between the C-H and C-D bonds were taken into account.

Yang (105) criticized this theory on the basis that a difference in energy, ΔE, originating from the zero-point energies of the C-H and C-D bonds would contribute a factor

$\exp(\Delta E/RT)$ to the k_H/k_D ratio which he did not observe for the C_3H_8 and $CH_3CD_2CH_3$ pair. He proposed a quenching mechanism which assumed that the excited mercury atom, characterized by its total angular momentum quantum number J, and the paraffin, which was approximated as a diatom, formed a complex with C_s symmetry. The quenching efficiency was then assumed to be maximum if the same symmetry of the complex could be attained from the reactant or product side of the quenching reaction. The products were taken to be HgH and R. This model predicts that quenching of Hg^0 atoms to the ground state is allowed if R has p character but not if R is in an s state. Quenching of Hg* atoms is allowed, regardless of the state of R. According to this model, quenching of Hg^0 atoms by hydrogen should be very inefficient which is not the case (62,63).

To explain band emission and the temperature independence of the isotope effect, the planar complex was viewed (105) as being weakly bound, depending on the polarizabilities of the excited mercury atom and the paraffin. The rate of decomposition depends on the bond strength of the bond being broken. This model, however, does not explain the isotope effect or the formation of Hg^0 atoms in the propane reaction.

The quenching of Hg', Hg* and Hg^0 atoms by alkanes was investigated by Vikis and Moser (107). They assumed that a

relatively long lived (HgHR)* complex was formed which decomposed primarily by R-HHg bond rupture in a unimolecular process, the rate of which they calculated by the RRKM theory. The energy content of the complex was dependent on the excitation energy of the mercury atom (Hg^+, Hg* or Hg^0) which were all made to pass through an identical Hg^+ H^- R ionic surface prior to crossover to potential surfaces leading to products. This theory predicts reasonably well the various trends in the quenching of Hg* and Hg^0 atoms, the isotope effect and the relative quenching of Hg^+, Hg* and Hg^0 atoms by 1°, 2° and 3° C-H bonds.

The assumption that both Hg*HR and Hg^0HR complexes pass over the same ionic surface along the reaction path is incompatible with Campbell's results (23) on quenching of Hg* and Hg^0 atoms by propane. Furthermore, the arbitrary selection of the crossover points, the minimum in the ionic potential surface and the vibrational force constants that were necessary in order to apply the RRKM theory, detract from the credibility of the results.

A unified mechanistic model which accounts for all the known experimental observations in the triplet mercury-paraffin system has been proposed by Gunning and co-workers (108). These authors view the quenching process to be initiated by the formation of an Hg*HR or Hg^0HR complex. The intersection of these two potential surfaces allowed for

spin-orbit relaxation while crossover from each of these two surfaces to potential curves which correlate with product formation was believed to account for the independent behaviour of Hg^* or Hg^0 towards an alkane substrate. The decomposition of the alkane was viewed as a simple hydrogen atom abstraction by the excited mercury atom which possesses an activation energy compatible with the strength of the C-H bond involved. Application of the semi-empirical bond-energy-bond-order method (109), with appropriate modification, correctly predicted the trend in the experimental rate data.

(d) Hydrogen.

Yang and co-workers (105,110) noted that quenching of Hg^* atoms by hydrogen is some 3.3×10^3 times faster than for Hg^0 atoms and this was explained by the same symmetry arguments used to describe the Hg-RH system. They calculated the quantum yield of formation of H, HgH and undissociated H_2 to be 0.26, 0.16 and 0.58, respectively by phase space theory (111). However, the quantum yield of hydrogen decomposition was later found to be unity (112) which indicates an inadequacy in this approach.

Callear and co-workers (60,61,64,113) observed a large yield of HgH in the quenching of Hg^* and Hg^0 atoms by hydrogen but not with hydrocarbons (except C_2H_2). From the yields of HgH and HgD in flashed mixtures of mercury and HD

(61,64), it was proposed that the quenching proceeds by the insertion of the excited mercury into the H-H bond to give an electronically excited (H-Hg-H)* species which predissociates to a second electronically excited complex which decomposes to HgH and H in their ground states.

(e) Unsaturated Hydrocarbons.

The olefins are very efficient quenchers of Hg* and Hg^0 atoms as compared to their alkane counterparts. Le Roy and Steacie (114) proposed that the primary act in the case of ethylene, and for olefins in general (115), is triplet energy transfer to produce a relatively long lived, vibrationally excited triplet state of the olefin and a ground state mercury atom.

The quenching of Hg* atoms by protiated and deuterated aromatics has been suggested (116,117) to proceed by exciplex formation, followed by intersystem crossing to a complex which correlates with, and dissociates to, Hg and an electronically excited triplet state of the aromatic molecule. The intersystem crossing step seems to be enhanced whenever deuterium atoms are substituted in adjacent positions on the benzene ring.

(f) Nitrogen-Containing Compounds.

(i) Ammonia.

The interaction of excited mercury atoms is with the nonbonding electrons in the NH_3 molecule (82). Like methane, the mercury sensitized decomposition of ammonia has a low quantum yield (118,119) which increases with an increase in temperature (101).

Phillips and co-workers (26-29) have studied the kinetics of the band emission from excited mercury and NH_3 or ND_3 complexes as a function of substrate, third body and Hg concentrations, using rotating sector and phase shift methods. These workers found (26,27) that Hg* atoms are rapidly relaxed to the $^3P_0$ level with quantum yields of 0.7 and 1.0 for NH_3 and ND_3, respectively. The rate determining step in the quenching of metastable atoms was the formation of a complex between Hg^0 atoms and the substrate

$$Hg^0 + NH_3 \rightarrow (HgNH_3)^0$$

and this exciplex has a high probability for radiative relaxation,

$$(HgNH_3)^0 \rightarrow Hg + NH_3 + h\nu,$$

resulting in a continuous emission band centered at 3460Å for NH_3 and 3500Å for ND_3.

Callear and co-workers studied the mercury-ammonia system with the resonance flash apparatus (30,62). In addition

to the bimolecular relaxation of Hg^0 by complex formation, a third order process was observed in the quenching of metastable atoms

$$Hg^0 + NH_3 + M \rightarrow (HgNH_3)^0 + M$$

The kinetics could be broken down into the elementary reactions (30)

$$Hg^0 + NH_3 \rightarrow (HgNH_3)^{0\prime} \qquad [2a]$$

$$(HgNH_3)^{0\prime} \rightarrow Hg^0 + NH_3 \qquad [2b]$$

$$(HgNH_3)^{0\prime} \rightarrow Hg + NH_3 + h\nu \qquad [2c]$$

$$(HgNH_3)^{0\prime} + M \rightarrow (HgNH_3)^0 + M \qquad [3a]$$

where $(HgNH_3)^{0\prime}$ represents a nascent and $(HgNH_3)^0$ a vibrationally stabilized complex. Third order rate constants were obtained for M = N_2, NH_3 and ND_3. Large differences in the measured values between NH_3 and ND_3 were attributed to a dependence of the emission rates of $(HgNH_3)^0$ and $(HgND_3)^0$ on the internal energy of these complexes.

Phillips and co-workers (29) observed that at high NH_3 pressures the decay constant of the band luminescence reached a limiting value which they identified with the radiative lifetime of the $(HgNH_3)^0$ complex. Improved rate constants for the bimolecular and termolecular modes of Hg^0 relaxation were obtained by allowing for the finite emission

lifetime. A value of 5.0 kcal/mole was derived for the dissociation energy of the stabilized mercury-ammonia complex (28) from measurements of the difference in the peak wavelength of the emission band at high and low ammonia pressure.

Further investigation of the wavelength distribution as a function of NH_3 pressures up to 10 atmospheres with the resonance flash led Callear and Connor (120) to postulate that Hg^0 could attach clusters of NH_3 molecules to form $(Hg(NH_3)_n)^0$ complexes with n up to at least 5. Emission profiles of the complexes were determined for n = 1-4 and the dissociation constants for complexes with n = 2-4 were calculated. Evidence for the quenching of the stabilized complexes by ground state mercury atoms,

$$(HgNH_3)^0 + Hg \rightarrow Hg_2^* + NH_3$$

was also obtained.

(ii) Aliphatic Amines.

Aliphatic amines were found to undergo sensitized reactions essentially identical to those of ammonia (34,35). The lower efficiency of Hg^0 atom formation by amines as compared to ammonia suggests that Hg* atoms play a more significant role in these systems, particularly for methylamine. Rate constants for bimolecular and termolecular reactions

with Hg^0 atoms, the lifetimes of complexes with metastable atoms and lower limits for dissociation energies of these complexes were obtained (34). The main process competing with luminescence was found to be α-hydrogen abstraction (35).

(g) Oxygen-Containing Compounds.

(i) Water.

Mercury sensitized H_2O reactions closely parallel those of NH_3. Both substrates exhibit band emission (23) and a low quantum yield of decomposition at room temperature, less than 0.02 at 45°C for water (121).

A study by Phillips and co-workers (34) of the band emission in H_2O and D_2O sensitization showed that rapid spin-orbit relaxation of Hg* atoms was followed by a rate determining bimolecular reaction between the substrate and Hg^0 atom to form an exciplex. The quantum yield of luminescence was 0.19 and 0.49 for H_2O and D_2O, respectively. In a later publication (33) these workers obtained rate constants for the relaxation of Hg^0 atoms by bimolecular and termolecular reactions with the phase shift technique. The third order rate constants were somewhat uncertain due to the presence of 10 ppm of O_2 in the nitrogen used as a third body.

(ii) Alcohols.

The mercury sensitized decomposition of alcohols has been studied by Knight and Gunning (122-124). The products of the reactions could be explained by an O-H bond split by an Hg* atom in the primary step

$$Hg^* + RCH_2OH \rightarrow Hg + RCH_2O + H$$

followed by a rapid abstraction of the α-hydrogen on the substrate by an alkoxy radical

$$RCH_2OH + RCH_2O \rightarrow RCHOH + RCH_2OH$$

in a secondary reaction. Kato and Cvetanovic (125), however, suggested that the primary step could be abstraction of an α-hydrogen instead of O-H bond scission, a process which is more favored energetically.

The results of the alcohol sensitization experiments were interpreted entirely in terms of interaction with Hg* atoms. For methanol and ethanol, the σ^2 values measured by the physical method are 13.4 (45) and 32 Å^2 (3[illegible] respectively, in contrast to 2.3 and 5.4 Å^2 measured by Bellas and co-workers (42) using the chemical method. These authors suggested the involvement of metastable atoms as an explanation for the large differences in the values measured by the two techniques.

Recent studies of Hg-alcohol systems (32,33) have demonstrated the existence of comparatively weak band emission

which was similar to the $(HgNH_3)^o$ and $(HgH_2O)^o$ emission spectra and therefore attributed to radiative decay of an Hg^o + alcohol exciplex. From the variation of luminescence intensity with the structure of the various alcohols it was concluded that the main process competing with emission is abstraction of an α-hydrogen by metastable atoms formed during the quenching of Hg* (32). Phillips and co-workers (33) obtained evidence for the quenching of Hg^o atoms by bimolecular and termolecular reactions

$$Hg^o + ROH \rightarrow \text{products}$$

$$Hg^o + ROH + M \rightarrow \text{products}$$

where M = ROH or N_2 and derived rate constants for these processes for a few alcohols. It appeared that N_2 was very inefficient as a chaperone for the termolecular reaction.

The available data on Hg^o quenching rate constants in the literature for NH_3, H_2O, and alcohols are summarized in Table IV.

(iii) Ethers.

The primary step in the mercury photosensitization of saturated ethers at room temperature and moderate pressures is exclusively C-H bond scission (126-129). The kinetics were based on the major process being

TABLE IV

Rate Constants for Reactions of Ammonia, Water and Alcohols With $Hg(^3P_0)$ Atoms.

Compound (M)	k (a) sec^{-1}	k (b) $cc\ mole^{-1}\ sec^{-1}$	k (c) $cc^2 mole^{-2}\ sec^{-1}$	k (d) $cc^2 mole^{-1}\ sec^{-1}$	Ref.
NH_3	5.83×10^5	1.9×10^{11}	8.3×10^{17}	2×10^{16}	(36)
	5.4×10^5	1.88×10^{11}	7.5×10^{17}	7.55×10^{16}	(32)
ND_3	5.5×10^5	1.47×10^{11}	1.23×10^{18}	1.7×10^{17}	(32)
H_2O		3.4×10^9	5.26×10^{14}		(130)
	4.5×10^5	1.3×10^{10}	4.3×10^{15}	1.7×10^{15}	(33)
D_2O	4.5×10^5	8.13×10^9	3.45×10^{15}	1.01×10^{15}	(33)
CH_3OH	1.6×10^6	7.8×10^{11}	5.4×10^{17}		(33)
C_2H_5OH	8.3×10^6	3.6×10^{12}	3×10^{18}		(33)
$(CH_3)_3COH$	1.2×10^6	1.9×10^{12}	2.9×10^{18}		(33)
$(C_2H_5)(CH_3)COH$	3.6×10^6	4.2×10^{12}	4.7×10^{18}		(33)

a. Rate constant for the process $(HgM)^0 \rightarrow Hg + M + h\nu$

b. Rate constant for the process $Hg^0 + M \rightarrow (HgM)^0$

c. Rate constant for the process $Hg^0 + 2M \rightarrow (HgM)^0 + M$

d. Rate constant for the process $Hg^0 + M + N_2 \rightarrow (HgM)^0 + N_2$

$$Hg^* + RCH_2OR \rightarrow Hg + PCHOR + H$$

despite the implication that Hg^0 atoms were present in this system (42). Phillips and co-workers (32) were not able to detect band emission in the sensitization of diethylether, which may be indicative of a basic difference in quenching mechanism between alcohols and ethers.

(h) Rare Gases.

The interaction of excited mercury atoms with the rare gases has been of considerable interest for several decades since the quenching mechanism is confined to photophysical processes. Oldenberg (17) observed band fluorescence on both sides of the 2537Å line in irradiated mixtures of mercury and the rare gases and these were attributed (18) to transitions from loosely bound complexes of Hg* and the substrate gas. These bands have often been referred to as satellite bands. Preston (131) noted band emission associated with 13 mercury lines from a mercury lamp containing helium or Ar. Recently, the Hg-Xe satellite, which appeared as a broad structureless band extending from the 2537Å line to about 3000Å with a maximum at 2750Å, has been recorded by Phillips and co-workers (25). They attributed the emission to a Hg^0-Xe complex, although previous attempts to detect Hg^0 atoms in this system had failed (45). Quenching rate constants for Hg^0 by Xe and Hg were obtained from kinetic

studies by measuring the phase shift between the incident and band emission radiation using the rotating sector method. Campbell (23) obtained medium resolution spectra of the noble gas-mercury systems. Helium and neon displayed only asymmetrical broadening on both sides of the resonance line while Ar and Xe showed at least two, and krypton three, blue satellites. Ar and Kr exhibited faint fine structure near the resonance line which was superimposed on the continuum that extended to longer wavelengths. In the case of Xe, fine structure was observed throughout the broad continuum which displayed a maximum at approximately 2650Å. The emission was assigned to a Hg* + Xe complex.

Several proposals have been advanced to explain the origin of these bands. It has been suggested that band emission is due to transitions between vibrational (23,132-134) or vibrational-rotational levels (135,136) of (Hg*-rare gas) van der Waals molecules and their ground state molecules. Jefimenko (137) used semi-empirical calculations to demonstrate the existence of auxiliary maxima and minima in the upper state potential curves. Satellite bands were attributed to radiative transitions from these regions of the potential curves. An adaptation of the quasistatic theory of pressure broadening of atomic lines has been used (138,139) to predict the features of red satellites. Breene (140) has suggested that band emission is due to a process that is the precise analogue of predissociation of stable molecules.

Cunningham and Olsen (141) obtained quenching cross-sections by measuring the depolarization of 2537Å radiation. Gunning and co-workers (24) measured band emission intensities to obtain σ^2 values which were in fair agreement with the earlier results. They also showed that quenching occurs entirely by radiative relaxation of the excited mercury-noble gas complex and that the curve crossing mechanism proposed earlier by Jablonski (142) is of little importance.

4. Aims of the Present Research.

It can be seen from the preceding discussion that although the general quenching mechanism in several mercury sensitized systems has been well established some aspects remain obscure. The role of Hg^0 and Hg^* atoms in the sensitization of several compounds remains undefined and, in some areas, conflicting data has slowed the development of a clear understanding of the various phenomena. The effect of temperature on the quenching process has received little attention, despite the potentially useful information that may be gained.

The aim of the present work is

(i) to study the various relaxation processes involved in the Hg^* sensitization of nitrogen in order to determine their effects on the measurement of Hg^0

atom quenching rate constants in Hg-N_2-substrate mixtures,

(ii) to elucidate the mechanism of Hg^0 atom quenching for a variety of substrates from a study of effects of deuterium substitution and temperature on the quenching rate and,

(iii) to determine the relative participation of Hg^* and Hg^0 atoms in the photosensitization of Xe atoms and ether molecules from band emission studies.

CHAPTER II

EXPERIMENTAL

1. Apparatus

A two-stage mercury diffusion pump and a Welsh "Duo-Seal" mechanical pump were used to evacuate a conventional vacuum apparatus to 10^{-6} torr. The distillation train, storage bulbs and cell section were kept grease-free by using Springham stopcocks, Delmar mercury float valves and Hoke valves. Pressure was measured using a mercury manometer, a Baratron MKS gauge and a Pirani gauge.

Kinetic studies were carried out in a circulating system (Figure 2) using a flash technique while experiments designed to investigate band emission employed a flow system with continuous irradiation (Figure 3).

(a) The Circulating System

Mercury vapour concentration was controlled by circulating the substrate gas(es) over a pool of mercury at ambient temperature and then through a 10 cm long condenser (stripper) packed with 1/8 inch glass helices. The stripper temperature was maintained at 20.0 ± 0.1°C, except where otherwise noted.

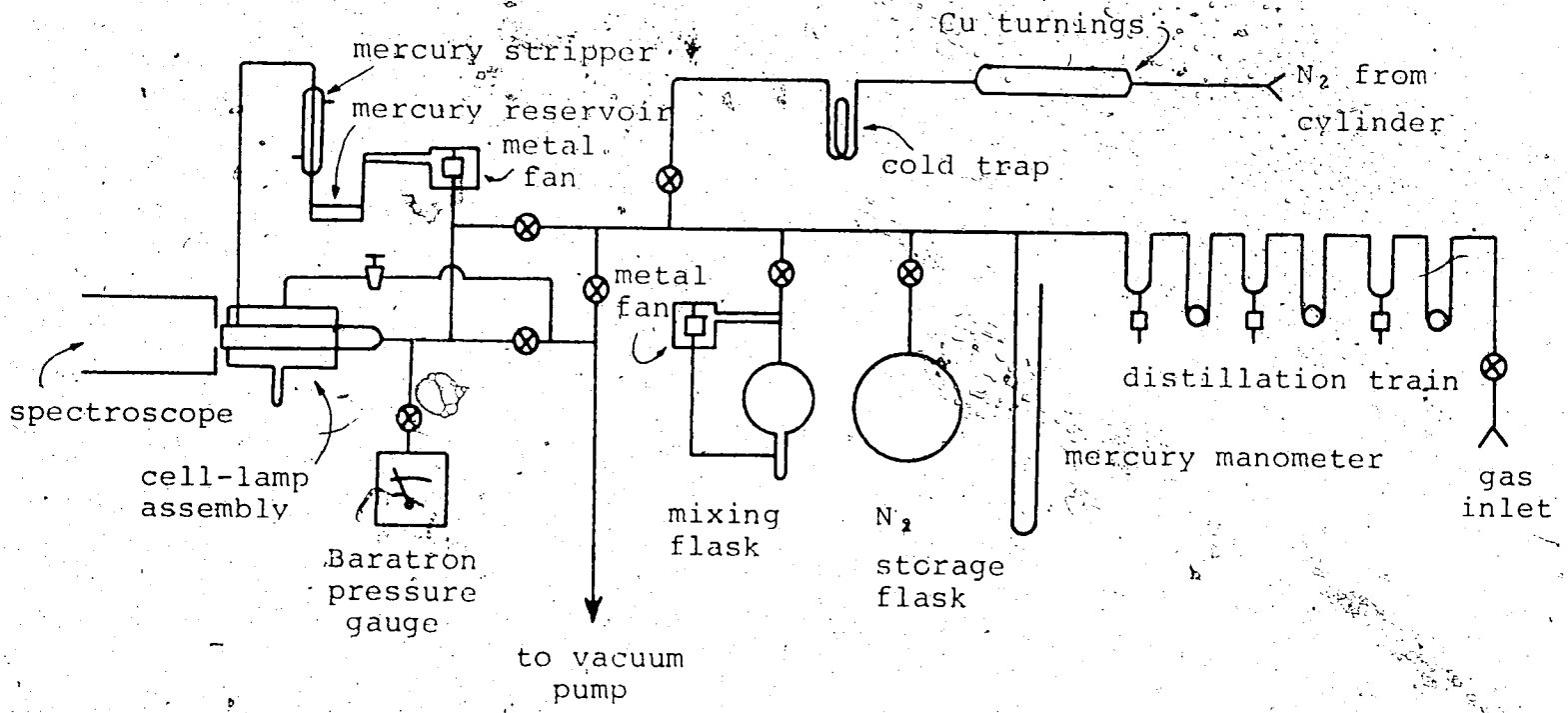

FIGURE 2: The circulating system vacuum apparatus.

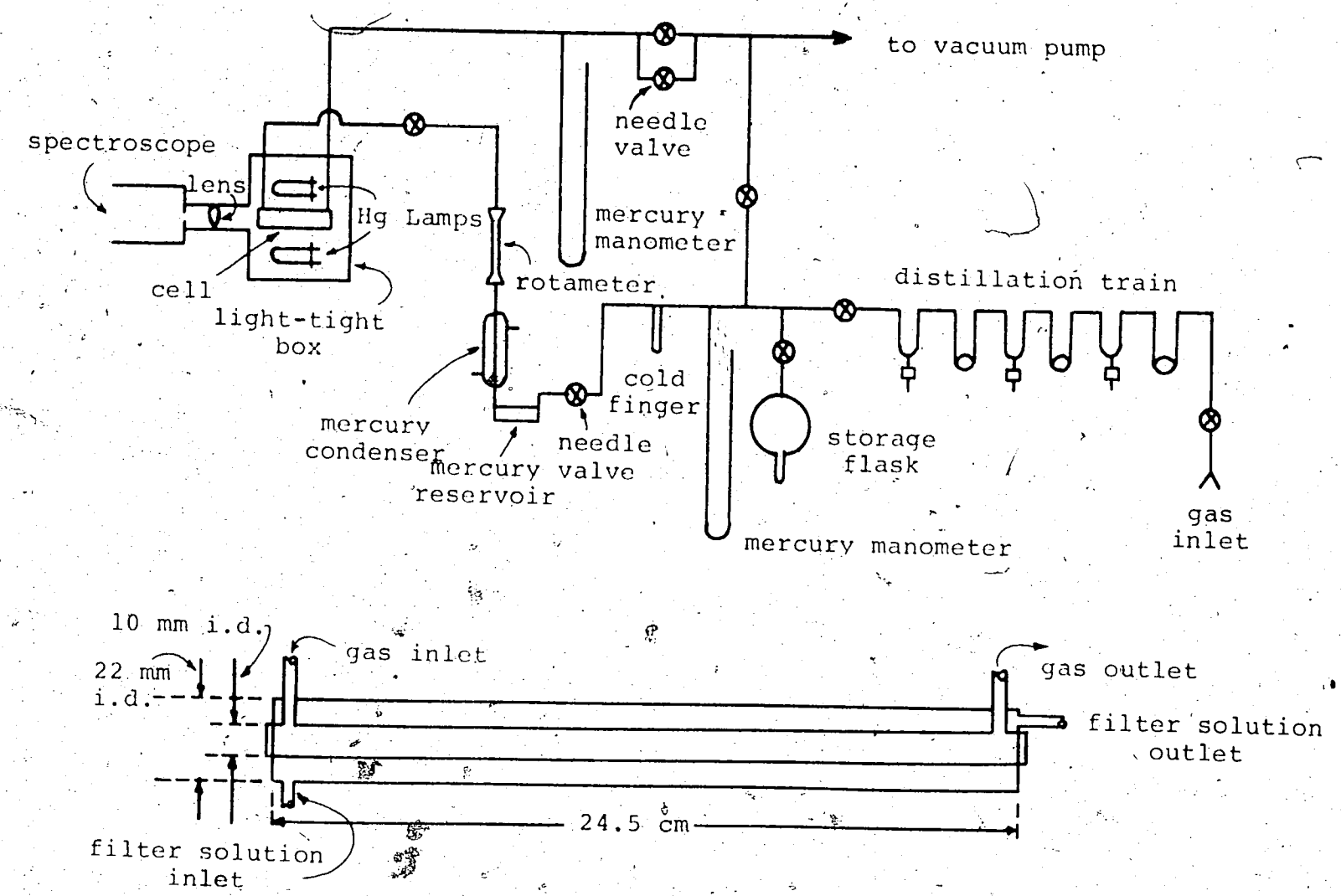

FIGURE 3: The flow system vacuum apparatus and cell used in band emission studies.

The reaction cell was connected to the mercury stripper by a two foot length of tubing wrapped with heating tape which allowed for pre-heating of the gases for the experiments conducted at elevated temperatures. Heating tape was wrapped around the entire circulating system in the runs which required high mercury vapour pressures.

Circulation of the gases was effected by means of a metal fan on "Rulon-A" bearings which was magnetically coupled to a drive motor operating at about 1800 rpm. The gases were circulated for approximately one minute before flashing to establish a constant mercury vapour pressure.

(i) Cell-Lamp Assembly

The basic features of the flash lamp-cell combination (Figure 4) were adopted from Callear and McGurk (113). The lamp was constructed of two 50 mm long quartz tubes, 22 and 50 mm i.d., sealed together at the ends. The lamp contained two torr of helium and the saturation vapour pressure of mercury at room temperature. A silicone greased ground glass stopcock isolated the lamp from the vacuum apparatus. Two tungsten electrode pairs were connected by co-axial cable to a one microfarad NPG low inductance capacitor. The decay lifetime of the flash was two microseconds or less when the capacitor was operated at 12 kV. A weak tail after the main flash had a decay lifetime of 50 to 60 microseconds.

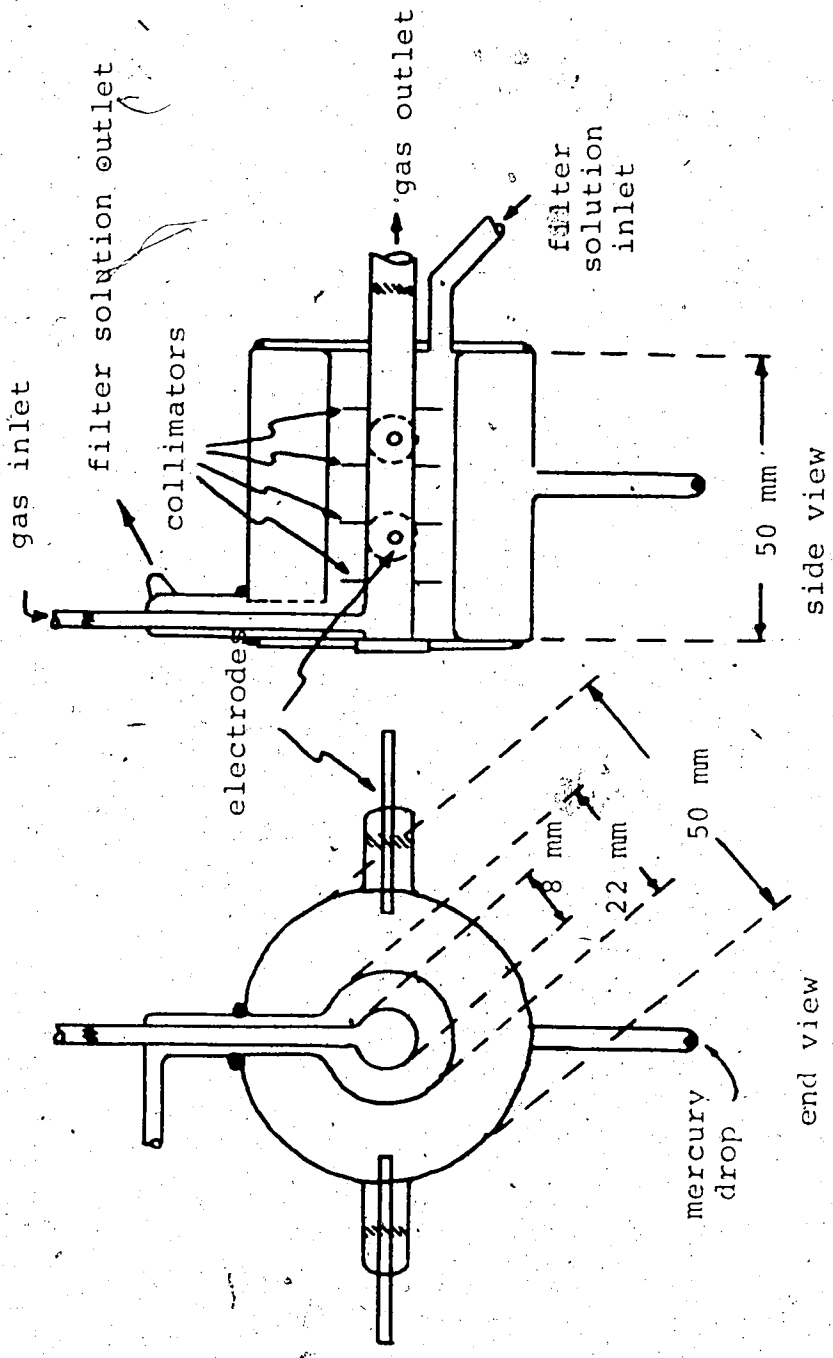

FIGURE 4: Flash lamp - cell assembly.

Two arborite plates, glued to the ends of the lamp, served to center an 8 mm i.d. spectrosil cell along the lamp axis and to enclose an annular compartment through which a filter solution was circulated. The cell temperature was controlled by regulating the temperature (± 2°C) of the filter solution. Rubber collimators attached to the cell at one cm intervals minimized the stray light radiated from the cell but did not hamper the flow of the filter solution.

A photograph of the spectrum observed through the cell window of 100 lamp firings showed a strong 2537Å line and other, much weaker, mercury and tungsten lines.

(ii) The Filter Solution.

A saturated 1:1 aqueous solution of $NiSO_4$-$CoSO_4$ containing 200 mg/liter of the u.v. dye 2,7-dimethyl-3,6-diazocyclohepta-1,6-diene perchlorate (143) was used. This solution had a transmission of 20% at 2537Å, 0.2% at 4047Å and about 0.6% at 2967Å and 4358Å. No change in the spectral characteristics of the solution was detected over a period of several months or upon heating to 80°C.

(iii) The Spectrograph.

The end window of the cell was placed immediately in front of the slit of a Hilger-Watts Model E498 medium-quartz spectrograph. The slit width was set at 500 microns.

(iv) The Light Detection and Recording Instruments.

An RCA 1P28 photomultiplier, housed in a E720 scanning unit that replaced the plate holder, was used to monitor the emitted light intensity. The photomultiplier could be moved to any desired location in the focal plane of the spectrograph to record the light intensity at a particular wavelength. A slit in front of the photomultiplier admitted a five angstrom bandwith. Power for the photomultiplier was supplied by a Harrison 6110A DC power supply operating at 900 volts. The pre-amplifier was powered by a Stark model PS-501 power supply delivering 80 volts. The output signal was amplified and displayed on the screen of a Hewlett-Packard 130C oscilloscope and recorded on type 107 Polaroid film.

(v) Data Processing.

The curves on the photographs were converted to digital form using a digitizer facility at the University of Alberta computing center. The (x,y) co-ordinates of points on the curves were determined electronically and stored on magnetic tape. Points were recorded at what corresponded to 10 microsecond intervals, beginning 50 microseconds after the flash. Fifteen to 45 points could be obtained, depending on the curve being measured. The data were then processed by an IBM 360/67 computer.

The slopes and intercept values of straight line plots were determined by least-squares analysis of the data points wherever possible. For plots which were not straight lines, curve fitting was carried out using iterative procedures to determine the value of a particular variable which would give the best fit.

(vi) Operating Procedure.

The experiments with nitrogen-substrate gas mixtures were carried out by initially filling a 6 liter storage bulb to a pressure of about 1200 torr with purified nitrogen (see below). A suitable quantity of the substrate gas was introduced into a three liter mixing flask to which nitrogen from the storage bulb was added. Successive reduction of the original nitrogen/foreign gas ratio was carried out by the addition of more nitrogen to the mixing flask. The mixtures were stirred for a minimum of five minutes before use. In most cases, two flashes of each mixture and four of the purified nitrogen were taken. The nitrogen concentration was kept at 1.06×10^{-5} mole cc^{-1}, except where otherwise noted. In cases where pure substrate gas was flashed, the gas was simply introduced into the cell from the storage vessel. The cell section was evacuated after each flash to eliminate possible interference from reaction products.

(b) The Flow System.

The experiments designed to record the spectra of (Hg*-substrate) complexes were carried out in a single pass flow system. In these experiments, the photomultiplier attachment was replaced by a plate holder.

(i) Emission Cell.

A double wall spectrosil cell, 10 x 245 mm, was constructed with the inlet and outlet tubes as close to the end windows as possible to eliminate dead space. The double wall enabled the filter solution (6 mm radial path length) to be circulated around the cell. Blackened plates, spaced one inch apart, collimated the incident radiation from the exciting source. Light emerging from the window was focused onto the slit of the spectrograph.

(ii) Light Source.

The incident radiation was provided by two Hanovia low pressure resonance lamps, #87a-45, situated on opposite sides of the cell. The lamps and cell were enclosed in a light-tight box which was flushed with a stream of nitrogen that cooled the lamps and prevented ozone formation in the enclosure.

(iii) Photographic Plates.

Kodak 103a-o photographic plates having a linear response to wavelengths between 2400Å and 5000Å were used

af[illegible] 15 second exposure [illegible] weak white light. This treatment ensured the linearity of the optical density with the l[illegible] of the intensity. The plates were developed for 3.5 m[illegible]es at 25°C in Kodak [illegible]19 developer. A Joyce-Loebl automatic recording MK II[illegible] microdensitometer was used for measuring optical [illegible]ties.

(iv) Operating Procedure.

Suitable temperature baths were used to establish a known pressure of substrate gas in a ballast volume. Mercury vapour was included in the input stream by passing the gas over a pool of mercury at 45°C and then through an efficient condenser maintained at 20.0 ± 0.1 °C. The gas pressure and flow in the cell were controlled by two Edwards needle valves, located upstream and downstream from the cell. A Matheson R-2-15AAA rotameter was used to measure the gas flow.

2. Materials

The gases studied were of highest purity available. Those condensable at -196°C were subjected to several freeze-pump-thaw cycles. Where the purity was suspect, the gases were distilled from appropriate low temperature slushes until only a single peak appeared when analyzed by vapour phase chromatography. Mass spectrometry was used to

assay the methane used, which was found to contain less than two ppm of impurities.

Nitrogen gas used in the kinetic studies was obtained from Canadian Liquid Air and had a stated purity of 99.993 mole percent. Further purification was carried out by passing the nitrogen through 20 x 400 mm glass tube packed with copper turnings heated to 275°C. At this temperature, oxygen impurity is converted to CuO. Water impurity was removed by condensation in a trap containing a molecular sieve maintained at -78°C. Comparison of some sample results using the purified nitrogen and Airco analyzed nitrogen (maximum impurities of 2 ppm) showed no significant differences, thus assuring acceptable purity of the prepared nitrogen.

CHAPTER III

THE INTERACTION OF EXCITED MERCURY ATOMS WITH NITROGEN

A detailed kinetic study of the processes occurring in flashed Hg-nitrogen mixtures was undertaken in order to establish a framework for experiments on the quenching of Hg^0 atoms to be described in Chapter IV.

1. Results.

The rate of removal of Hg^0 atoms in mercury-nitrogen mixtures was determined by measuring the exponential decay of the delayed fluorescence intensity as a function of nitrogen pressure (Figures 5 and 6) and temperature (Figure 6). The results have been interpreted in terms of the following reaction scheme:

$$Hg + h\nu(2537\text{Å}) \rightarrow Hg^* \qquad [1]$$

$$Hg^* \rightarrow Hg + h\nu(2537\text{Å}) \qquad [2]$$

$$Hg^* + N_2 \rightarrow Hg^0 + N_2(v=1) \qquad [11]$$

$$Hg^0 + N_2 \rightarrow Hg^* + N_2 \qquad [12]$$

$$Hg^0 + Hg + N_2 \rightarrow Hg_2^*\ A(^3\Sigma_u) + N_2. \qquad [13]$$

Quenching of Hg^* and Hg^0 to the ground state and spontaneous emission from Hg^0 are negligibly slow in comparison to the other relaxation processes and are omitted from the reaction

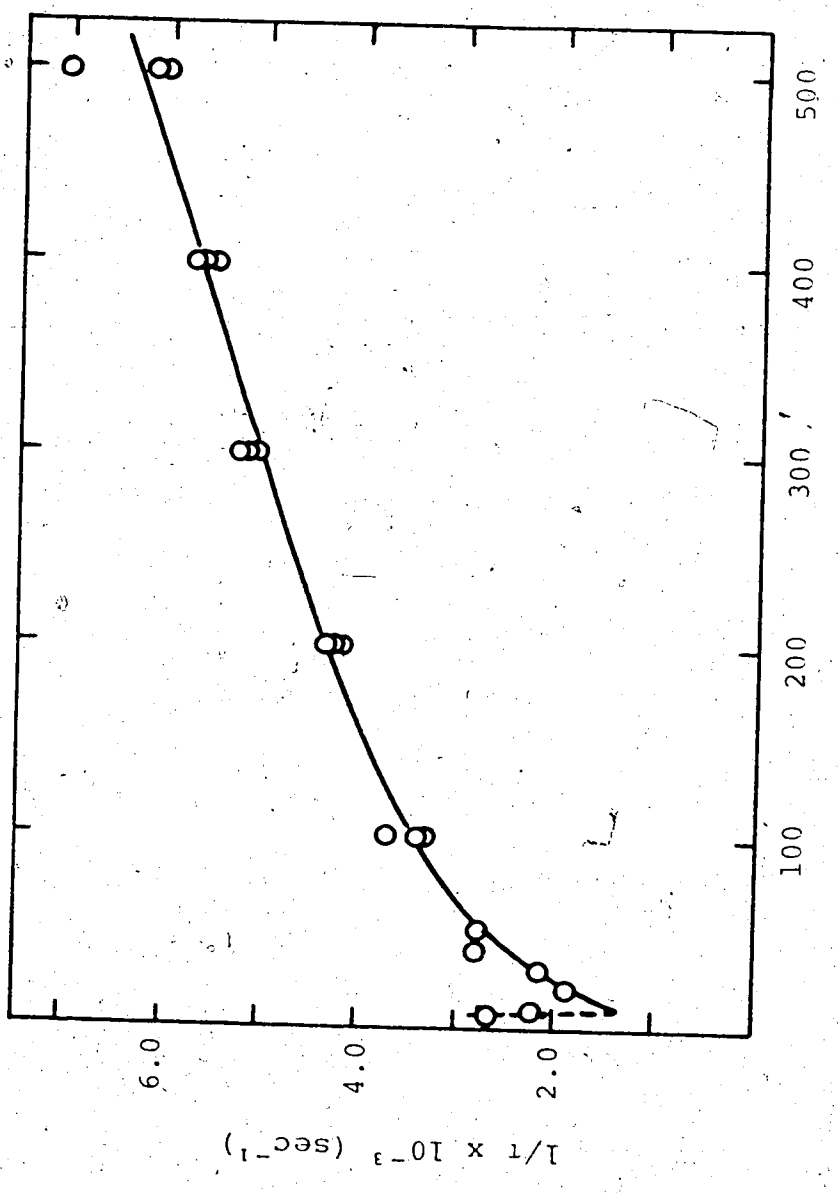

FIGURE 5: $1/\tau$ vs nitrogen pressure at 29°C.

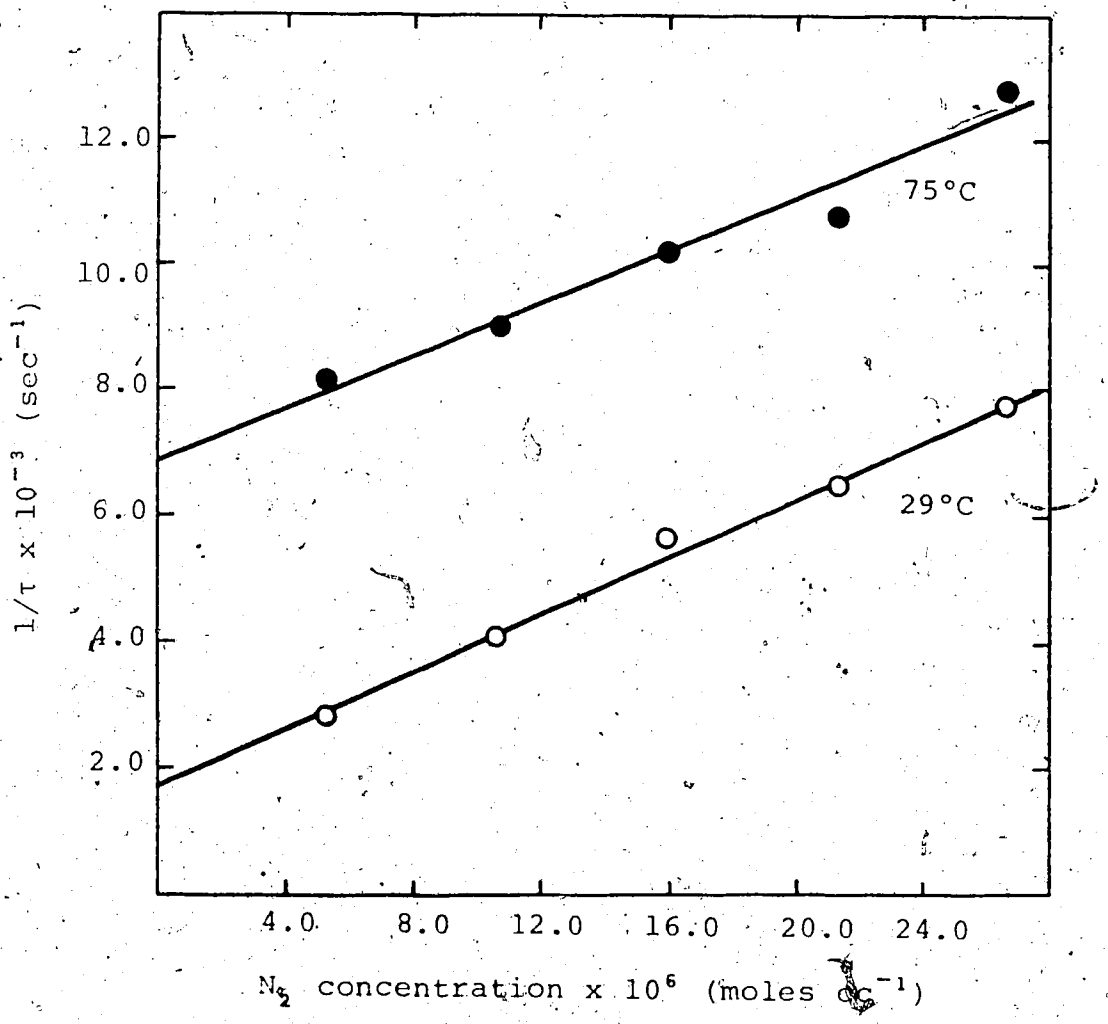

FIGURE 6: $1/\tau$ vs nitrogen concentration at 29°C and 75°C.

mechanism. Loss of Hg^0 atoms by diffusion to the walls only becomes important at N_2 pressures less than 10 torr which was indicated by an upward curvature in Figure 5 in this region, in qualitative agreement with Pitre and co-workers (71).

The experimental decay constant, k_{N_2}, of the delayed fluorescence is given by the expression

$$1/\tau = k_{N_2} = \frac{k_2[N_2]\{k_{13}[Hg] + k_{12}\} + k_{11}k_{13}[Hg][N_2]^2}{k_2 + k_{11}[N_2]} \quad [14]$$

which was obtained as a solution of the simultaneous differential equations involving Hg^* and Hg^0 by the standard method of differentiation and elimination (see Appendix A).

The values of the appropriate rate constants, listed in Table V, were applied to equation [14] to determine the value of k_{13} which best fitted the experimentally observed decay rate at nitrogen pressures ranging from 5 to 500 torr for a constant mercury pressure of 4.9×10^{-4} torr at 29°C, (Figure 5). The derived value of k_{13} was 4.3×10^{18} $cc^2 mole^{-2} sec^{-1}$, in fair agreement with 1.1×10^{18} $cc^2 mole^{-2} sec^{-1}$ (90), probably the best previous value.

At high nitrogen pressures equation [14] can be simplified to the form

TABLE V

Rate Constant Values Employed in the Kinetic Calculations in the $Hg(^3P_1)$ + N_2 System.

Rate	Rate Constant	Reference
k_2	5.76×10^6 sec^{-1} (a)	
k_{11}	3.93×10^{12} cc $mole^{-1} sec^{-1}$ with a temperature dependence of $\exp(-1600/RT)$	(44)
k_{12}	$3k_{11} \exp(-5.0 \times 10^3/RT)$	(88)
k_{16}	1.0×10^7 sec^{-1} 2.0×10^4 sec^{-1}	(85), (89) (86)
k_{17}	2.6×10^{13} cc $mole^{-1} sec^{-1}$	(81)
k_{18}	3×10^{12} cc $mole^{-1} sec^{-1}$	(80)
k_{19}	20.0 sec^{-1} 0.5 sec^{-1}	(85) (6)

a. Calculated for 4.9×10^{-4} torr Hg at 29°C using Yang's imprisonment formula (15), with $\tau_0 = 1.41 \times 10^{-7}$ sec^{-1} (5).

$$1/\tau = K_{N_2} = 3.0 \exp(-5.0 \times 10^3/RT) k_2 + k_{13}[Hg][N_2] \quad [15]$$

(see Appendix A) and describes the contribution to the decay rate of Hg^0 by delayed fluorescence and excimer formation. The predicted linear dependence of the decay rate on the nitrogen concentration has been observed, at least for nitrogen pressures greater than 100 torr (Figures 5 and 6). Since both terms in equation [15] depend on the mercury concentration and tend to counteract each other, the decay rate as a function of mercury concentration is expected to be complex. Within experimental error, no change in the rate of decay of Hg^0 atoms was observed on varying the mercury pressure from 2.5×10^{-4} to 1.2×10^{-3} torr at 29°C. Data taken from different experiments indicate a linear dependence of the rate at higher mercury concentrations where the imprisonment of resonance radiation is increased, i.e., the value of k_2 is drastically reduced.

The increase in the decay rate of metastable atoms as the temperature is increased is a manifestation of the five kcal/mole energy difference separating the Hg^0 and Hg^* states. This theoretical activation energy for reaction [12] is expressed by the exponential term in equation [15] and can be derived from the intercepts in Figure 6. Using the two intercept values, and correcting for the change in the radiative lifetime of Hg^* at the two different temperatures using Yang's formula (15), an activation energy of 5.4 ± 0.9

kcal/mole was calculated.

The mercury excimer bands centered at 3350Å and 4850Å could not be observed under conditions of low imprisonment of the resonance radiation. With nitrogen pressures greater than 200 torr and the mercury pressure at 5.47×10^{-2} torr at 81°C, the value of k_2 was decreased sufficiently to allow the detection of the 4850Å band and a concurrent decrease in the delayed fluorescence intensity was also observed. The 3350Å band could not be detected owing to the efficient conversion of the Hg_2^* excimer to the $(^3O_u^-)$ state at the nitrogen pressures used in the experiments. Figure 7 displays the time dependence of the 4850Å band with 800 torr nitrogen.

In addition to the reactions on page 64, the following mechanism has been employed to explain the observed results:

$$Hg_2^* \; A(^1\Sigma_u^+) \rightarrow 2Hg + h\nu(3350Å) \qquad [16]$$

$$Hg_2^* + N_2 \rightarrow Hg_2^{**} \; A(^3O_u^-) + N_2 \qquad [17]$$

$$Hg_2^* + N_2 \rightarrow 2Hg + N_2' \qquad [18]$$

$$Hg_2^{**} \rightarrow 2Hg + h\nu(4850Å) \qquad [19]$$

$$Hg_2^{**} + N_2 \rightarrow 2Hg + N_2' \qquad [20]$$

where the prime denotes vibrational and the asterisk electronic and vibrational excitation. Deactivation of Hg_2^{**} on the walls (85) is much slower than collisional relaxation and is not included in the reaction mechanism.

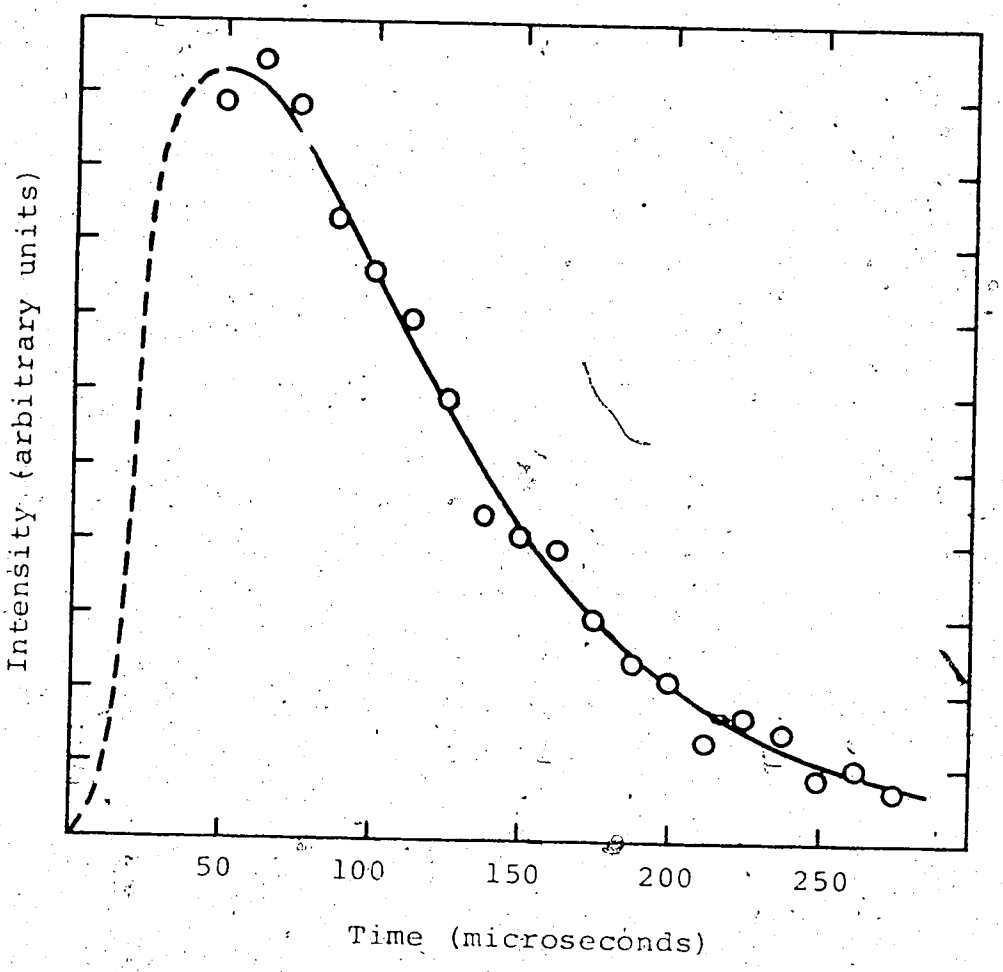

FIGURE 7: Time dependence of 4850 Å band intensity with 800 torr N_2 at 81°C.

Given that $[Hg^0] = A \exp(-k_{N_2} t)$, where k_{N_2} can be measured from the decay of delayed fluorescence intensity, successive integration of the rate equations involving Hg_2^{**} yields the following expression for the 4850Å band intensity in time (see Appendix B):

$$I_{4850} = \frac{A' k_{13} k_{17} k_{19} [Hg][N_2]^2 \{ X - Y + Z \}}{(p-m)(v-m)(v-p)} \qquad [21]$$

where $m = k_{N_2}$

$p = k_{16} + (k_{17} + k_{18})[N_2]$

$v = k_{19} + k_{20}[N_2]$

$X = (v-p)\exp(-mt)$

$Y = (v-m)\exp(-pt)$

$Z = (p-m)\exp(-vt)$ and

A' is a constant of proportionality which includes such factors as the photomultiplier response and dispersion of the spectroscope.

k_{20} was evaluated by matching the decay of the 4850Å band intensity given by equation [21] to the experimentally observed decay rate measured with 200, 400, 600 and 800 torr nitrogen. Rate constant values for the various reactions involved were taken from Table V, along with the value of 4.8×10^{18} $cc^2 mole^{-2} sec^{-1}$ for k_{13}. The best value of k_{20} for each of the four nitrogen pressures was obtained by minimizing the standard deviation between the calculated and experimental points. The average value of k_{20} obtained in this

manner is approximately 7 x 10^8 cc $mole^{-1}sec^{-1}$ for either of the two values of k_{16} and k_{19} listed in Table V. This figure is about two orders of magnitude greater than that noted by Penzes and co-workers (81). The estimated error in the present value is a factor of five.

Ladd and co-workers (86) have postulated a pressure induced emission process for the 4850Å band. If the above mechanism is modified so that the reactions

$$Hg_2^{**} + N_2 \rightarrow 2Hg + N_2 + h\nu(4850Å) \qquad [22]$$

$$Hg_2^{**} + Hg \rightarrow 3Hg + h\nu(4850Å) \qquad [23]$$

replace reactions [19] and [20], no improvement in fitting the appropriately modified equation [21] to the results was observed.

2./Discussion.

The mercury photosensitization of nitrogen has attracted a great deal of study since it is unique in efficiently bringing about spin-orbit relaxation of Hg* to Hg^0 without appreciably quenching either of these two species to the ground state. It has been considered that the major mode of deactivation of the metastable atoms produced in this system is by the formation of the diatomic $A(^3\Sigma_u^+)$ mercury excimer with nitrogen as a chaperone (81,89,90). The results of the present investigation clearly demonstrate that under con-

ditions of low imprisonment of resonance fluorescence, collisional promotion of metastable atoms to the $^3P_1$ state, followed by 2537Å emission is the chief process by which Hg^0 atoms are removed. This can be seen by reference to equation [15] which predicts that at low mercury concentrations, where k_2 is large, the first term accounts for almost all of the observed decay rate. If k_2 is made very small by increasing the mercury concentration, thus increasing the radiative lifetime of Hg* atoms, the major contribution to the observed decay rate is due to the second term, i.e. excimer formation. This prediction has been verified in the high temperature experiments. At low mercury concentrations, the delayed fluorescence appeared strongly whereas the emission bands from the mercury excimers could not be detected. Increasing the mercury concentration some 50-fold resulted in a 10-fold decrease of the delayed fluorescence intensity and the appearance of the 4850Å band.

The fact that the decay rate of delayed fluorescence at 29°C was independent of mercury pressures between 2.5×10^{-4} and 1.2×10^{-3} torr can be explained in terms of the critical role of imprisonment of the resonance radiation. Under these conditions, increasing the mercury concentration results in an increase by the decay rate in the second term in equation [15] but this is offset by a decrease in k_2 in the first term. Since the formation of excimer varies from 3.0 to 22.2% of the total decay of Hg^0 atoms in 500 torr N_2, a

much larger increase in this mode of decay is needed to offset a smaller decrease in the radiative lifetime to obtain a cancellation of the two factors. The 4.8-fold increase in the mercury concentration would produce a 9.1% increase in the rate of decay of Hg^0 atoms, but the 1.25 reduction of k_2 corresponds to a 10.1% decrease in the decay rate. This difference is well within experimental limits. The dependence of the decay rate on the mercury concentration could only be measured at much higher Hg vapour pressures where the contribution to the decay rate by delayed fluorescence becomes very small in comparison to the decay of Hg^0 atoms by excimer formation.

It is evident that interpretation of the reactions of Hg^0 atoms with added substrates in mercury-nitrogen mixtures may be complicated by the presence of Hg* atoms in this system. The extent of the interference by Hg* atoms will depend on the experimental technique and conditions used in the investigation.

Vibrationally excited nitrogen molecules formed in the spin-orbit relaxation of Hg* atoms appear to be of little importance in contributing to the reverse reaction rate. The measured activation energy of 5.4 kcal/mole for the promotion of Hg^0 atoms to the $^3P_1$ level suggests that this is brought about by collisions with thermally equilibrated nitrogen molecules.

Callear (130) has measured the decay rate of 2537Å radiation in Hg-N_2 mixtures with essentially the same apparatus as used in the present work. He calculated that the major mode of relaxation of Hg^0 atoms was by delayed fluorescence for nitrogen pressures less than 50 torr. He also suggested that the increase in the decay rate for nitrogen pressures greater than 100 torr was probably due to oxygen impurity. The present work demonstrates that delayed fluorescence is the primary mode of decay for N_2 pressures up to several atmospheres, under conditions of low imprisonment, and that the gradual increase in the decay rate with increasing nitrogen pressure is due to the increasing rate of excimer formation. Callear has also assumed that the decay rate of delayed fluorescence decreases to zero as the nitrogen pressure is reduced to zero. In the present work it was noted that an increase in the decay rate becomes apparent at nitrogen pressures less than 10 torr. This can be explained in terms of the increased importance of deactivation of Hg^0 atoms at the wall (9,74).

The experimental data concerning the time dependence of the 4850Å band intensity could be equally well described by assuming either a spontaneous emission of the Hg_2^{**} excimer (81,89) or a pressure induced emission (86) since the arbitrary factor, A', in equation [21] can be adjusted to suit both possibilities. The fast decay rate of the 4850Å band

intensity obtained under the present conditions implies that the $(^3O_u^-)$ state is relaxed primarily by a collisional process, but whether this results in quenching (81) or pressure induced emission (86) cannot be determined from the data. In either case, the two order of magnitude increase in the rate constant measured at 810C (present work) from that measured at 20°C (81) would suggest that the reaction is temperature dependent.

CHAPTER IV

INTERACTION OF $Hg(^3P_0)$ ATOMS WITH FOREIGN GASES

Rate constants for the quenching of Hg^0 atoms by foreign gases, except NH_3, were determined by measuring the time dependence of the delayed fluorescence intensity as a function of the partial pressure of quencher gas in flashed $Hg-N_2$ mixtures. Data was obtained at 27(±2) °C and at 75(±1) °C.

The results were interpreted in terms of reactions [1], [2], and [11]-[13] used in Chapter III and the following:

$$Hg^* + Q \rightarrow Hg + \text{products} \qquad [24]$$

$$Hg^* + Q \rightarrow Hg^0 + Q \qquad [25]$$

$$Hg^0 + Q \rightarrow Hg + \text{products} \qquad [26]$$

where Q denotes a quencher molecule and "products" indicate decomposition, electronic excitation, etc., of the molecule or band emission. The above mechanism is a simplified but experimentally indistinguishable version of a more detailed scheme that includes complex formation:

$$Hg^* + Q \rightarrow (HgQ)^* \qquad [27]$$

$$(HgQ)^* \rightarrow Hg^* + Q \qquad [-27]$$

$$(HgQ)^* \rightarrow Hg + \text{products} \qquad [28]$$

$$(HgQ)^* \rightarrow Hg^0 + Q \qquad [29]$$

$$Hg^0 + Q \rightarrow (HgQ)^0 \qquad [30]$$

$$(HgQ)^0 \rightarrow Hg^0 + Q \qquad [-30]$$

$$(HgQ)^0 \rightarrow Hg + \text{products.} \qquad [31]$$

The rates of the reactions considered above are related to the decay rate constant, k_T, of the delayed fluorescence intensity by the formula (see Appendix C):

$$1/\tau = k_T = k_{13}[Hg][N_2] + k_2k_{12}/k_{11} + (k_{24}k_{12}/k_{11} + k_{26})[Q] \qquad [32]$$

The intercept of k_T vs [Q] plots, $(k_{13}[Hg][N_2] + k_2k_{12}/k_{11})$, represents the rate of removal of Hg^0 atoms by nitrogen molecules which, as pointed out in Chapter III, is via excimer formation and emission of 2537Å radiation. The slope, $(k_{24}k_{12}/k_{11} + k_{26})$, k_Q, describes the contribution to the decay rate by the quencher gas and indicates that the relaxation of Hg^0 atoms is affected by two processes when a quencher is present, namely:

(i) quenching of Hg* atoms (produced by collisions of Hg^0 atoms with N_2) expressed by the term $k_{24}k_{12}/k_{11}[Q]$ and

(ii) quenching of Hg^0 atoms directly, given by the term $k_{26}[Q]$.

k_{26} values were calculated from the slopes by subtracting the correction term, $k_{24}k_{12}/k_{11}$, and inserted into

$$= k_{26}/\{8\pi RT(M_{Hg}+M_Q)/(M_{Hg}M_Q)\}^{1/2} \quad [33]$$

to obtain quenching cross-sections.

The correction term was calculated using the values of k_{11} and k_{12} found in Table V and assuming that k_{24} equals $k^*(1-\phi^0)$ where k^* is the quenching rate constant for Hg* atoms measured by the physical method and ϕ^0 is the quantum yield of Hg^0 formation. k^* values were taken from Table I, with preference given to those of reference (45) and (38) since these represent the most extensive and unified set of determinations available in the literature. The quantum yield for spin-orbit relaxation were taken from reference (65) of Table II. Where ϕ^0 values are not available, a range of values for k_{26} were calculated corresponding to $\phi^0 = 0$ and $\phi^0 = 1$ (identical to k_Q) for the room temperature data. Lack of data on k^* and ϕ^0 at higher temperatures prevented the calculation of the correction term and, consequently, of k_{26}. In these cases, k_Q values were used without modification to calculate $(\sigma^0)^2$ values.

1. Isotopic Hydrogen and Hydrocarbon Compounds.

(a) Results.

Quenching cross-sections were determined as outlined above for several light and deuterated alkanes, hydrogen,

deuterium, ethylene and deuterated ethylene and the results are presented in Table VI. A detailed description follows.

The decay lifetime, $1/\tau$, of delayed fluorescence was measured as a function of propane and neopentane concentrations at 29 and 75°C, and a nitrogen bath concentration of 2.12×10^{-5} moles cc^{-1} as well as the standard 1.06×10^{-5} moles cc^{-1} (Figures 8 and 9). The k_Q values were the same, within experimental error, at both temperatures and nitrogen concentrations. The data from the two nitrogen experiments were averaged before calculating $(\sigma^0)^2$ at each of the two temperatures.

Experiments with methane, ethane, cyclo-pentane, cyclo-hexane and deuterated cyclo-pentane and cyclo-hexane were done at ambient temperatures and at 75°C with the lower nitrogen concentration only. Plots of $1/\tau$ vs the quencher gas concentration are displayed in Figures 10-12.

$1/\tau$ values were measured at various concentrations of hydrogen, deuterium, propane-d_2, n-butane, iso-butane, ethylene and deuterated ethylene at room temperature (Figures 13-16), with the nitrogen bath concentration kept at 1.06×10^{-5} moles cc^{-1}.

As can be seen in Figure 10 and Table VI, k_Q for CH_4 is about doubled in going from 29 to 75°C. However, the correction term accounted for 92% of k_Q at the lower temperature.

TABLE VI

Quenching Data for $Hg(^3P_0)$ Atoms by Isotopic Hydrogen and Hydrocarbon Molecules (a).

Compound	k_Q, cc mole^{-1}sec^{-1} (b) 29°C	k_Q, cc mole^{-1}sec^{-1} (b) 75°C	$(\sigma^0)^2$, Å^2 29°C (c)	$(\sigma^0)^2$, Å^2 75°C (d)
H_2	$(4.4\pm.2)\times10^{13}$		0.92	
D_2	$(1.9\pm.1)\times10^{13}$		0.55	
CH_4	$(3.8\pm.5)\times10^{8}$	$(7.8\pm.9)\times10^{8}$	2×10^{-6}	5.8×10^{-5}
C_2H_6	$(1.3\pm.1)\times10^{10}$	$(1.4\pm.1)\times10^{10}$	0.0014	0.0014
C_3H_8	$(2.3\pm.1)\times10^{11}$	$(2.2\pm.2)\times10^{11}$	0.028	0.026
$CH_3CD_2CH_3$	$(9.1\pm.6)\times10^{10}$		0.011	
$n\text{-}C_4H_{10}$	$(7.9\pm.4)\times10^{12}$		1.1	
$i\text{-}C_4H_{10}$	$(2.6\pm.2)\times10^{13}$		3.6	
$C(CH_3)_4$	$(3.9\pm.2)\times10^{10}$	$(3.9\pm.3)\times10^{10}$	0.0053	0.0055
$c\text{-}C_5H_{10}$	$(2.5\pm.2)\times10^{12}$	$(1.8\pm.3)\times10^{12}$	0.38 -0.37	0.17
$c\text{-}C_5D_{10}$	$(5.3\pm.4)\times10^{11}$	$(5.1\pm.5)\times10^{12}$	0.084-0.077	0.074
$c\text{-}C_6H_{12}$	$(3.3\pm.4)\times10^{12}$	$(2.4\pm.3)\times10^{12}$	0.53 - 0.52	0.36
$c\text{-}C_6D_{12}$	$(3.0\pm.4)\times10^{11}$	$(4.5\pm.8)\times10^{11}$	0.051-0.045	0.071
C_2H_4	$(2.4\pm.2)\times10^{14}$		25	
C_2D_4	$(2.3\pm.1)\times10^{14}$		26	

a. Error limits are given in standard deviation.

b. k_Q = slope of $1/\tau$ vs. [Q] plots = $k_{24}k_{12}/k_{11} + k_{26}$.

c. Calculated from $k_{26} = k_Q - k^*(1-\phi^0)k_{12}/k_{11}$. Where ϕ^0 is not available, a range of $(\sigma^0)^2$ values are reported for $\phi^0=0$ and $\phi^0=1$.

d. Calculated directly from k_Q.

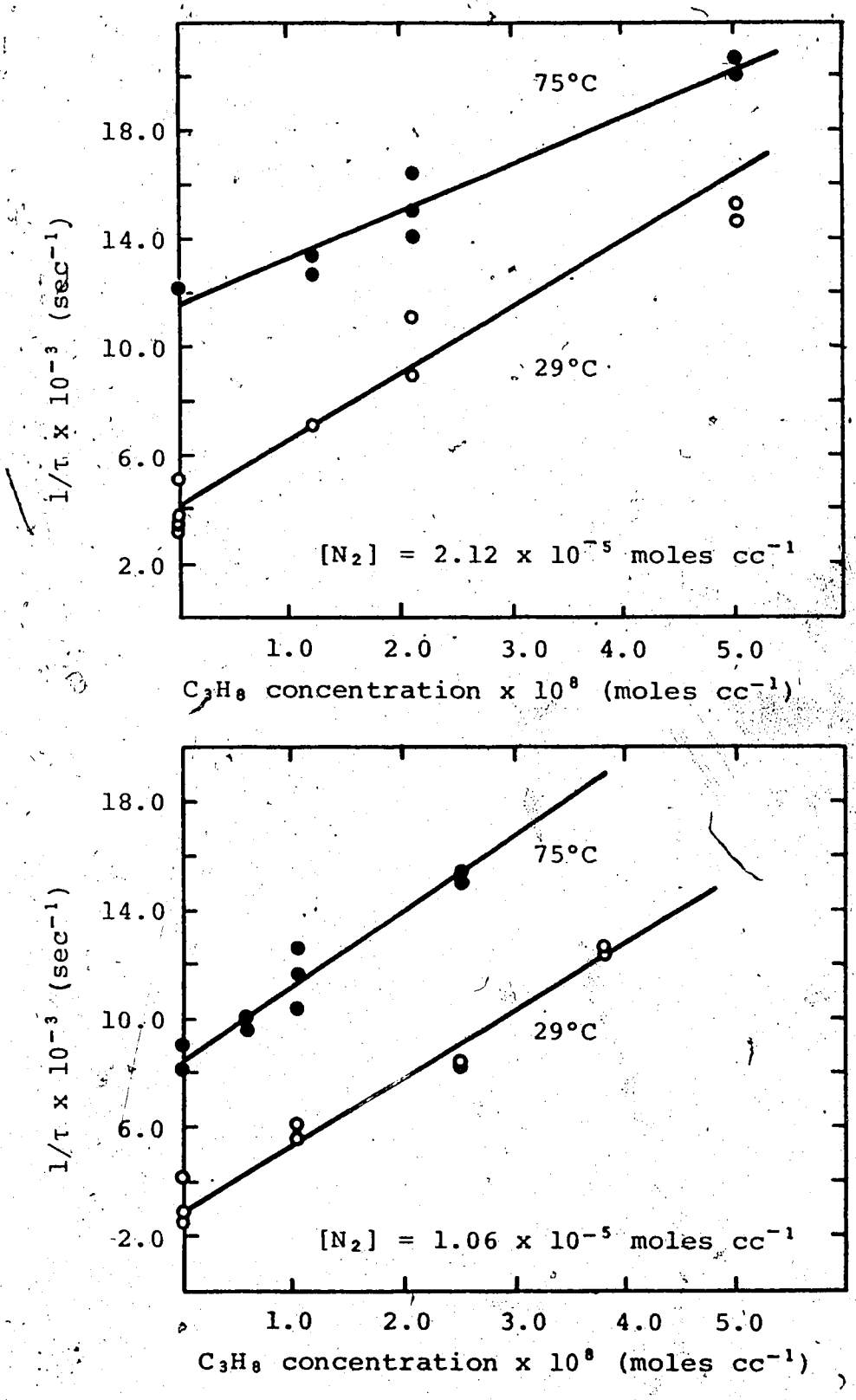

FIGURE 8: $1/\tau$ vs C_3H_8 concentration.

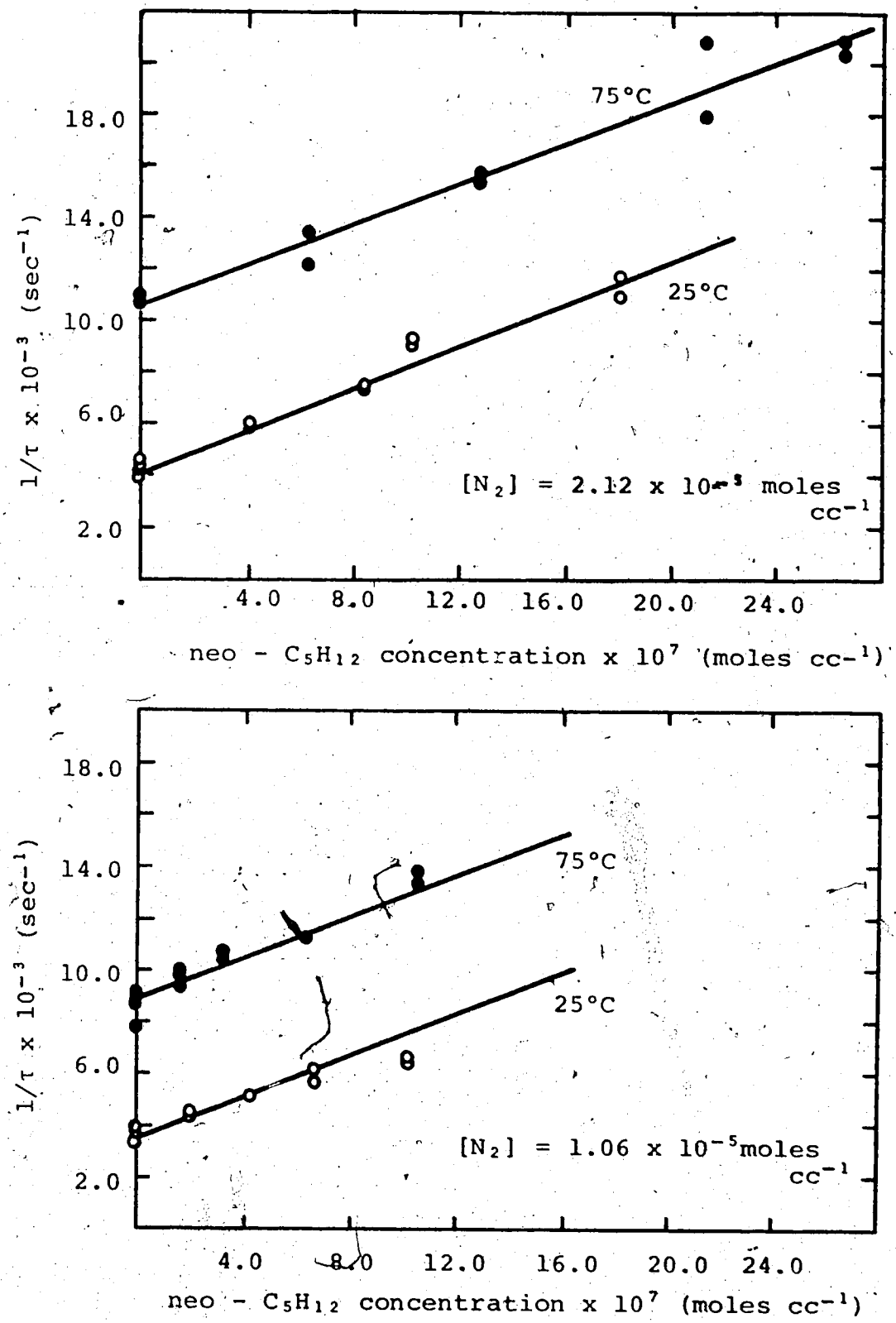

FIGURE 9: $1/\tau$ vs neo-C_5H_{12} concentration.

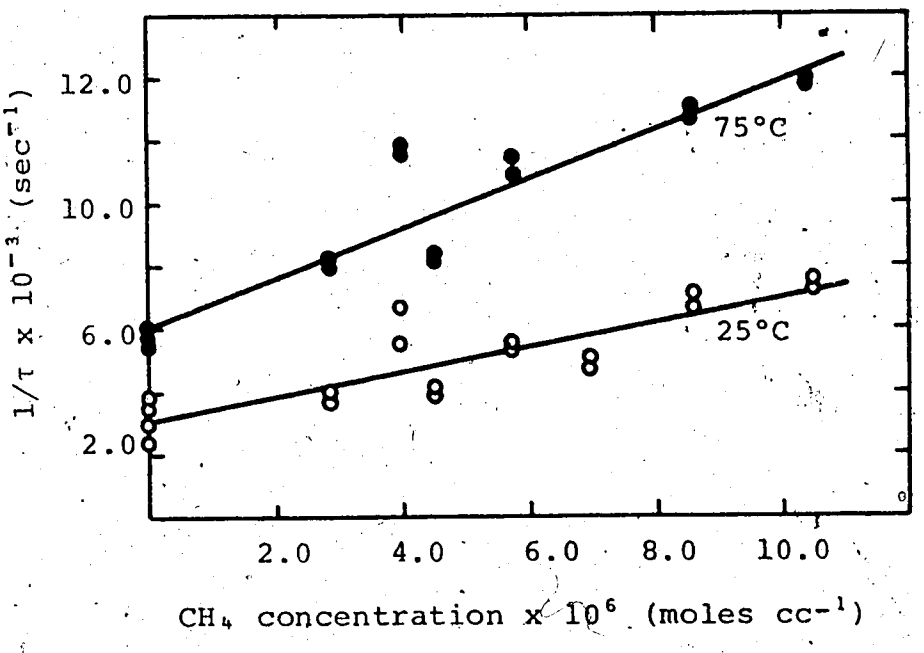

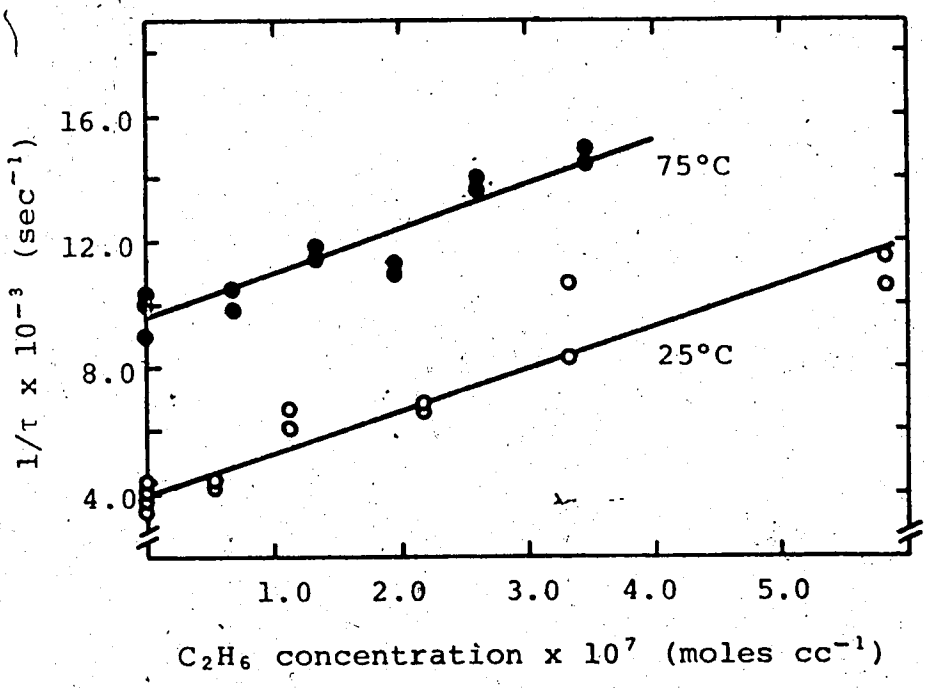

FIGURE 10: $1/\tau$ vs CH_4 and C_2H_6 concentration.

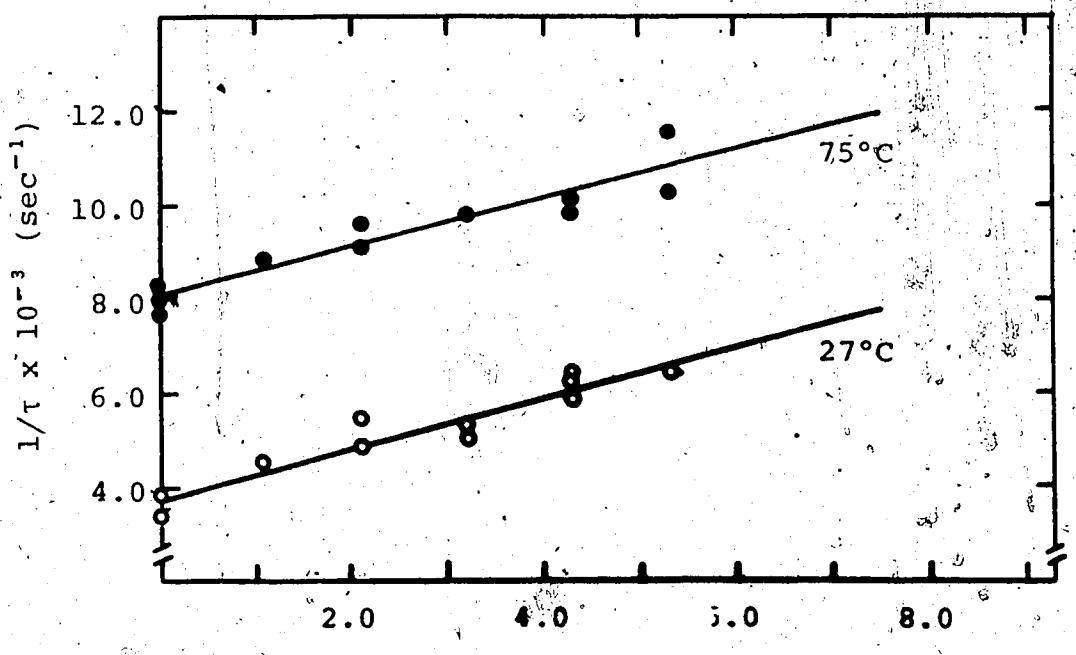

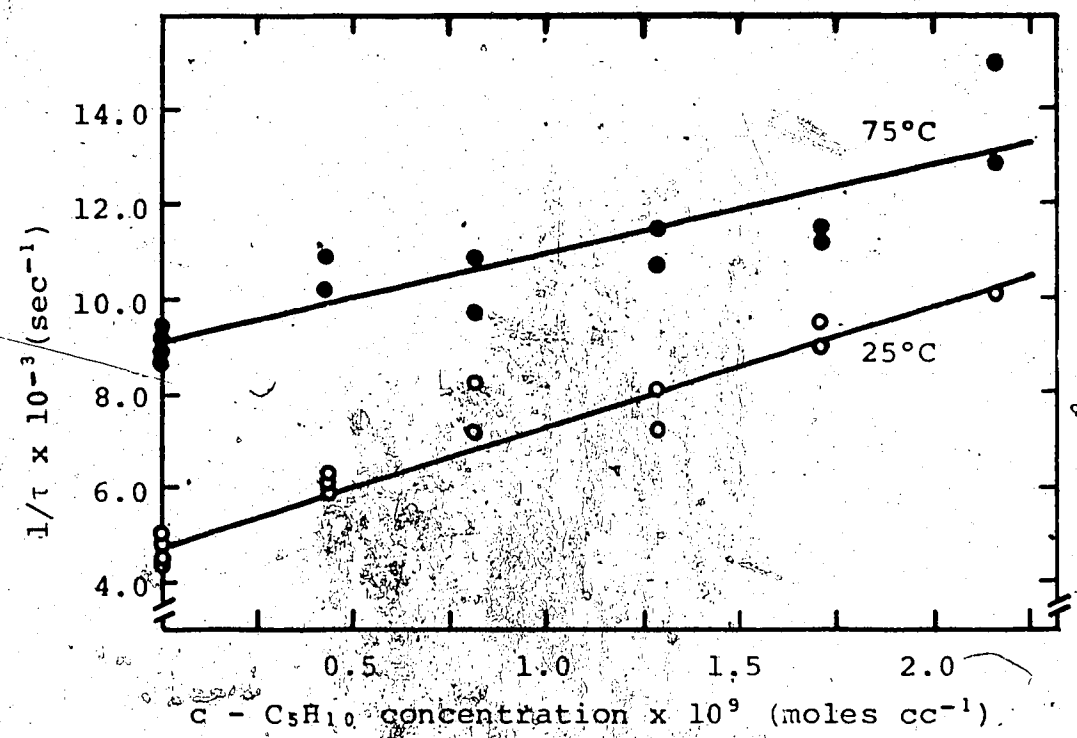

FIGURE 11: $1/\tau$ vs c-C_5D_{10} and c-C_5H_{10} concentration

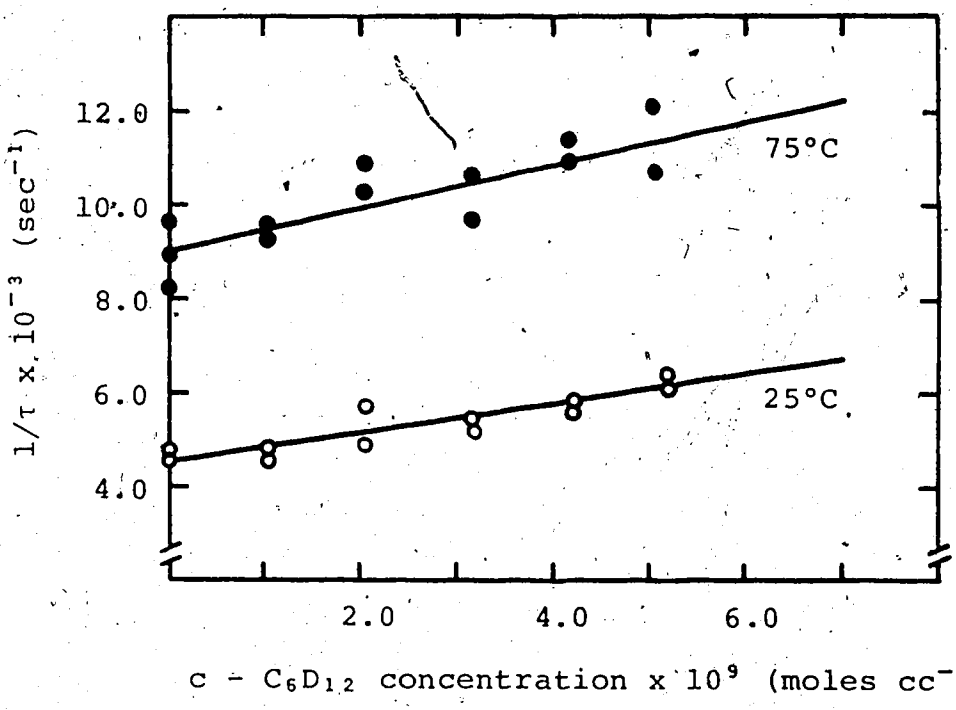

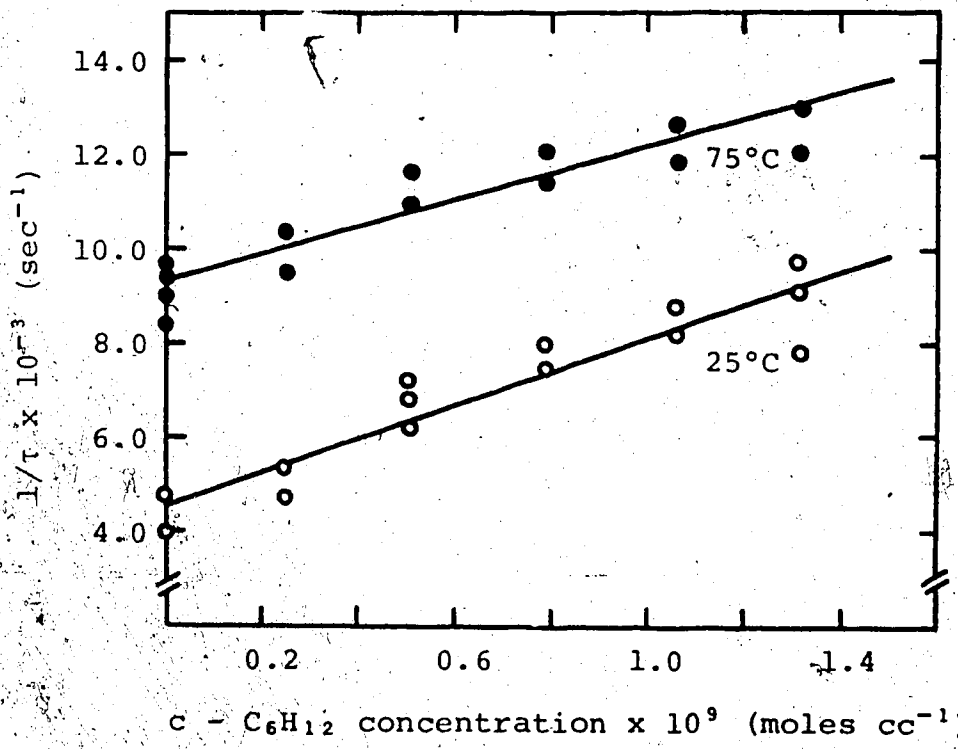

FIGURE 12: $1/\tau$ vs c - C_6D_{12} and c - C_6H_{12} concentration.

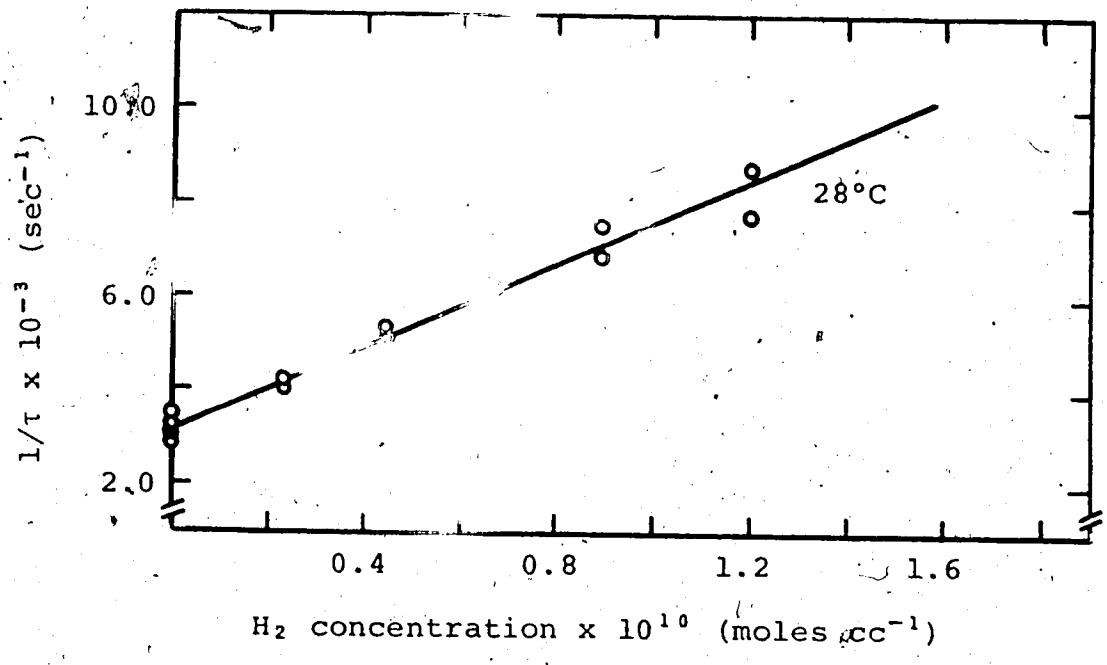

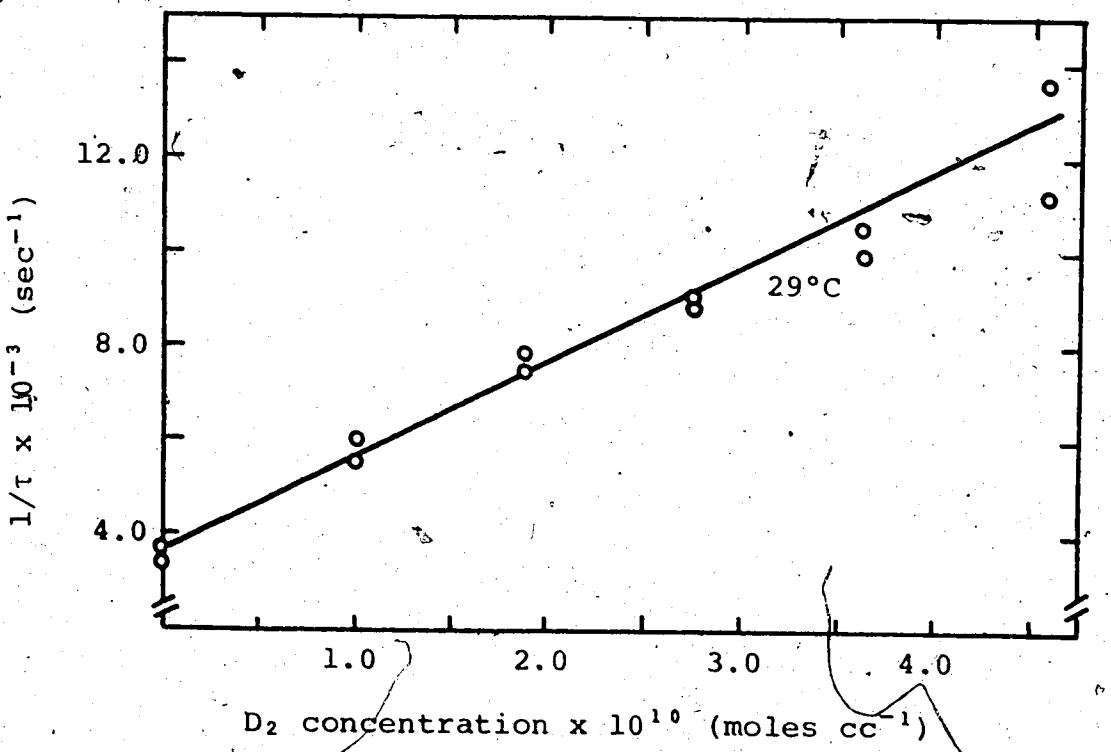

FIGURE 13: $1/\tau$ vs H_2 and D_2 concentration.

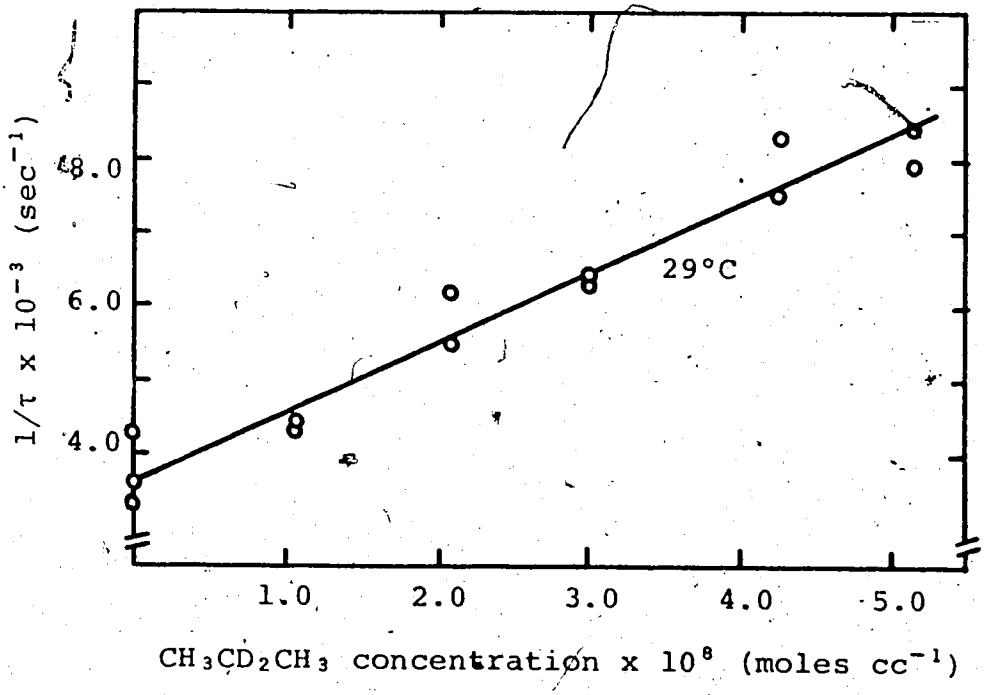

FIGURE 14: 1/τ vs $CH_3CD_2CH_3$ concentration.

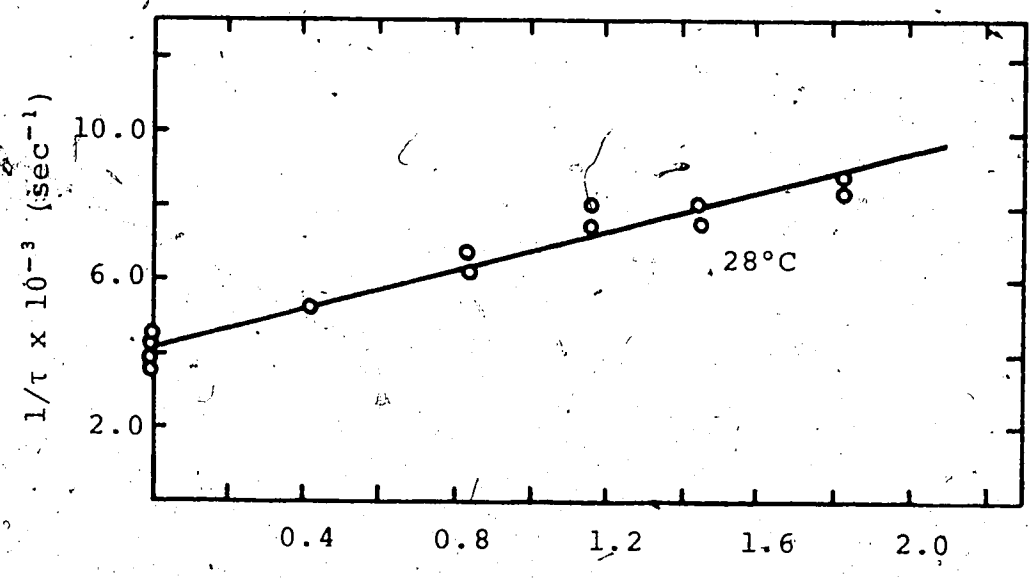

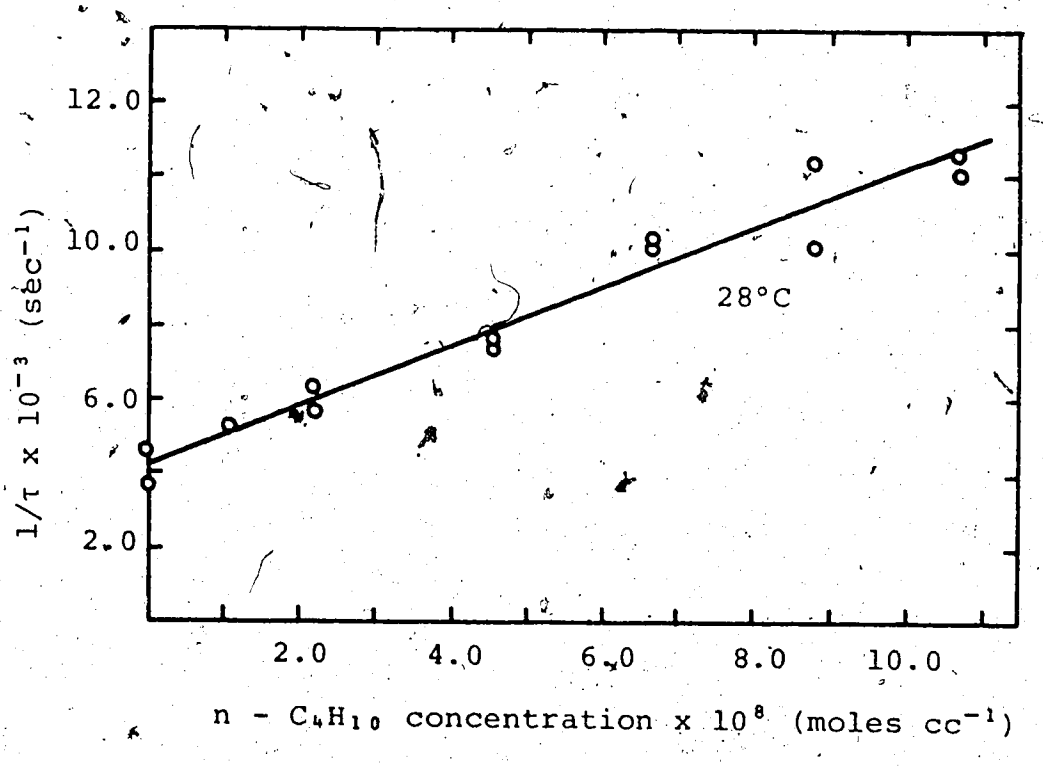

FIGURE 15: $1/\tau$ vs i - C_4H_{10} and n - C_4H_{10} concentration.

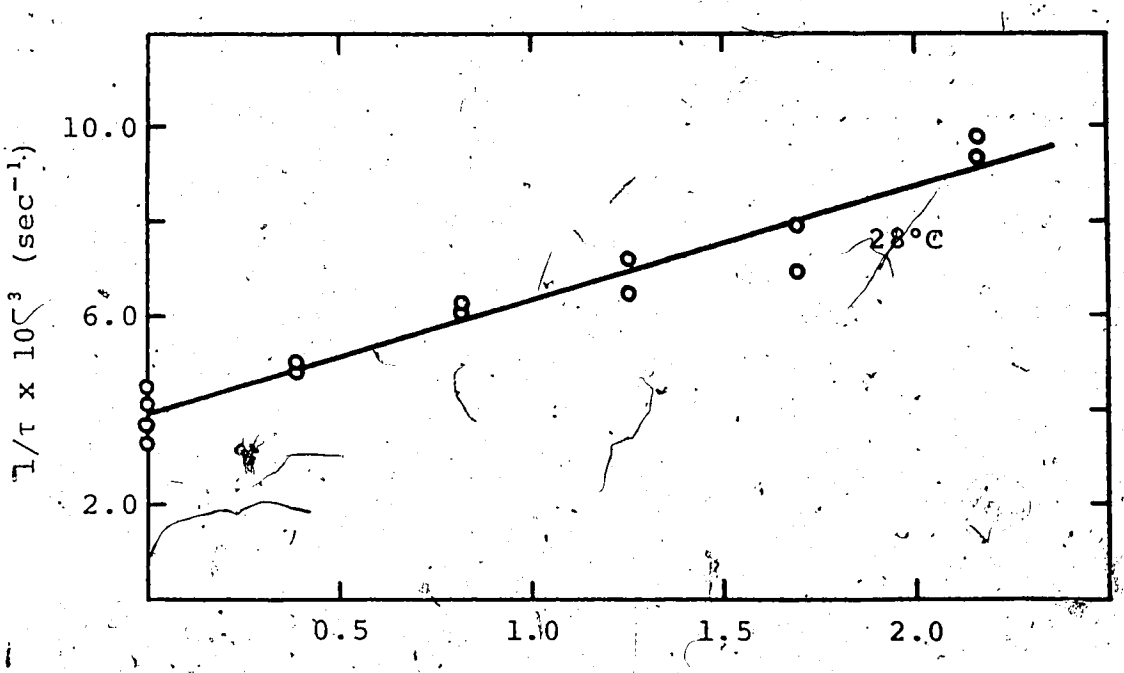

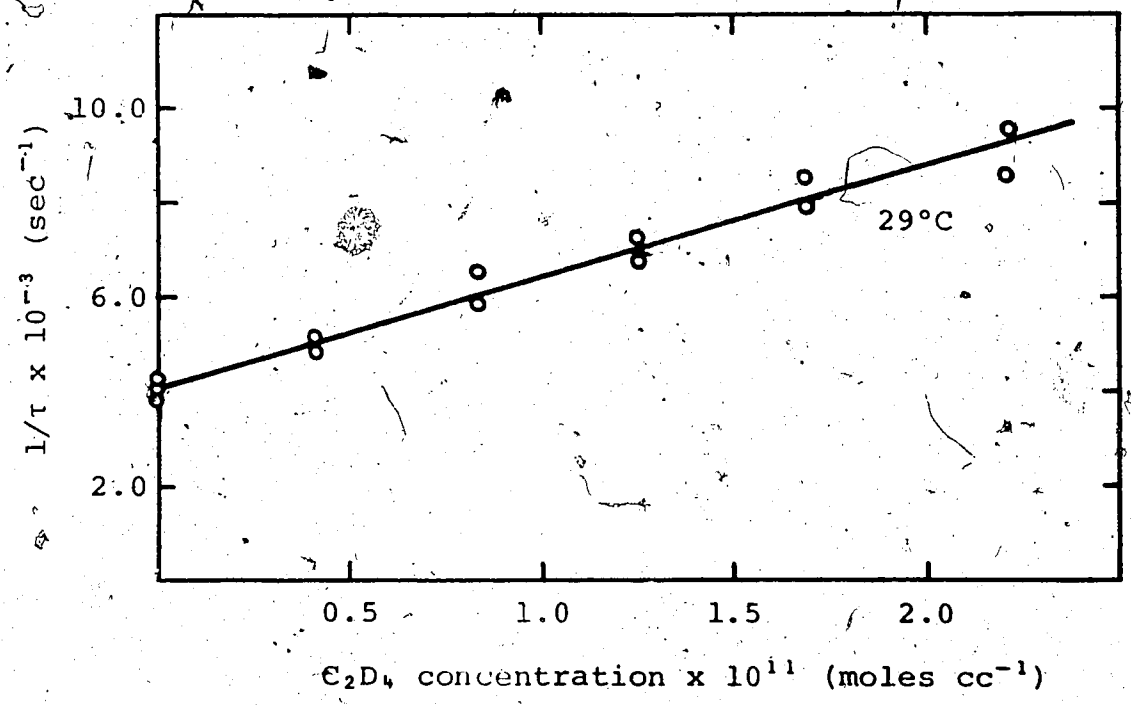

FIGURE 16: $1/\tau$ vs C_2H_4 and C_2D_4 concentration.

The value of 4.9×10^{11} cc mole^{-1}sec^{-1} for k_{24} was taken from Horiguchi and Tsuchiya (67) to determine k_{26} in this case. The correction term plays a key role in the evaluation of the experimental data at 75°C also. If k_{24} remains constant, then the exponential term in k_{12}/k_{11} would account for a three-fold increase in k_Q. The observed increase is between 1.6 and 2.6, considering the statistical error. The quenching cross-section for CH_4 at 75°C entered in Table VI was calculated from k_Q, which includes the correction term, and is, therefore, an upper limit by at least an order of magnitude.

Methane is such a poor quencher that up to 100 torr of this substrate were required in mixtures with nitrogen in order to achieve detectable quenching. This large amount of substrate could complicate the kinetics. For this reason the effect of CH_4 alone on the 2537Å fluorescence was investigated. The decay rate of the resonance line was identical with pure mercury vapour or with 200 torr of methane in the cell, and assures that the assumptions made in deriving equation [32] are still valid, even for the large percentage of methane in the mixture.

With the exception of CH_4, the correction term varied from a high of 10% for neopentane and c-C_5D_{10} to less than 1% for H_2, D_2, n-C_4H_{10}, i-C_4H_{10}, C_2H_4 and C_2D_4. The correction term for the other alkanes was between one and 5%

which is within the standard deviation of the slope. A ratio of about 10^2 to 10^3 for $(\sigma^*)^2/(\sigma^0)^2$ and a low quantum yield of Hg^0 formation is necessary in order to produce a discernable difference between k_Q and k_{26}. For this reason, the data of only those substrates which are very weak quenchers of Hg^0 atoms required adjustment to account for the quenching of Hg* atoms. At 75°C, where k_{12}/k_{11} is a factor of three larger than at room temperature, the reported $(\sigma^0)^2$ values for the weak quenchers are overestimated by as much as 15% if k_{24} remains constant. For neopentane and c-C_5D_{10} the higher temperature value may be 45 and 30% too high, respectively, and the actual quenching cross-section for these two substrates could be smaller than at room temperature. For most of the alkanes studied, quenching of Hg^0 atoms appears to be temperature independent or possibly decreases slightly with an increase in temperature, although the scatter in the data would mask an activation energy of about ±1.5 kcal $mole^{-1}$. Duplicate runs with c-C_6H_{12} and a single run with c-C_5H_{10} clearly showed a decrease in k_Q as the temperature was increased.

(b) Discussion.

All of the gases studied exhibit lower quenching cross-sections for Hg^0 atoms than for Hg* atoms. The discrepancy between the two values increases as the ability to quench Hg* atoms decreases. For instance, the $(\sigma^*)^2/(\sigma^0)^2$ ratio for

$i\text{-}C_4H_{10}$, a strong Hg* quencher, is approximately two whereas it is 350 for neopentane, a weak quencher of Hg* atoms. In general, alkanes quench Hg^0 atoms 100 times more slowly than Hg* atoms, in good agreement with the results reported by Callear and McGurk (62) using the same technique as the present study. The $(\sigma^0)^2$ values reported by Vikis and Moser (73) indicate a factor of 500 difference between Hg^0 and Hg* quenching. Their values were relative to that of ethylene which determined to be 2.5Å². The present work reports a value of 25Å² for ethylene quenching of Hg^0 atoms so that reasonable agreement would be attained if their values were scaled accordingly.

Apart from the different magnitudes of Hg^0 and Hg* quenching by the foreign gases the trends in the $(\sigma^0)^2$ values with respect to the nature of the quencher are very similar to those found for Hg* quenching. The quenching cross-sections vary as C_2H_4 > $i\text{-}C_4H_{10}$ > $n\text{-}C_4H_{10}$ > C_3H_8 > $C(CH_3)_4$ > C_2H_6 > CH_4 in both cases which is clear evidence that Hg^0 and Hg* atoms are quenched by the same mechanism. This is further supported by the similar effect of deuterium substitution. Ethylene and deuterated ethylene quench Hg* atoms by interaction with the π bond and do not show an isotope effect. Paraffins quench Hg* atoms via C-H bond rupture and these gases exhibit a pronounced deuterium isotope effect, particularly if substituted at the weakest bond (82,92-94). Deuterium substitution has a similar effect

on Hg^0 atom quenching by propane and the cyclo-alkanes in the present s[illegible]. Hydrogen and deuterium do not follow this pattern in [illegible]nching of Hg* and Hg^0 atoms.

The present study, like most previous studies of Hg^0 reactions, employed nitrogen to populate the $^3P_0$ level. A small population of Hg* atoms has been shown to exist in this system (see Chapter III). These atoms may have a crucial bearing on the interpretation of studies of Hg^0 reactions made using an Hg^*-N_2 system. This is illustrated by the quenching data obtained with methane.

The correction term which was applied to the apparent rate of relaxation of Hg^0 atoms was almost sufficient to account for all of the measured quenching by CH_4 at room temperature and probably at 75°C. This implies that Hg^0 atoms were promoted to the $^3P_1$ level by collisions with nitrogen and the Hg* atoms were subsequently quenched by the methane. Very little direct quenching of metastable atoms occurred at either temperature.

The role of Hg* atoms becomes relatively more important at 75°C than at 25°C. Lack of kinetic data under such conditions precludes a definite assessment of the extent of this complication. In most cases it is not expected to be too significant unless a radical change in the relative quenching of Hg* atoms to the ground state or to the $^3P_0$ level takes place.

Callear and McGurk (62) have determined quenching cross-sections for Hg^0 atoms using the same technique as in the present study. Since these workers did not consider the role of Hg* atoms, their $(\sigma^0)^2$ values should be regarded as upper limits. Fortunately, the correction for Hg* quenching is small in most cases.

The quenching rate constant of Hg^0 by Xe, in the presence of N_2, has been measured by Phillips and co-workers (25). The reported value was very small and it is likely that the quenching was due to Hg* atoms in the system, as is the case for methane in the present study.

The salient features of Hg^0 quenching with regard to trends in reactivity, deuterium isotope effect and the temperature dependence of $(\sigma^0)^2$ exhibited by the various alkanes may be explained in terms of a hydrogen abstraction mechanism (108), as illustrated by the schematic potential energy curves displayed in Figure 17.

The alkane and a Hg* or Hg^0 atom combine along an attractive potential surface with a shallow well of depth ϵ^* and ϵ^0, respectively, proportional to the polarizabilities of the two reactants. The complex is trapped in the potential well as a result of the redistribution of the collision energy amongst the various degrees of freedom in the substrate molecule. Since the excited mercury atom interacts

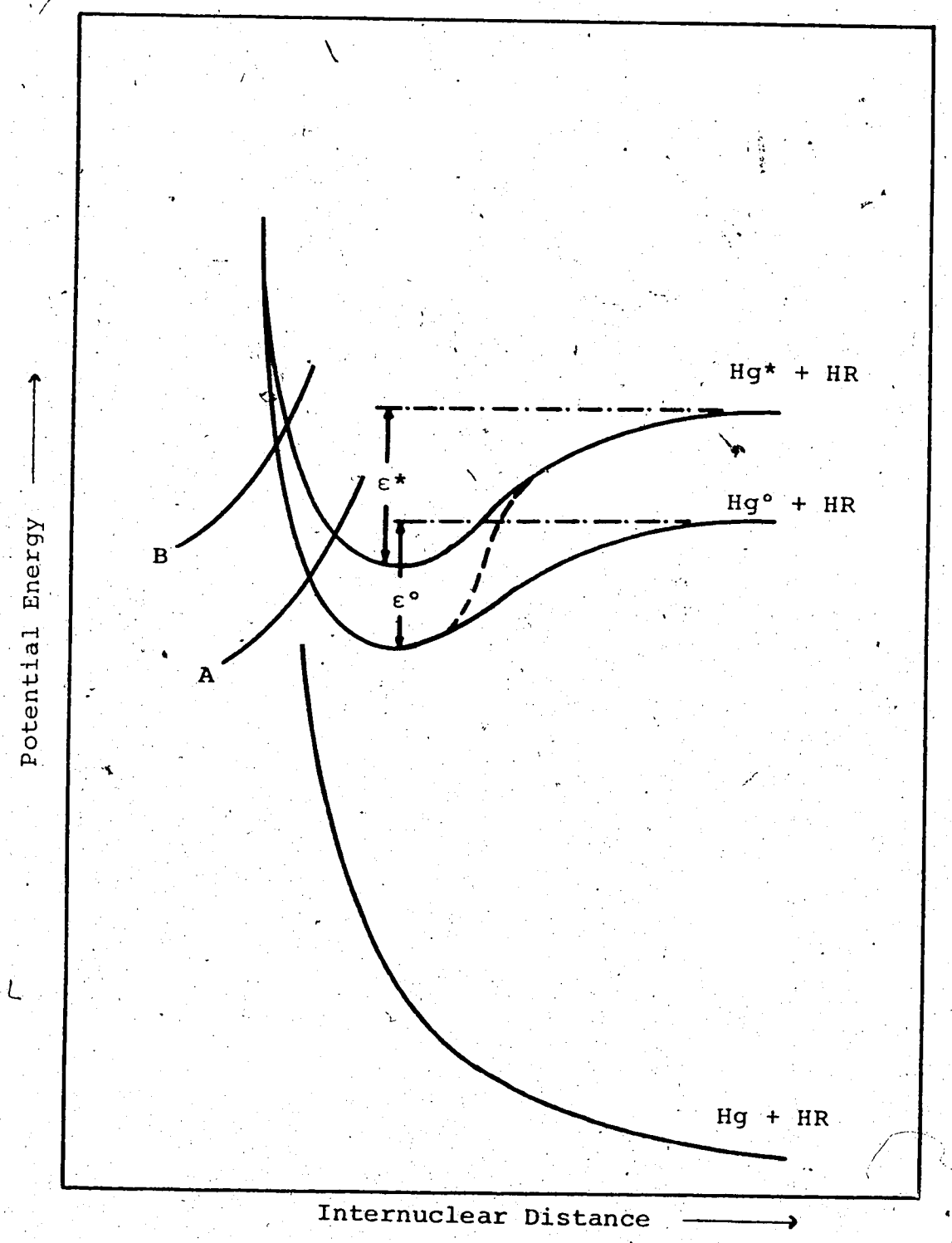

FIGURE 17: Schematic potential energy diagram for the interaction of Hg ($^3P_0$) and Hg ($^3P_1$) atoms with alkanes.

with a specific hydrogen atom in the paraffin (82), a separate potential surface exists for each different C-H bond (1^o, 2^o or 3^o) in both Hg* and Hg^o sensitization. The splitting of the (HgHR)* complex into the $\Omega = \pm 1$ and $\Omega = 0$ states, arising from the perturbation on the J vector of the Hg* atom by the alkane (136), is not a crucial point and has been omitted in the figure to maintain clarity.

The existence of (HgHR)* and $(HgHR)^o$ complexes having finite lifetime allows for radiative transitions to the ground state. Band emission in the mercury photosensitization of alkanes has been attributed to the (HgHR)* complex (23). Emission from the $(HgHR)^o$ complex is apparently an inefficient process compared to other relaxation modes.

At high molecular compression, the (HgHR, $\Omega = \pm 1$)* surface intersects the $(HgHR)^o$ potential energy curve. This provides a reaction channel for spin-orbit relaxation of Hg* atoms and the reverse process, vis., promotion of a Hg^o atom to the $^3P_1$ level. An additional low energy route available to deuterated alkanes for Hg^o production has been suggested (108) and is indicated by the dashed line in Figure 17.

The rupture of a C-H bond proceeds via predissociation to a repulsive surface which correlates with an HgH molecule (104) and the respective alkyl radical. The energy level of the crossover point depends on the depth of the potential well and the strength of the C-H bond being broken, with the

weakest bond having the lowest crossover point. Thus, i-C_4H_{10}, which possesses a 3° bond, has a larger $(\sigma^0)^2$ value than n-C_4H_{10} which has only 1° and 2° bonds. The decrease in the $(\sigma^0)^2$ values as the bond strength increases from i-C_4H_{10} to CH_4 may also be explained by this rationale.

Alkanes display $(\sigma^*)^2$ values (Table I) which are lower than the gas kinetic collision frequency, the discrepancy being largest for the first few members of the series. This is even more evident for Hg^0 quenching (Table VI). Since the level at which crossover to products takes place may lie at a higher or lower energy than the level of the separated reactants, indicated by curves A and B in Figure 17, respectively, the lower than unit quenching efficiency and the temperature dependence of the $(\sigma^0)^2$ values may be explained in two ways: (i) if predissociation occurs within the potential well, the crossover must have a lower probability of occurring than the breakup of the complex back to the reactants. The relative rates of these two processes depend on the efficiency with which the collision energy is redistributed in the alkane molecule. This explanation would be consistent with a decrease in $(\sigma^0)^2$ values as the temperature is increased if the probability of crossover is independent of temperature, since the redissociation rate increases because of its activation energy. This proposal appears to be applicable in the case of the protiated cyclo-alkanes because of the comparatively lower C-H bond strength and

higher $(\sigma^0)^2$ values than those of CH_4, C_2H_6, C_3H_8 and neo-C_5H_{12}; or (ii) in the case where predissociation takes place at a higher energy than the dissociation energy of the complex, the existence of the energy barrier involved in the relaxation of Hg^0 atoms provides a reason for low quenching efficiency. Methane, ethane, neopentane and propane are likely to belong in this category since they all have comparatively high C-H bond energies. This model predicts an increase in the quenching rate with increasing temperature which is not substantiated by the present data. However, this apparent contradiction may be resolved by inspection of the Hg* and Hg^0 sensitized reactions of these gases. A comparison of the features exhibited in Hg* sensitization shows a distinct similarity between them which implies that these alkanes may be considered collectively as a group. Compared with the rest of the alkanes, these show the largest difference between the quenching rate and the collision frequency, a direct result of their high bond strength. A second feature is that the Hg* sensitized quantum yields, Φ^*_d, are less than unity at room temperature so that spin-orbit relaxation (Table II) and band emission (23) are significant relaxation processes. Based on the parallel trends in the $(\sigma^*)^2$ and $(\sigma^0)^2$ values, it may be assumed that the Hg^0 sensitization of these gases follows a reaction mechanism applicable to all members of the group, to a greater or lesser degree. The temperature independence of the $(\sigma^0)^2$

values has an explanation based on the observation that the propane Hg^0 sensitized quantum yield, ϕ^0_d, increases from 0.59 at 63°C to 0.94 at 200°C (103). In order to account for the low ϕ^0_d at the lower temperature, an intersystem crossing to the ground state potential energy surface has been suggested (108). It would seem that the rate of intersystem crossing decreases with an increase in temperature which, to a large extent, cancels the increase in the rate of decomposition since the $(\sigma^0)^2$ value does not change appreciably over the temperature range of the present study. It is to be expected that the rate at which $(HgHR)^0$ are promoted to $(HgHR)^*$ complexes also increases as the temperature is raised but the products of this reaction, a Hg^* atom and the alkane, would recreate a Hg^0 atom in a subsequent collision via crossover at the high energy intersection of the $(HgHR)^*$ and $(HgHR)^0$ surfaces. The overall effect would appear as only a minor increase in the rate of relaxation of Hg^0 atoms via Hg^* sensitized decomposition. Similar arguments would apply to explain the negligible temperature effect on Hg^0 quenching by the other members of this group.

In cases (i) and (ii) above, the lower $(\sigma^0)^2$ values compared to $(\sigma^*)^2$ values are probably due to the smaller polarizability of the Hg^0 atom and thus a shallower potential well. Redissociation of the complex to reactants would be more important in this case and the quenching cross-sections would reflect the decreased probability of the

decomposition reaction.

The H/D kinetic isotope effect may be interpreted on the basis of the energetics of the hydrogen abstraction mechanism. The activation energy for abstraction of a deuterium atom is greater than for the abstraction of a hydrogen atom by virtue of its lower zero point energy (109) and thus more energy is required to rupture a C-D bond. This would have the effect of reducing the $(\sigma^0)^2$ value of a deuterated alkane with respect to its protiated analogue, in agreement with experiment.

The results of the study of the effect of nitrogen pressure on the quenching of Hg^0 atoms by propane and neopentane indicate that quenching of the $(HgHR)^0$ complex by N_2 is very inefficient, and omission of this process from the reaction mechanism is experimentally justifiable. It appears that $(HgQ)^0$ complexes are very stable with respect to collisional relaxation in the cases where Q is a mercury atom, as shown in Chapter III, or an alkane molecule which is apparent from this and other studies (130).

Callear and McGurk (113) have proposed a mechanism for the quenching of Hg^* and Hg^0 atoms by hydrogen and deuterium which involves an intersystem crossing between a triplet upper complex and a singlet ground state complex,

$$Hg(^3P) + H_2\,^1\Sigma^+ \rightarrow HHgH\ ^3B_2 \rightarrow HHgH\ ^1A' \rightarrow HgH\ ^2\Sigma^+ + H.$$

The $^3B_2$ state splits into an A_2, A_1, and B_1 state, the first of which correlates with a Hg^0 atom and the other two with a Hg* atom. The intersystem crossing step is completely allowed for quenching of Hg* atoms but is allowed only through rotation-electronic coupling for Hg^0 quenching. This explains the nine-fold lower $(\sigma^0)^2$ values and provides a basis for the factor of two difference between the H_2 and D_2 quenching cross-sections. As an alternative explanation, they suggested that the intersystem crossing step might be sensitive to deuterium substitution in the sense that tunnelling at configurations close to the turning point would be lower for D_2. The results of the present investigation provide experimental evidence for an isotope effect in hydrogen quenching of Hg^0 atoms.

2. Organic Oxygen- and Sulfur-Containing Compounds.

(a) Results.

Decay rates of 2537Å delayed fluorescence were measured as a function of ethancl concentration with 200, 300, 400 and 500 torr nitrogen pressure at 28°C (Figure 18). No evidence that the nitrogen pressure affected the quenching rate was detected. A similar study with ethylmercaptan also showed no variation in the quenching rate when the nitrogen pressure was varied from 200 to 400 torr. These observations

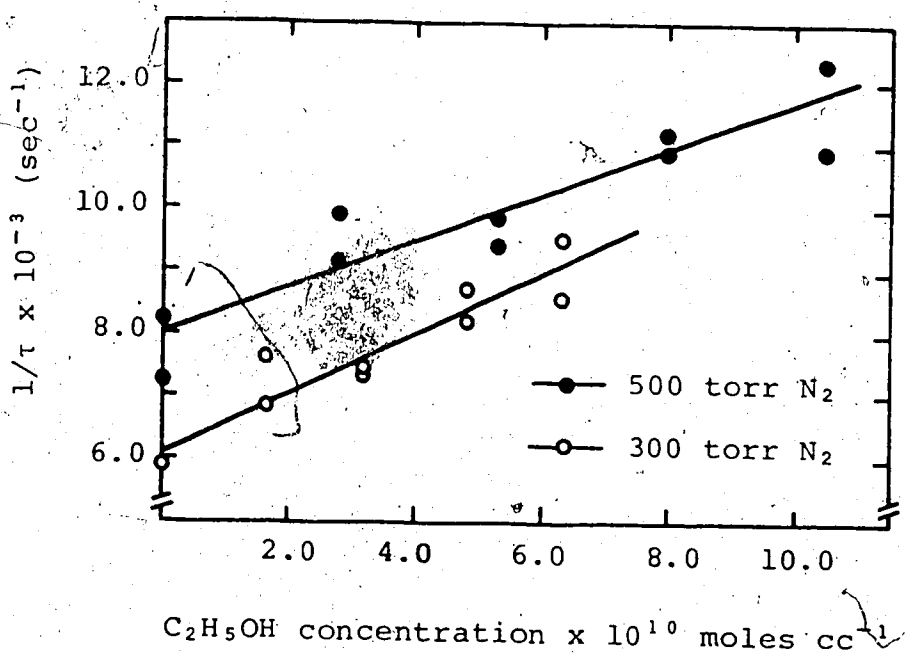

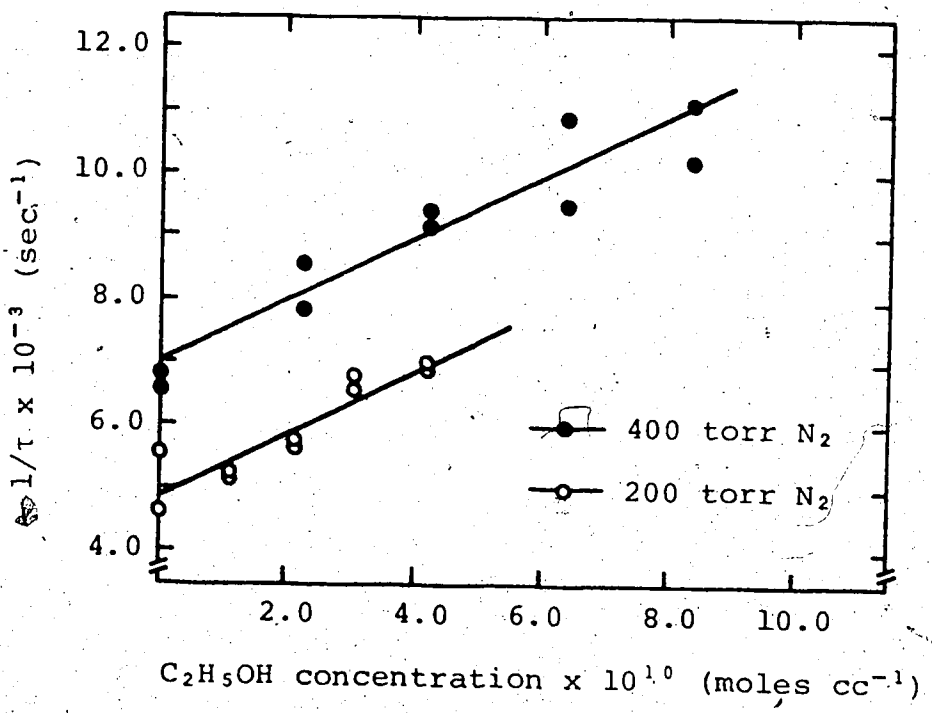

FIGURE 18: $1/\tau$ vs C_2H_5OH concentrations in different nitrogen bath pressures.

indicate that a termolecular deactivation process

$$Hg^0 + Q + N_2 \rightarrow \text{products}$$

is too slow to be detected in the present experiments. Phillips and co-workers (33) were able to measure small rate constants for the above process where Q = methanol and ethanol, and also for the reaction

$$Hg^0 + 2A \rightarrow \text{products}$$

for a variety of alcohols, A, in the range 10^{18} to 10^{19} $cc^2 mole^{-2} sec^{-1}$. This process is negligible in the present work due to the low alcohol concentrations used.

The temperature dependence of Hg^0 quenching by C_2H_5OH, CH_3CD_2OH, $(CH_3)_2O$, $(C_2H_5)_2O$, $(CH_3CD_2)_2O$, $(C_2D_5)_2O$, CH_3SH, C_2H_5SH, and $(CH_3)_2S$ was determined, from measurements of $1/\tau$ at various substrate concentrations (Figures 19-26), and the results are presented in Table VII. The maximum value of the correction term at room temperature was less than 2% of k_Q so that the k_Q values can be taken to be k_{26} values. In the case of CH_3CD_2OH, however, the correction term could amount to 15% of k_Q if $\phi^0 = 0$. Since this extreme is unlikely (32), it is assumed that the correction is within the experimental error in k_Q.

The quenching of Hg^0 atoms by ethanol and diethylether show a marked deuterium isotope effect, particularly at the

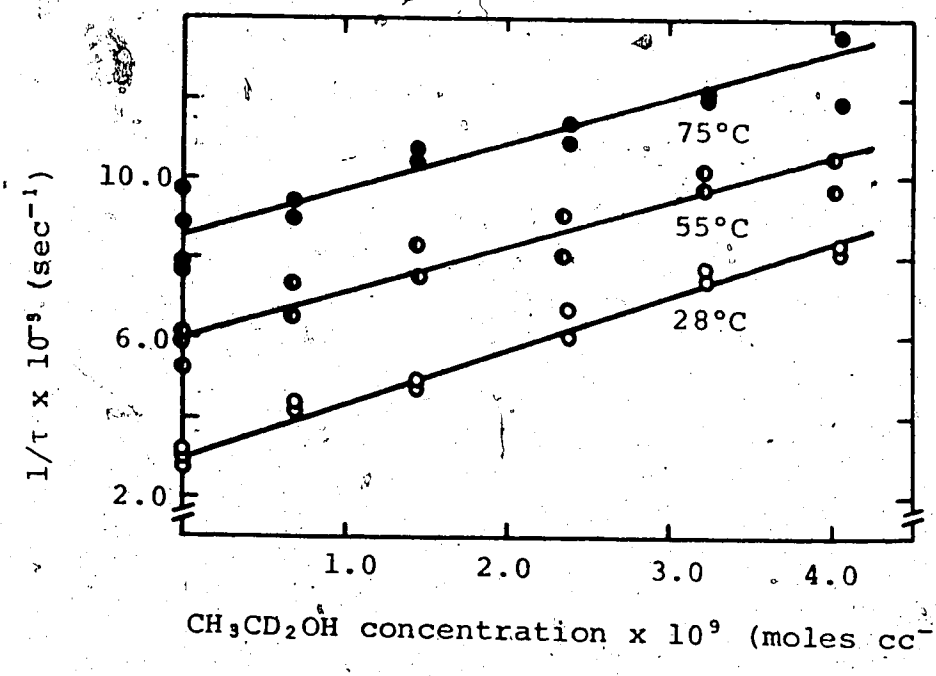

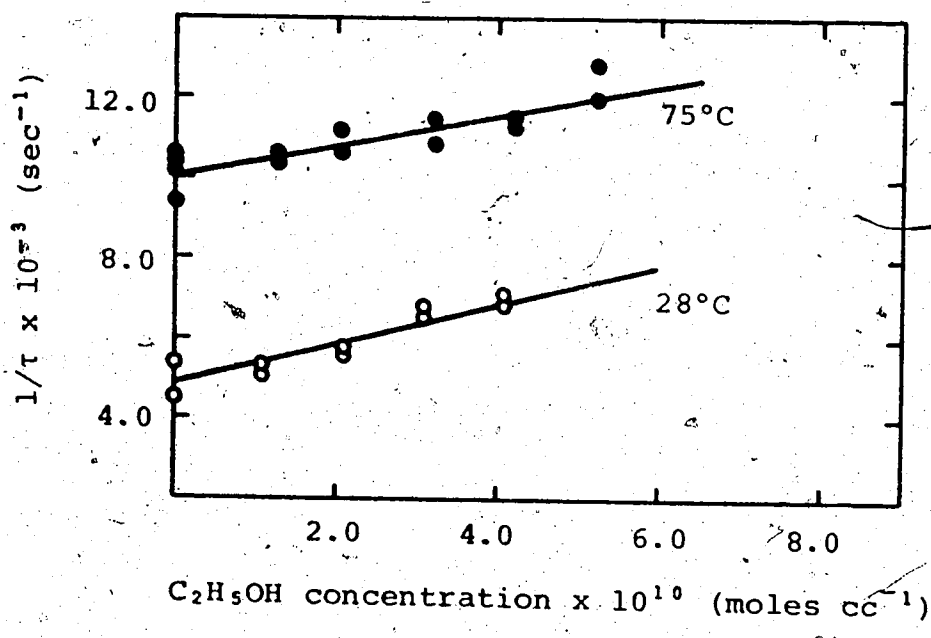

FIGURE 19: $1/\tau$ vs CH_3CD_2OH and CH_3CH_2OH concentration.

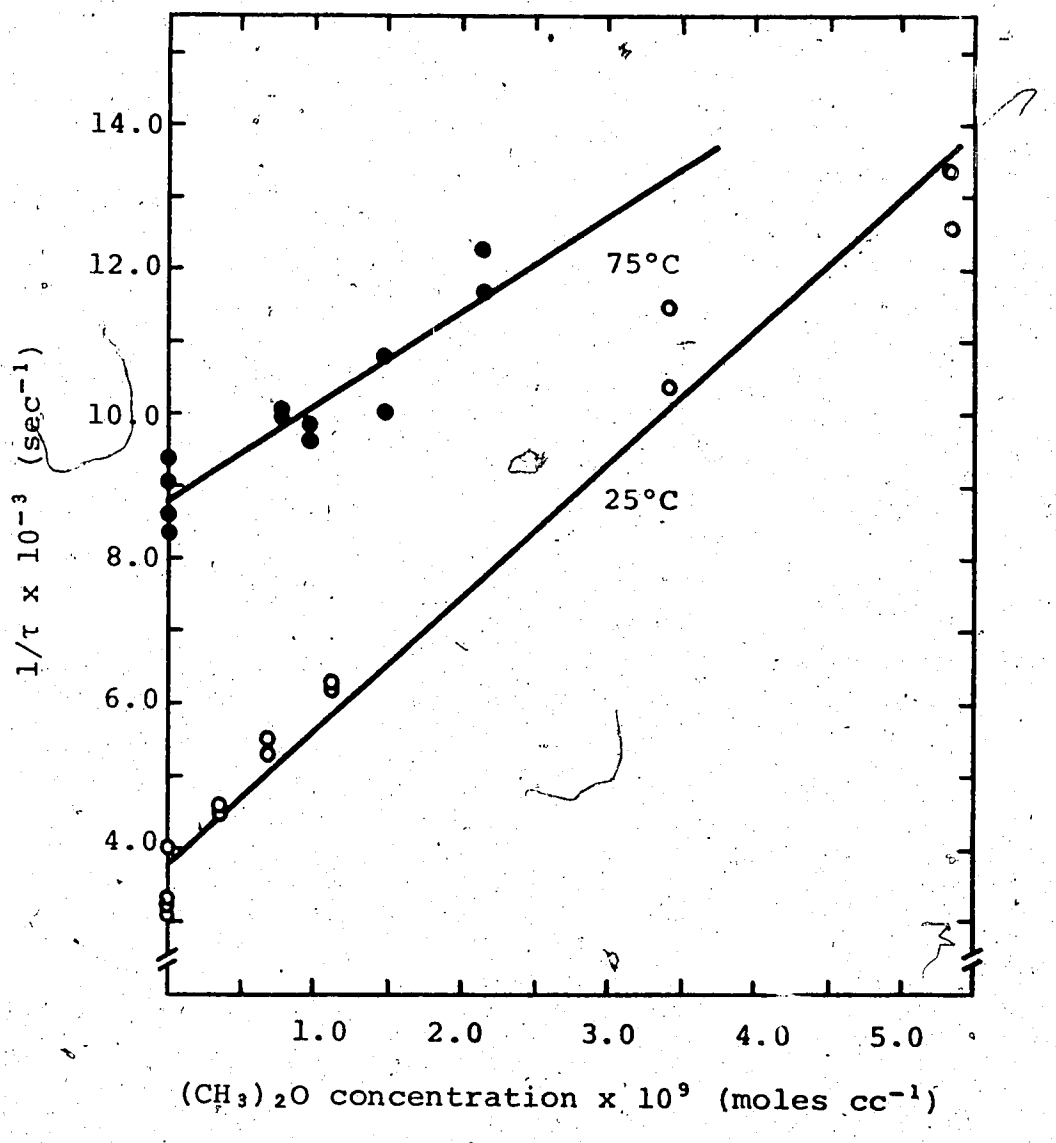

FIGURE 20: $1/\tau$ vs $(CH_3)_2O$ concentration.

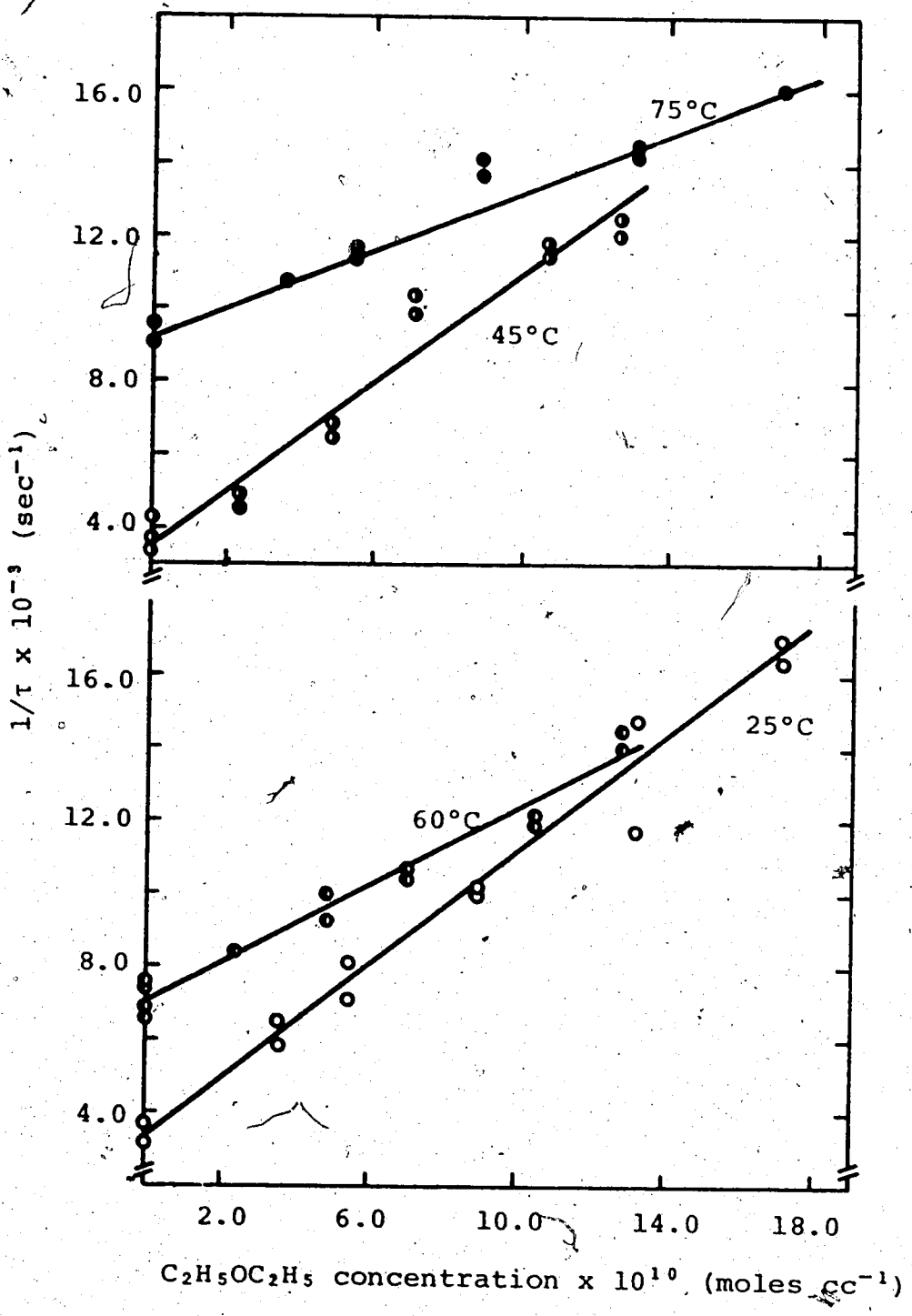

Figure 21: $1/\tau$ vs $(C_2H_5)_2O$ concentration.

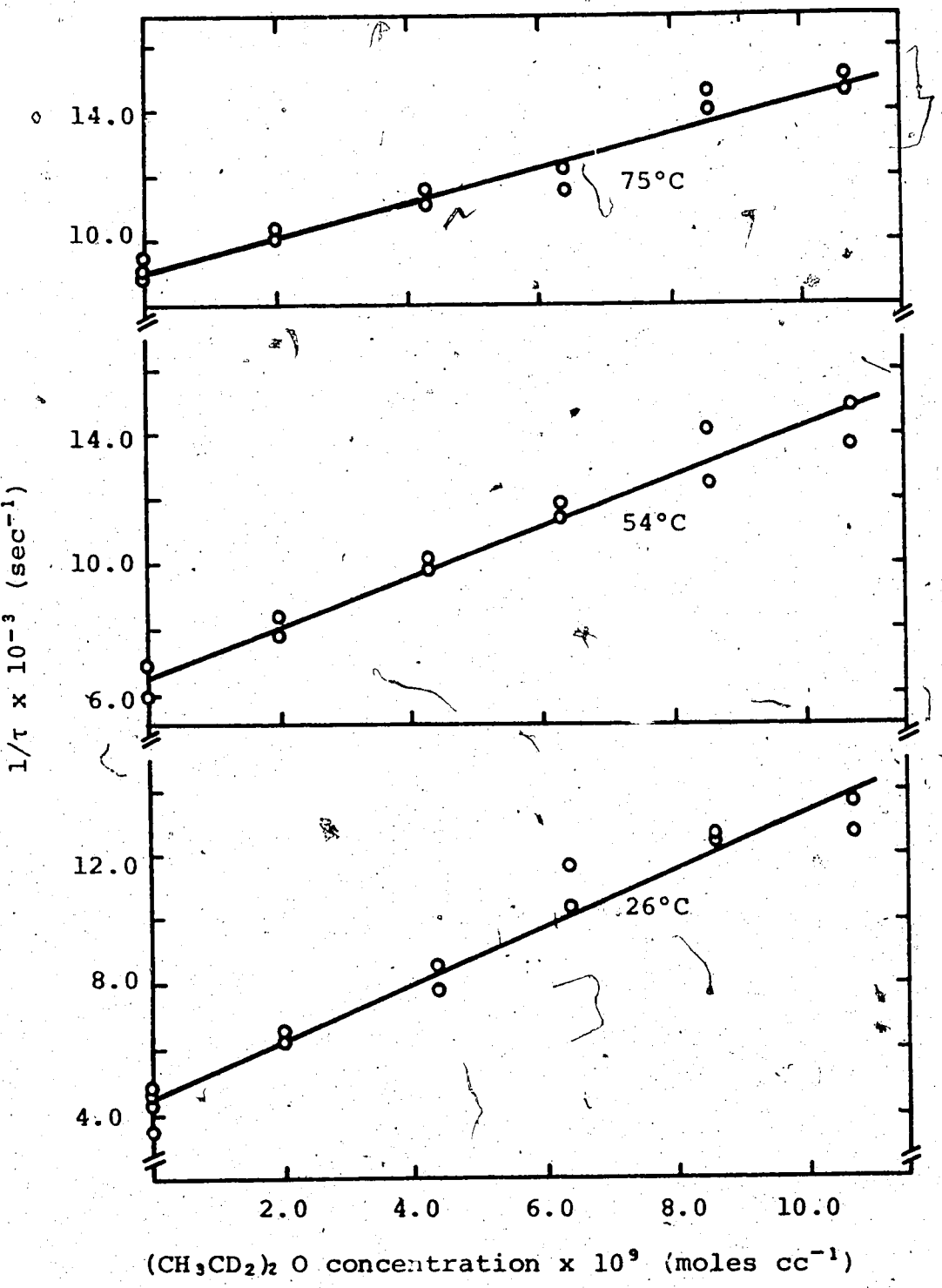

FIGURE 22: $1/\tau$ vs $(CH_3CD_2)_2$ O concentration.

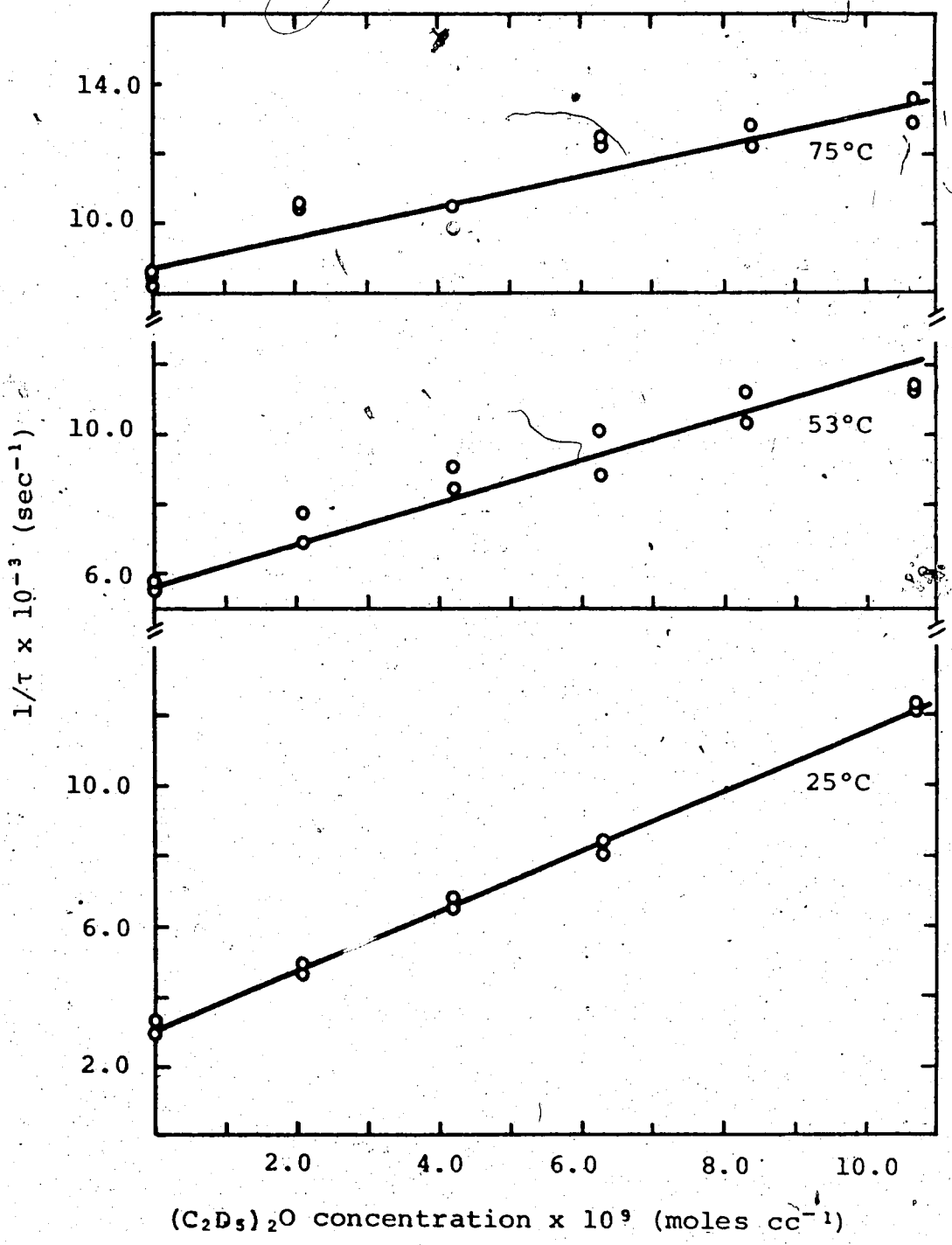

FIGURE 23: $1/\tau$ vs $(CD_3CD_2)_2O$ concentration.

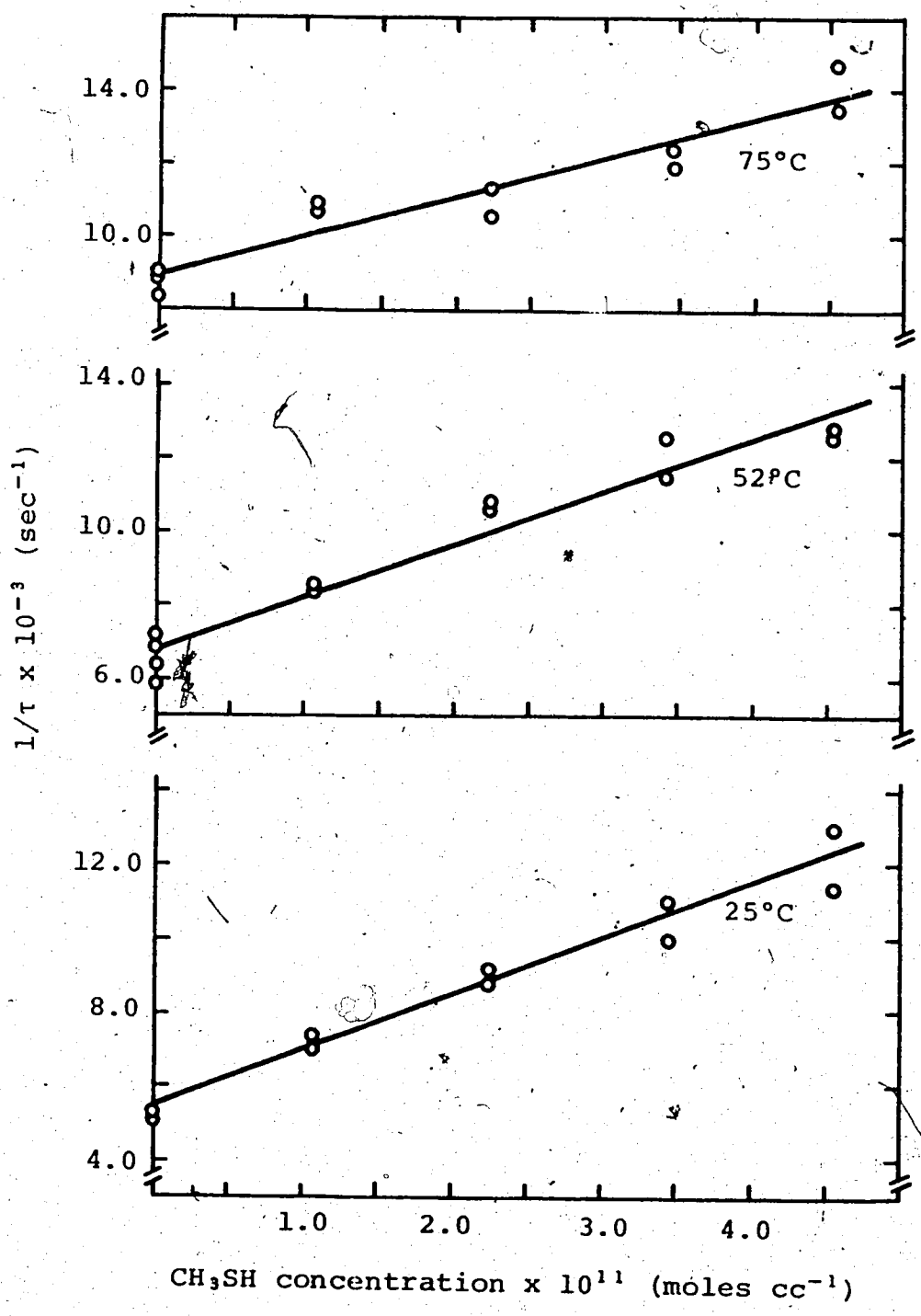

FIGURE 24: $1/\tau$ vs CH_3SH concentration.

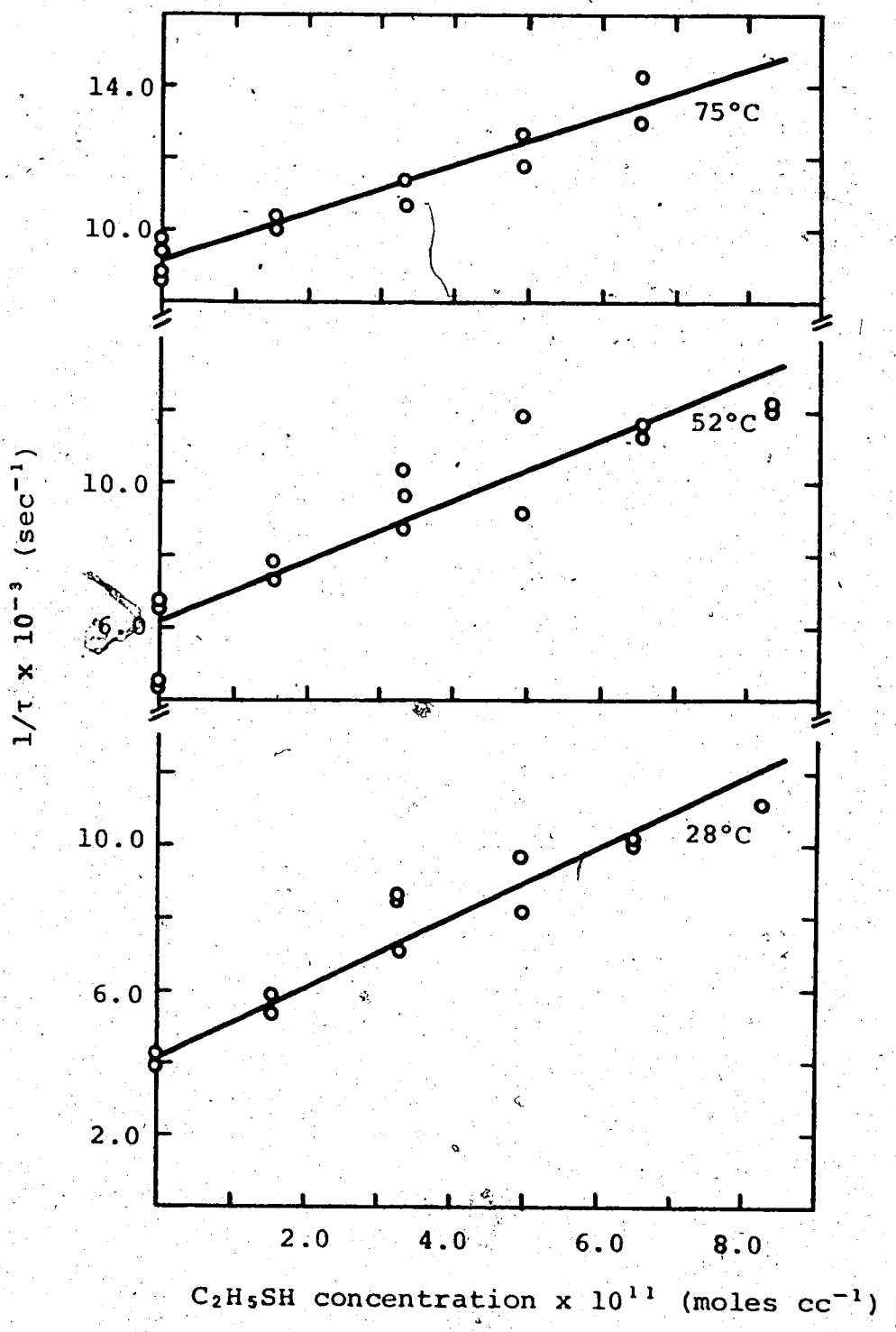

FIGURE 25: $1/\tau$ vs C_2H_5SH concentration.

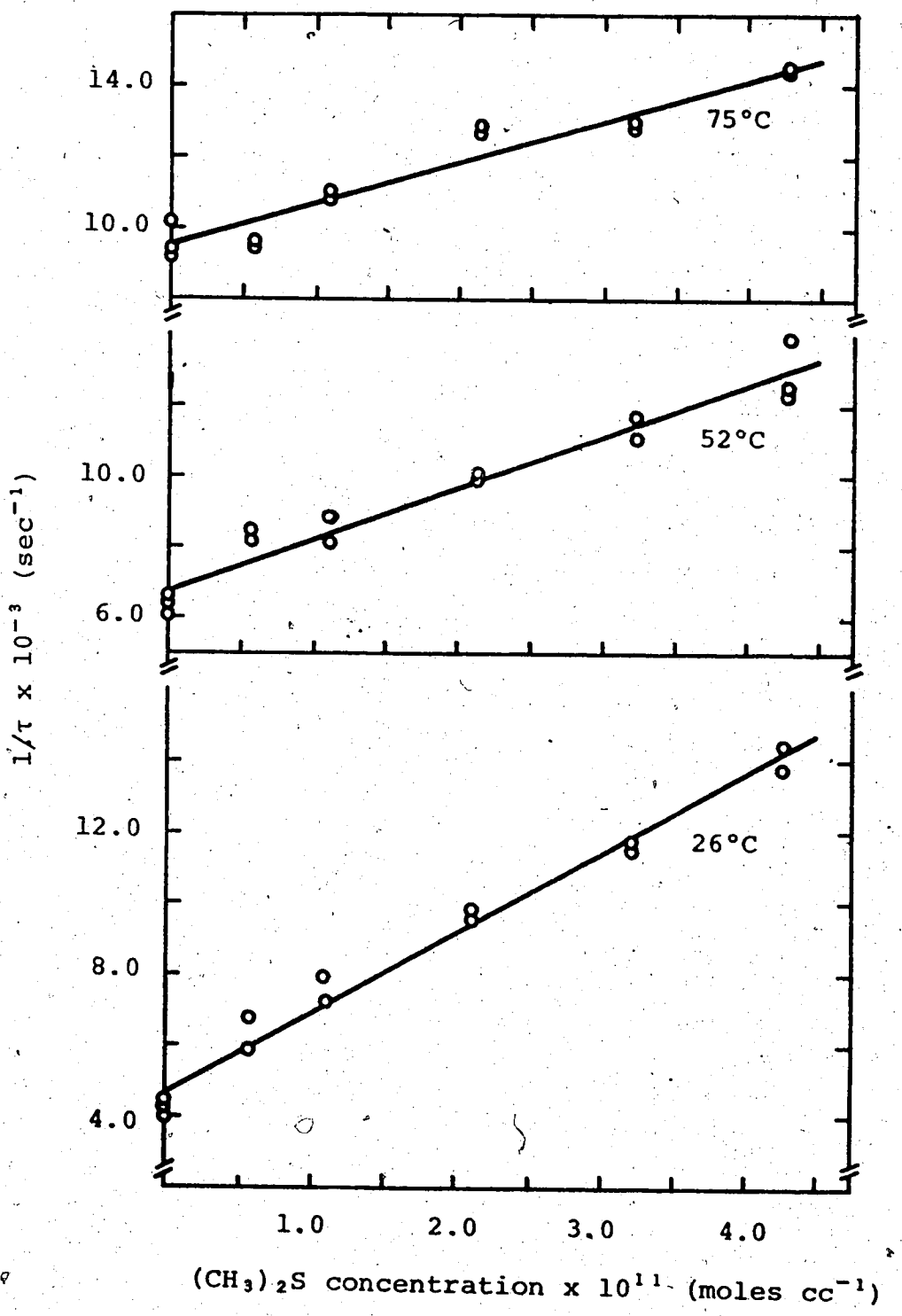

FIGURE 26: $1/\tau$ vs $(CH_3)_2S$ concentration.

TABLE VII

Quenching Data for $Hg(^3P_0)$ Atoms by Oxygen and Sulphur Containing Organic Compounds (a).

Compound	Temp. (°C)	k_Q (b) cc $mole^{-1}sec^{-1}$	$(\sigma^0)^2$ $Å^2$
CH_3CH_2OH	28	$(4.76\pm.69)\times10^{12}$ (c)	0.63±0.09
	75	$(3.93\pm.57)\times10^{12}$	0.59±0.09
CH_3CD_2OH	28	$(1.31\pm.05)\times10^{12}$	0.17±0.006
	55	$(1.12\pm.09)\times10^{12}$	0.14±0.01
	75	$(1.14\pm.11)\times10^{12}$	0.14±0.01
$(CH_3)_2O$	25	$(1.83\pm.09)\times10^{12}$	0.24±0.01
	75	$(1.33\pm.17)\times10^{12}$	0.16±0.02
$(CH_3CH_2)_2O$	25	$(7.55\pm.31)\times10^{13}$	11.6±0.5
	45	$(7.31\pm.44)\times10^{13}$	10.9±0.7
	60	$(5.22\pm.27)\times10^{13}$	7.6±0.4
	75	$(3.95\pm.22)\times10^{13}$	5.7±0.3
$(CH_3CD_2)_2O$	26	$(8.79\pm.51)\times10^{12}$	1.38±0.08
	54	$(7.80\pm.46)\times10^{12}$	1.17±0.07
	75	$(5.43\pm.33)\times10^{12}$	0.79±0.05

cont'd

TABLE VII (cont'd)

Quenching Data for $Hg(^3P_0)$ Atoms by Oxygen and Sulphur Containing Organic Compounds.

Compound	Temp. (°C)	k_Q [b] cc mole^{-1}sec^{-1}	$(\sigma^0)^2$ Å^2
	25	$(8.43\pm.16)\times10^{12}$	1.36±0.02
$(CD_3CD_2)_2O$	53	$(5.71\pm.37)\times10^{12}$	0.88±0.06
	75	$(4.50\pm.41)\times10^{12}$	0.67±0.06
	25	$(1.15\pm.11)\times10^{14}$	19.9±1.4
CH_3SH	53	$(1.42\pm.10)\times10^{14}$	17.9±1.3
	75	$(1.07\pm.11)\times10^{14}$	13.1±1.3
	28	$(1.08\pm.13)\times10^{14}$ [d]	15.7±1.7
C_2H_5SH	52	$(0.83\pm.09)\times10^{14}$	11.5±1.2
	75	$(0.67\pm.07)\times10^{14}$ [d]	8.9±0.9
	26	$(2.22\pm.08)\times10^{14}$	32.0±1.1
$(CH_3)_2S$	52	$(1.44\pm.09)\times10^{14}$	19.9±1.2
	75	$(1.14\pm.10)\times10^{14}$	15.3±1.3

a. Error limits are given in standard deviation.

b. k_Q values are quoted since k_{26} values differ by negligible amounts.

c. Average of four runs.

d. Average of two runs.

α-hydrogen position for diethylether, unlike Hg* quenching which does not demonstrate any significant isotope effect (Table I).

It is evident from Table VII that the quenching rate constants for Hg^0 relaxation by oxygen- and sulphur-containing compounds decrease as the temperature is increased. By assuming a temperature dependent pre-exponential factor, the modified Arrhenius equation

$$k_Q = (AT^{1/2}) \exp(-E_a/RT)$$

may be used to relate k_Q to the temperature, T. Plots of $\log(k_Q) - 1/2 \log(T)$ vs $1/T$ for these compounds, except C_2H_5OH and CH_3OCH_3, are found in Figures 27-28. Values of E_a and log(A) obtained from least-squares analysis are listed in Table VIII. Only two temperatures were investigated for C_2H_5OH and CH_3OCH_3 so that a least-squares treatment could not be carried out. For these two substrates, the slope and intercept were determined by drawing a straight line through the two points. Error limits were obtained from the two curves which can be drawn connecting the maximum and minimum error limits, and vice versa, of each individual point.

(b) Discussion.

A comparison of $(\sigma^0)^2$ values measured at room temperature for quenching by the alkanes (Table VII) and oxygen and

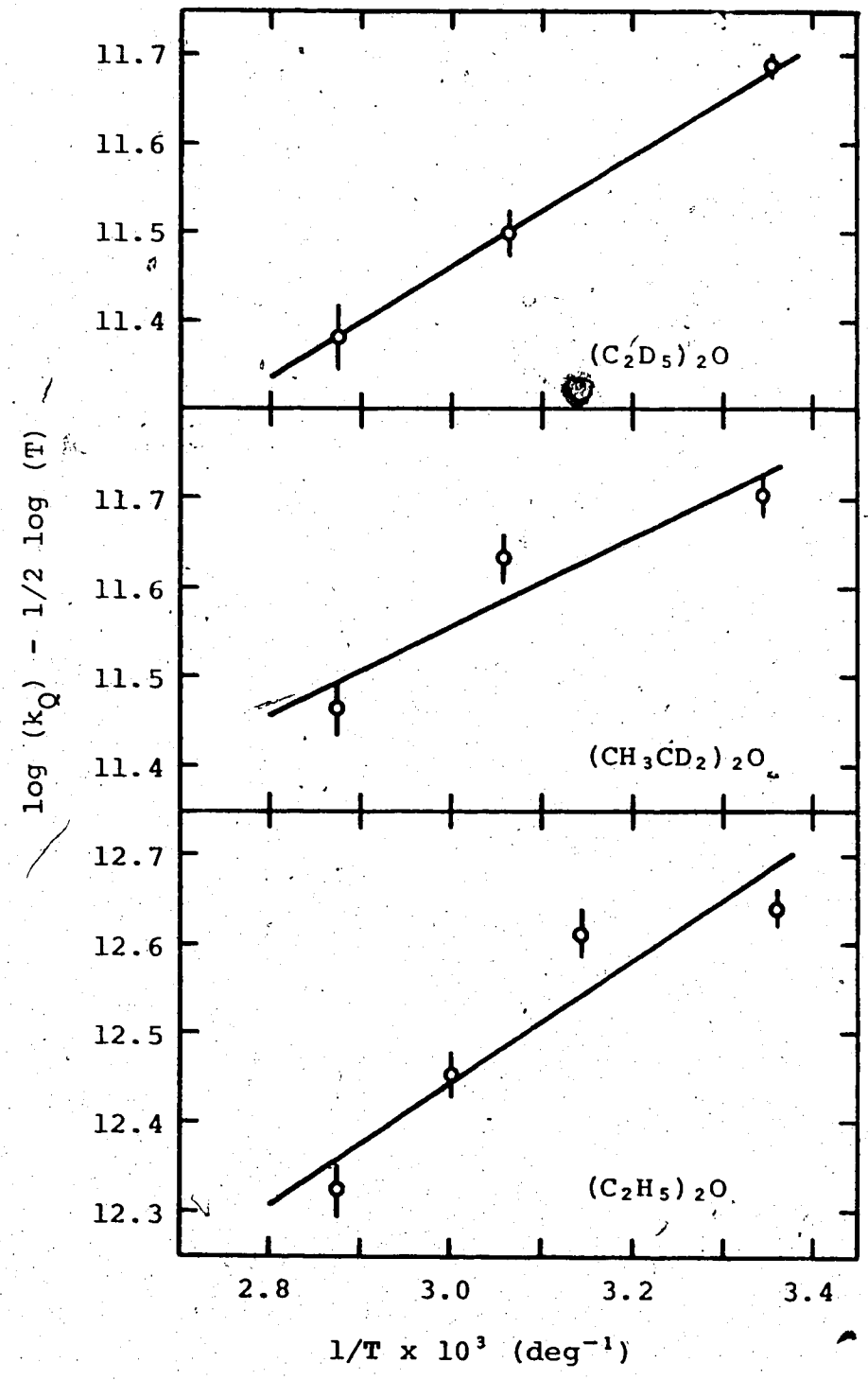

FIGURE 27: Arrhenius plots for $(C_2H_5)_2O$, $(CH_3CD_2)_2O$ and $(C_2D_5)_2O$ substrates.

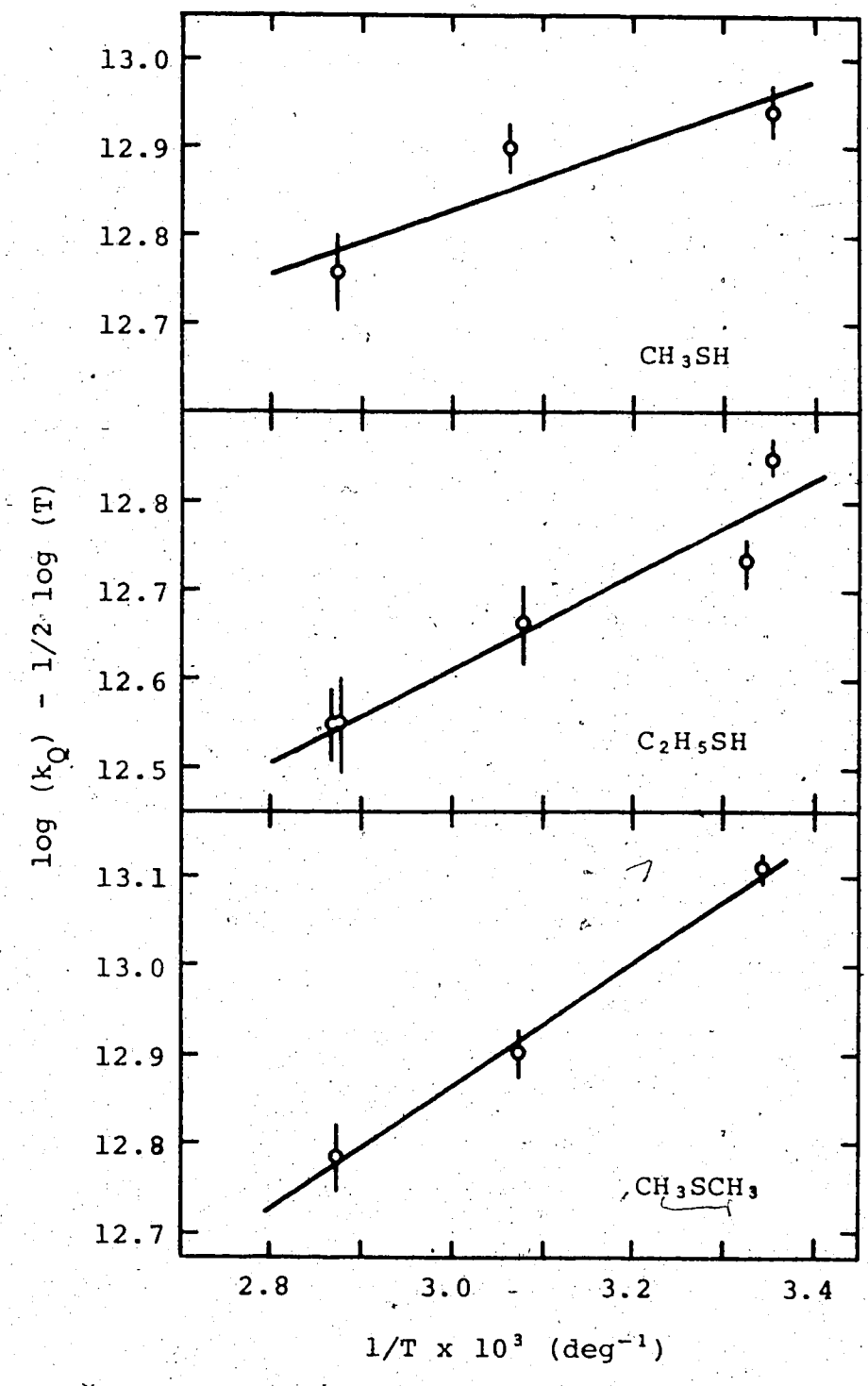

FIGURE 28: Arrhenius plots for $(CH_3)_2S$, C_2H_5SH and CH_3SH substrates.

TABLE VIII

Modified Arrhenius Parameters for the Quenching of $Hg(^3P_0)$ Atoms by Oxygen and Sulphur Containing Compounds (a).

Compound	E_a, kcal mole^{-1}	log(A)
CH_3CH_2OH	-1.2 ± 1.3 (b)	10.6 ± 1.1
CH_3CD_2OH	-1.0 ± 0.4	10.2 ± 0.2
$(CH_3)_2O$	-1.6 ± 0.8 (b)	9.8 ± 0.5
$(CH_3CH_2)_2O$	-3.0 ± 0.8	10.6 ± 0.6
$(CH_3CD_2)_2O$	-2.4 ± 0.8	10.1 ± 0.6
$(CD_3CD_2)_2O$	-2.9 ± 0.1	9.6 ± 0.1
CH_3SH	-1.7 ± 0.7	11.7 ± 0.5
CH_3CH_2SH	-2.4 ± 0.4	11.1 ± 0.3
$(CH_3)_2S$	-3.2 ± 0.3	10.8 ± 0.2

a. Determined from k_Q data over the range 25 to 75°C. Error limits are given in standard deviation.

b. Calculated from two temperature measurements. Error limits are estimated from the largest and smallest slopes that could be drawn through the error limits of $\ln(k_Q)$ values at the two temperatures.

sulphur compounds (Table VIII) demonstrate the distinct electrophilic nature of Hg^0 atoms. In all cases, the $(\sigma^0)^2$ value of a parent alkane is greatly increased by the presence of an oxygen atom and even more so by a sulphur atom. The substitution of an alkyl group for the hydrogen atom bound to an oxygen or sulphur in an alcohol or a mercaptan increases the quenching cross-section dramatically. However, the nature of the alkyl substituents and the central atom are significant factors in determining the reactivity of the molecule as a whole, as can be seen by comparing $CH_3OCH_3 < C_2H_5OH$ with $CH_3SCH_3 > C_2H_5SH$. Additional evidence for the electrophilic character of Hg^0 atoms is provided by the trends in $(\sigma^0)^2$ values of the paraffins. In this connection, it has been shown (91) that specific increments in σ for Hg^* quenching by methyl, methylene and methine groups follows their increasing electron donating ability. The same trend is apparent in Hg^0 quenching cross-sections.

Three important conclusions may be drawn regarding Hg^0 atom interaction with the compounds entered in Table VII, namely:

(i) all exhibit $(\sigma^0)^2$ values which are lower than the corresponding $(\sigma^*)^2$ values,

(ii) deuterium substitution in the α-position decreases the quenching cross-section of Hg^0 atoms in the case of ethanol and diethylether and,

(iii) there is a noticeable decrease in the $(\sigma^0)^2$ values as the temperature is increased.

A general mechanism to describe the processes involved in the Hg^0 sensitization of oxygen compounds may be formulated from the present data and the known photochemistry of alcohols and ethers.

Hg* atoms are quenched with near unit efficiency (45) resulting predominantly in Hg^0 formation (32,42). This can be attributed to the formation of a complex in which the Hg* atom is strongly bound to the oxygen atom. This implies that the complex exists long enough for this quenching process to occur. Since spin-orbit relaxation does not involve the rupture of a C-H bond, deuteration would have only secondary effects on the Hg* quenching cross-section, illustrated by the data in Table I. The high efficiency of this process, indicated by the large $(\sigma^*)^2$ values, precludes the possibility of relaxation of the complex by radiative transitions.

The $(\sigma^0)^2$ values are lower than the $(\sigma^*)^2$ values due to a different quenching mechanism. It may be assumed that Hg^0 atoms form a complex with the substrate which is relaxed via decomposition of the quencher, by exclusive C-H bond rupture (32,126-129), and by radiative decay. Band emission originating from $(Hg\text{-alcohol})^0$ complexes has been observed (23,32). Band emission has also been observed in the mercury photo-

sensitization of ethers (see Chapter V) which bears a close resemblance to the (Hg-alcohol)^0 spectra. The Hg^0 atom is again expected to be bound to the non-bonded electrons in the oxygen atom so that the complex must assume a configuration favorable for the abstraction of a hydrogen atom. The presence of an α-hydrogen would greatly facilitate the attainment of the required conformation. In this regard, the most pronounced isotope effect on the $(\sigma^0)^2$ values was noticed for deuterium substitution in the α-position. This observation provides direct experimental evidence that decomposition is enhanced by the presence of an α-hydrogen, a conclusion previously inferred (32) from band emission studies of (Hg-alcohol)^0 complexes.

In order for the Hg^0 atom to interact strongly with a nearby hydrogen atom, they must be in close proximity to each other concurrent with a weakening of the Hg^0-oxygen bond (Figure 29). The necessary configuration may be attained by appropriate twisting, wagging and stretching vibrations of the CH_2 group. These modes may become exaggerated by van der Waals attractions which come into play between the Hg^0 and hydrogen atoms. Decomposition would not necessarily follow once the Hg^0 atom is attached to a hydrogen atom since, at this point, the quenching mechanism would be similar to that operative in Hg^0-alkane systems. The comparatively weak α-hydrogen bond in an oxygen compound, however, would render abstraction more probable than in the

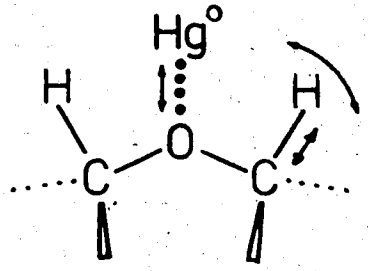

Configuration where the Hg° atom interaction is with the oxygen atom.

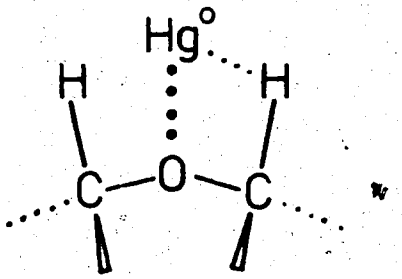

Configuration where the Hg° atom interaction shifts from the oxygen to the hydrogen atom.

FIGURE 29: Schematic configurations in Hg($^3P_0$) quenching by oxygen containing organic compounds.

case of the alkane analogue. This model is consistent with the observation that deuterium substitution results in a decrease in the $(\sigma^0)^2$ value since the amplitudes and frequencies of the vibrations are smaller.

An increase in the temperature would result in the population of higher vibrational levels of the mercury-oxygen bond in the complex. Consequently, the increase in the bond length would reduce the probability for attaining the configuration necessary for decomposition to occur and also increase the rate of dissociation back to reactants. Thus, a decrease in the quenching rate would be expected at higher temperatures, in agreement with experiment. As a corollary, an increase in the temperature should affect deuterated compounds to a greater extent than the protiated molecules and would be reflected in larger temperature variations in $(\sigma^0)^2$ values. This prediction cannot be verified by the data in Table VIII due to the large standard deviations of E_a values.

The proposed model accounts for the kinetic isotope effect, the lower reactivity of the Hg^0 compared to Hg* atoms and, due to the small $(\sigma^0)^2$ values, the ability of band emission to compete with decomposition as a mode of relaxation of metastable atoms. A discussion of band emission observed in the Hg* sensitization of ethers will be entered into more fully in the next chapter.

The results of Hg^0 atom quenching by sulphur-containing compounds may be interpreted in a fashion compatible with the limited information available in the literature. Of the sulphur compounds studied in the present work, only the Hg* sensitization of dimethylsulphide has been investigated (144,145). The primary decomposition reaction, attributed to quenching of Hg* atoms to the ground state (144,145), results in the fragmentation of the substrate into methyl and thiyl radicals arising from C-S bond rupture (144). Spin-orbit relaxation, however, has been suggested (42) as a primary process, although detection of Hg^0 atoms experimentally has not been attempted. The observation (144) that added carbon monoxide enhances the decomposition of the substrate indicates the involvement of Hg^0 atoms in the decomposition reaction (146).

The smaller values of $(\sigma^0)^2$ compared to the $(\sigma^*)^2$ values of the sulphur compounds is consistent with different quenching processes for the two excited mercury atoms. It would appear that spin-orbit relaxation of Hg* atoms is an important primary process whereas decomposition of the substrate results mostly from Hg^0 atom quenching.

It may be assumed that the electrophilic Hg^0 atom is strongly attracted to the lone pair electrons on the sulphur atom in a $(HgSR_2)^0$ complex. Unlike their oxygen analogues, decomposition of the sulphur compounds occurs directly from

this configuration since C-S bond cleavage is the almost exclusive decomposition mode. Quenching of Hg^0 atoms by sulphur-containing compounds is expected to be more efficient than by oxygen compounds because, in this case, predissociation of the complex to yield decomposition products does not require the attainment of a configuration where the Hg^0 atom interacts with a nearby hydrogen atom. This suggestion is supported by the higher A factors (see Table VIII) of the sulphur compounds.

The negative temperature dependence and the high values of the quenching rate constants suggest that predissociation to a potential energy surface leading to product formation occurs at a lower energy than the separated reactants. Since the crossover to products intersects with the $(HgSR_2)^0$ potential energy surface, the E_a values listed in Table VIII may be considered to represent lower limits for the binding energy of the complex.

The high $(\sigma^0)^2$ values, indicative of an efficient decomposition process, suggests that radiative relaxation of the $(HgSR_2)^0$ complex would be a minor process and the intensity of band emission would be very weak, if observable at all.

3. Aromatic Compounds.

(a) Results and Discussion.

The room temperature quenching rate constants for Hg^0 atoms by benzene, deuterated benzene and hexafluorobenzene were determined from the decay lifetime of the delayed fluorescence as a function of substrate pressure in $Hg-N_2$ mixtures (Figure 30), and the results compiled in Table IX.

There appears to be a factor of two difference between the $(\sigma^0)^2$ values of benzene and deuterated benzene. This may be a spurious result since the measured $(\sigma^0)^2$ value for C_6H_6 is three times larger than that reported for the quenching of Hg* atoms (117). The very strong quenching by the aromatic compounds required an extremely small amount of the substrate (approximately 2×10^{-4} to 1×10^{-5} torr in the case of benzene) to achieve sufficient quenching. Degassing from the walls of the circulating system cannot be discounted and would have the effect of increasing the apparent quenching rate. For this reason, the data obtained for these compounds should be viewed with caution. Despite this possible complication, it is apparent that aromatic compounds are very efficient quenchers of both Hg^0 and Hg* atoms.

The "superefficiency" of the Hg^0 quenching rate may be seen by comparing $(\sigma^0)^2$ values with the square of the hard sphere collision diameter, $(\sigma_s)^2$. An approximate value for σ_s can be obtained by equating it with the internuclear

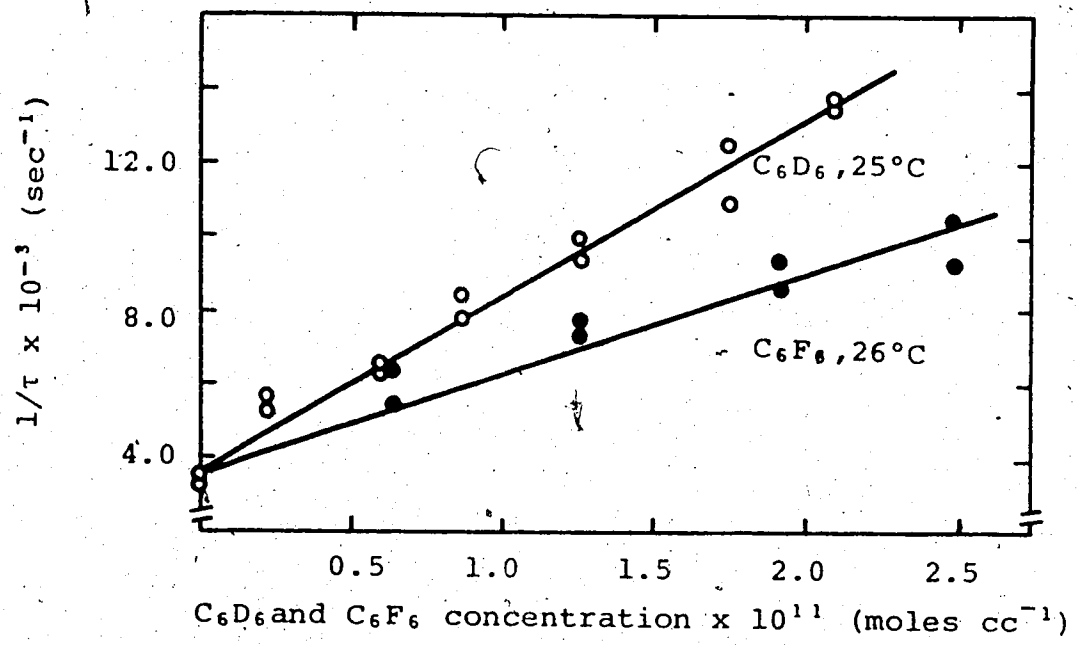

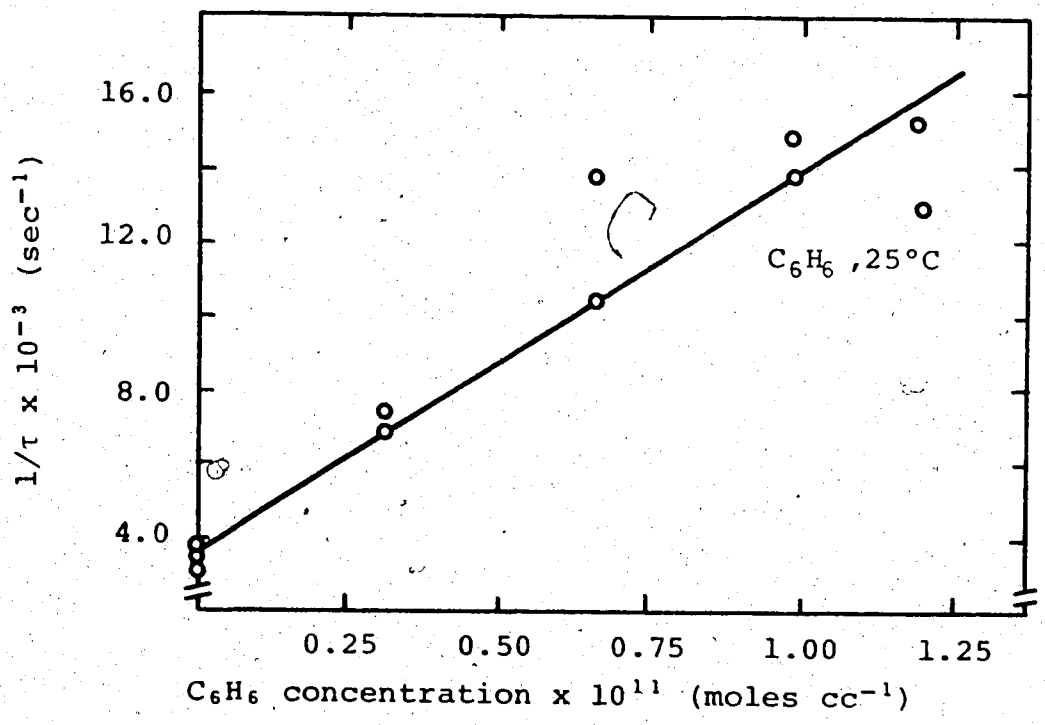

FIGURE 30: $1/\tau$ vs C_6D_6, C_6F_6 and C_6H_6 concentration.

TABLE IX

Quenching of $Hg(^3P_0)$ Atoms by Aromatic Compounds (a).

Comp'd	$(\sigma^*)^2$ (b) Å^2	k_Q (c) cc mole^{-1}sec^{-1}	$(\sigma^0)^2$ Å^2
C_6H_6	48 ± 3	(9.42±.65)x10^{14} (d)	150 ± 10
C_6D_6	74 ± 2	(4.69±.17)x10^{14}	76 ± 3
C_6F_6		(2.69±.20)x10^{14}	56 ± 4

a. Error limits are given in standard deviation.

b. Taken from reference 116.

c. k_Q values are quoted since k_{26} values differ by negligible amounts.

d. Average of two runs.

distance, r, at the minimum in the Lennard-Jones potential energy function. This distance is given by the expression

$$r^6 = 2\sigma^6 \qquad [34]$$

which is obtained by setting the derivative of the function to zero and solving for r. For the interaction between two unlike particles A and B, σ is given by the mixing rule

$$\sigma = (\sigma_A + \sigma_B)/2. \qquad [35]$$

Using the values σ_{Hg^*} = 2.4Å (147) and $\sigma_{C_6H_6}$ = 5.349Å (148), σ can be calculated from equation [35] and substituted into equation [34] to obtain a value of r = σ_s = [illegible]. Thus, the hard sphere collision cross-section, $(\sigma_s)^2$, for a Hg^* atom and a benzene molecule is approximately 19Å^2. This value should be about the same as that for a Hg^0 atom and benzene, and indicates that the quenching cross-section is about eight times larger than the hard-sphere collision cross-section.

4. Ammonia.

(a) Results and Disscussion.

The rate of decay of Hg^0 atoms in the presence of ammonia was measured from observations of the time dependence of the $(HgNH_3)^0$ complex emission intensity at 3600Å as

a function of ammonia concentration. The decay rate of the emission was determined from phase-plane plots (149). Since the emission lifetime of the complex is very short compared to its rate of formation (26,30), the decay rate of the band emission is an accurate measure of the rate of removal of Hg^0 atoms. The following mechanism has been adopted:

$$Hg + h\nu(2537\text{Å}) \rightarrow Hg^* \qquad [1]$$

$$Hg^* \rightarrow Hg + h\nu(2537\text{Å}) \qquad [2]$$

$$Hg^* + NH_3 \rightarrow H + NH_2 + H \qquad [36]$$

$$Hg^* + NH_3 \rightarrow Hg^0 + NH_3 \qquad [37]$$

$$Hg^0 + NH_3 \rightarrow (HgNH_3)^{0'} \qquad [38]$$

$$(HgNH_3)^{0'} \rightarrow Hg^0 + NH_3 \qquad [-38]$$

$$(HgNH_3)^{0'} \rightarrow Hg + NH_3 + h\nu \qquad [39]$$

$$(HgNH_3)^{0'} + NH_3 \rightarrow (HgNH_3)^0 + NH_3 \qquad [40]$$

$$(HgNH_3)^0 \rightarrow Hg + NH_3 + h\nu \qquad [41]$$

Kinetically, reactions [38]-[41] are indistinquishable from the following

$$Hg^0 + NH_3 \rightarrow Hg + NH_3 + h\nu \qquad [42]$$

$$Hg^0 + 2NH_3 \rightarrow Hg + 2NH_3 + h\nu, \qquad [43]$$

where the superscript (^{0}) denotes electronic excitation, ($'$) vibrational excitation and $h\nu$ signifies the band emission radiation.

The decay rate constant of Hg^0 atoms can be expressed by the formula

$$1/\tau = k_A = k_{42}[NH_3] + k_{43}[NH_3]^2. \quad [44]$$

A plot of $1/\tau \div [NH_3]$ vs $[NH_3]$ at 28°C is shown in Figure 31A, from which k_{42} and k_{43} were found to be $(1.2\pm0.2)\times10^{11}$ cc mole^{-1}sec^{-1} and $(6.9\pm0.5)\times10^{17}$ cc^{2}mole^{-2}sec^{-1}, in fair agreement with published values (see Table IV). A similar plot for the data obtained at 70°C showed appreciable curvature. At this temperature, a plot of $1/\tau$ vs $[NH_3]$ was an adequate representation of the results (Figure 31B). The slope of this line at 70°C is $(3.9\pm0.3)\times10^{11}$ cc mole^{-1}sec^{-1}. This result suggests that the third order reaction [43] is a minor process with respect to the second order process [42] at this temperature. The value of k_{42} appears to have increased three fold at the higher temperature. The activation energy and the log of the pre-exponential factor for reaction [42], 5.4 ± 1.2 kcal/mole and 13.8 ± 0.8, respectively, were calculated by the method outlined previously in the determination of Arrhenius parameters for ethanol and dimethylether quenching (see page 116).

At room temperature, the decay lifetime of Hg^0 atoms reached a limiting value of 1.6±0.3 microseconds as the ammonia pressure was increased up to 600 torr. This limiting value can be identified with the radiative lifetime of the $(HgNH_3)^0$ complex (29) and indicates that the complex is not readily quenched by ammonia.

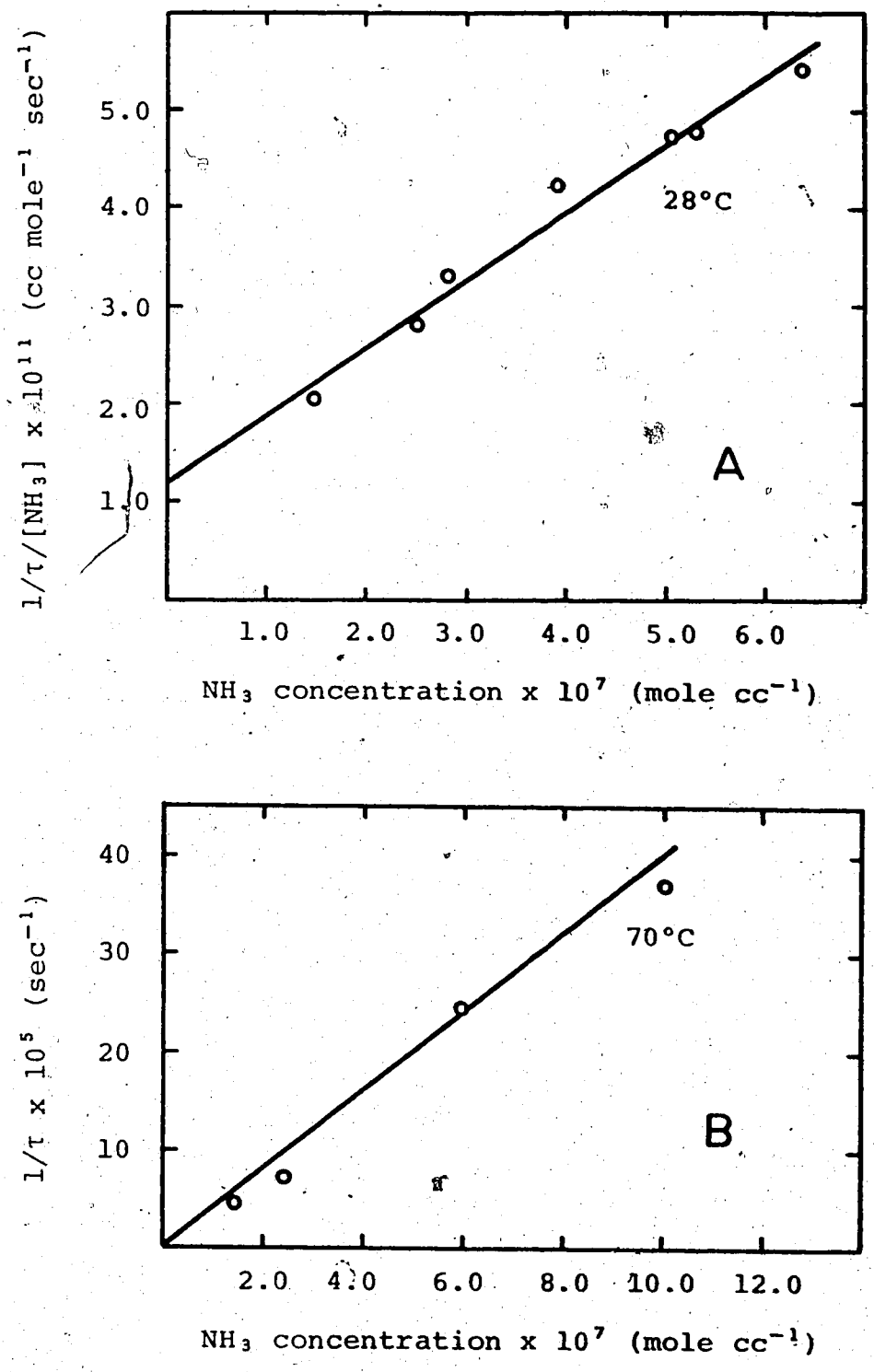

FIGURE 31: Rate data plots for the relaxation of $Hg(^3P_0)$ atoms by ammonia.
top: $1/\tau \div [NH_3]$ vs ammonia concentration
bottom: $1/\tau$ vs ammonia concentration.

The results of the ammonia study can be interpreted in terms of the potential energy diagram (Figure 32) and the following reaction

$$Hg^0 + NH_3 \rightarrow Hg + NH_2 + H. \qquad [45]$$

At room temperature, the interaction between Hg* and ammonia results in the decomposition of the molecule or in quenching to the metastable level. Spin-orbit relaxation is expected to be the favored process due to the energy barrier for decomposition. The complex formed between a Hg^0 atom and an ammonia molecule can be stabilized in a further collision with NH_3, leading to the presence of second and third order kinetics. Due to the energy barrier, reaction [45] will be less favorable than band emission. This interpretation accounts for the low quantum yield of decomposition and the observed second and third order kinetics at this temperature.

At higher temperatures, decomposition of NH_3 increases in importance due to the increased rate of crossover to products from both the $(HgNH_3)^*$ and $(HgNH_3)^0$ systems. Emission will become less likely for two reasons,

(i) the complex formed with Hg^0 in a bimolecular collision with ammonia will not be stabilized as easily by a consecutive collision since the length of time spent in the potential well will be shor-

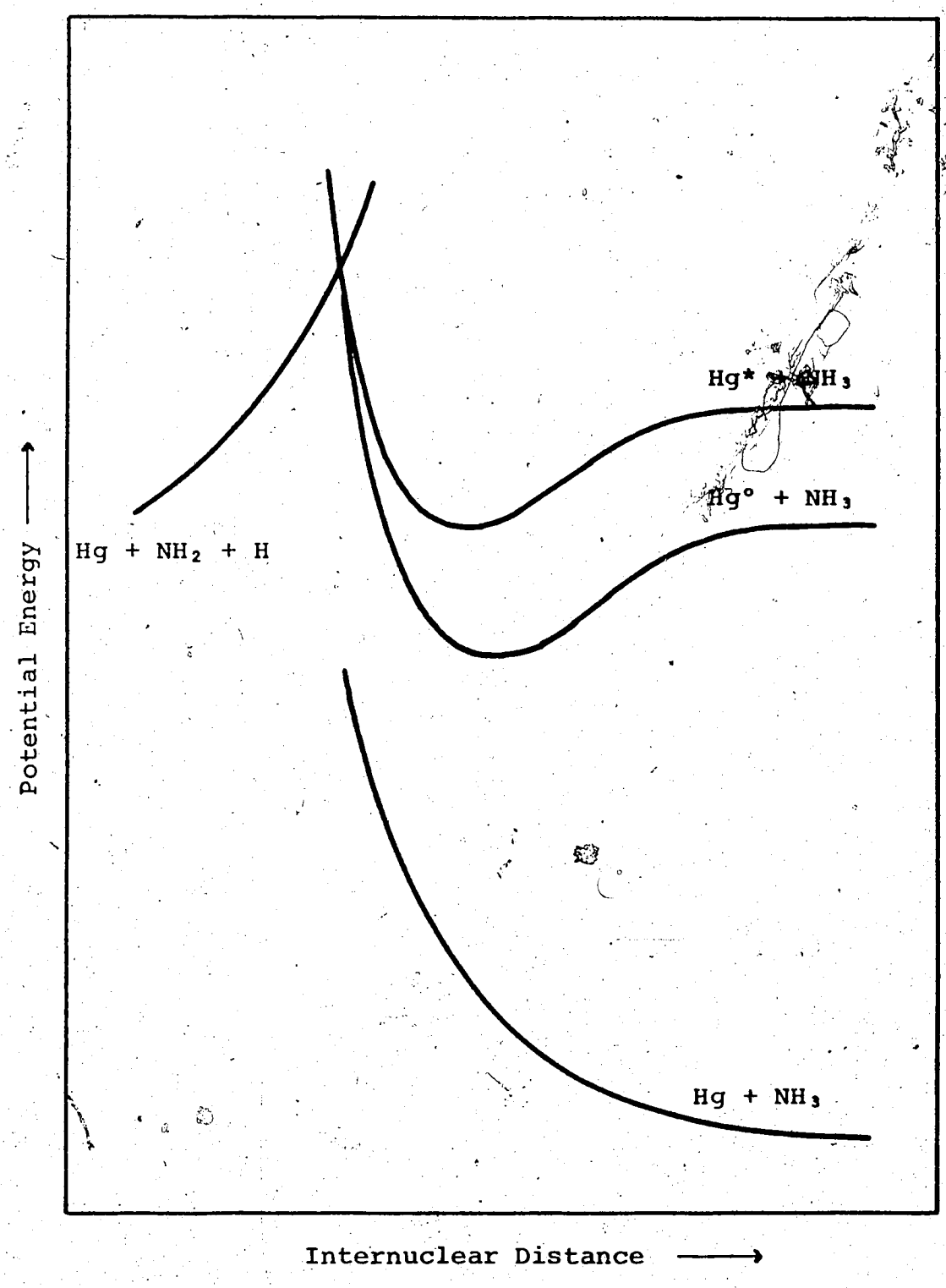

FIGURE 32: Schematic potential energy diagram for the interaction of $Hg(^3P_0)$ and $Hg(^3P_1)$ atoms with ammonia.

ter, and

(ii) the complex will have a greater tendency to revert back to the separated particles.

This will result in a slower rate of relaxation of metastable atoms and a lower band emission intensity, and accounts for the increase in the quantum yield of decomposition as well as the absence of a detectable third order process. This argument is supported by the observation that the band intensity at the higher temperature was about half that at the lower temperature. Since the second order rate increases at the higher temperature, reaction [45] has been postulated. However, the overall rate of decay of Hg^0 atoms is slower since the third order rate process is less important.

CHAPTER V

EMISSION FROM EXCITED MERCURY-SUBSTRATE MIXTURES

It has been shown from this laboratory (22,23) that measurements on band emission from mercury-substrate excimers gives pertinent information for the elucidation of the energy transfer process. Phillips and co-workers (25,32) have reported spectra of Hg-alcohol and Hg-Xe systems which they attributed to transitions from "charge transfer" complexes involving a Hg^0 atom. In view of the similarity between alcohol and ether quenching of Hg^0 atoms, an investigation for band emission in ether sensitization was carried out. A study of the band emission from various Hg-N_2-Xe mixtures was undertaken to define the role of Hg* atoms in this system. Several other substrates of interest were also examined for possible band emission.

1. Results and Discussion.

(a) Hg + Ether Systems.

Band spectra observed with dimethyl, diethyl, t-butylethyl ethers and tetrahydrofuran in Hg* photosensitization are displayed in Figures 33 and 34. The sharp lines in these figures are due to stray light from the mercury lamp. These

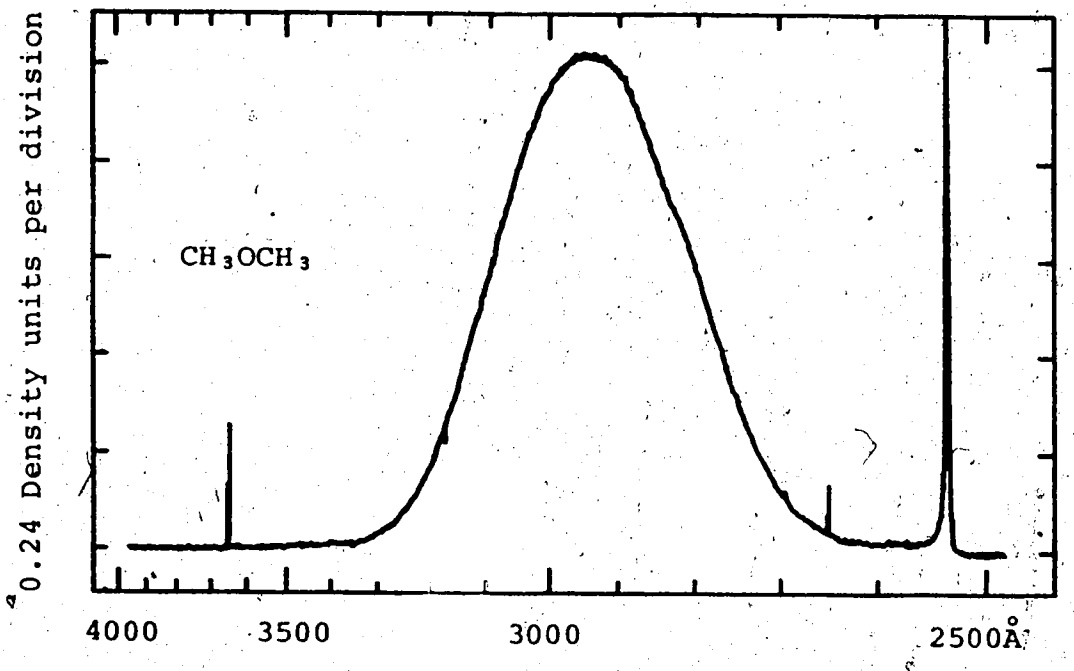

Band spectra with $(CH_3)_2O$; 235 torr, 1 hr.

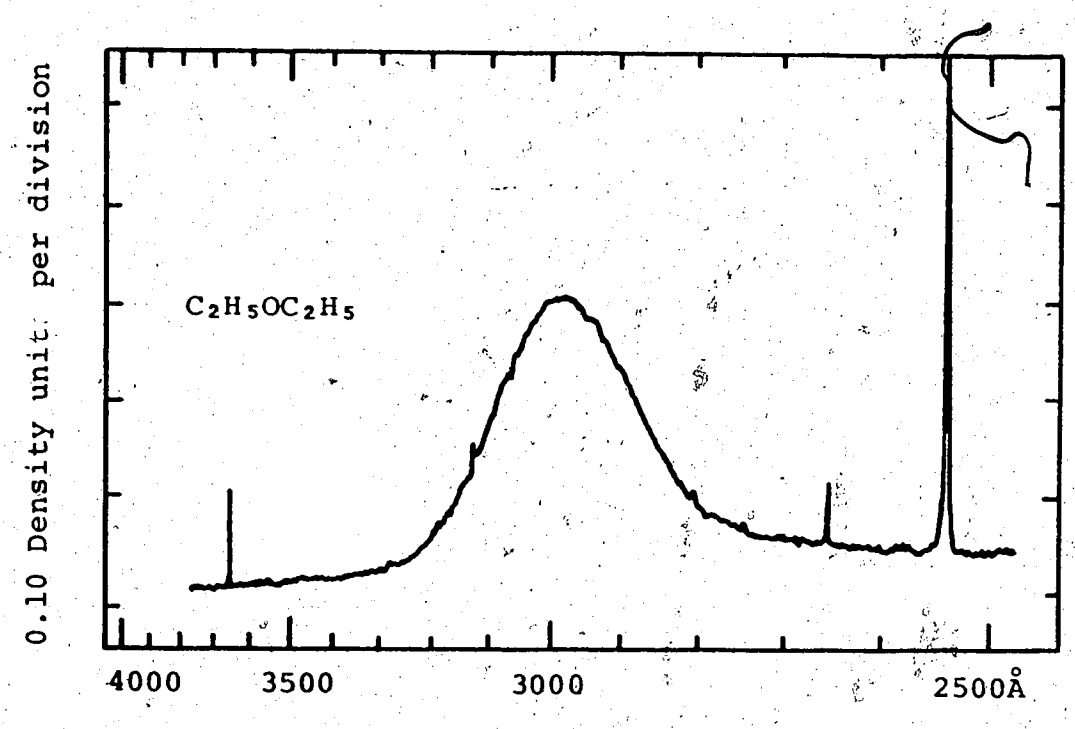

Band spectra with $(C_2H_5)_2O$; 240 torr, 145 min.

FIGURE 33: Microdensitometer traces of $(CH_3)_2O$ and $(C_2H_5)_2O$ band emission spectra.

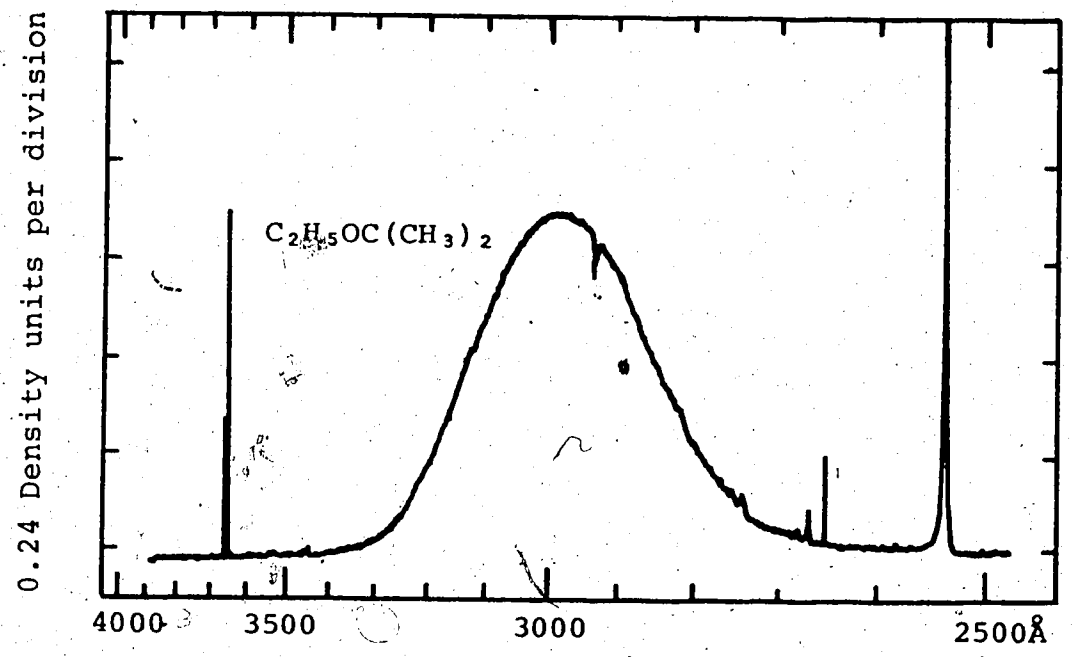

Band spectra with $C_2H_5OC(CH_3)_3$; 88 torr, 5 hrs.

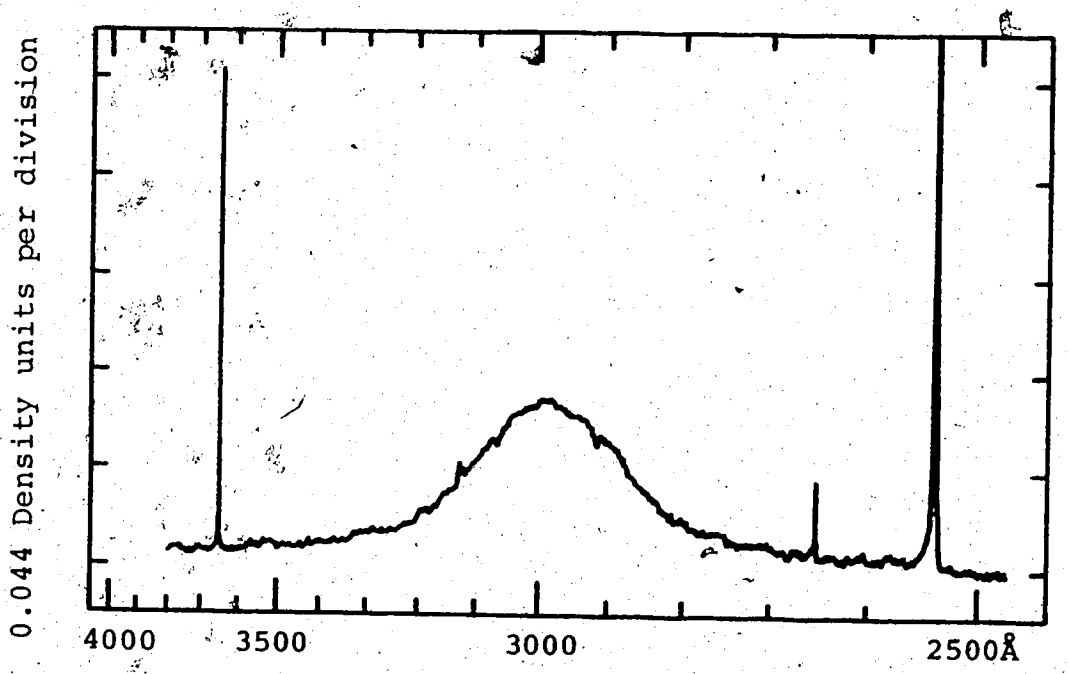

Band spectra with tetrahydrofuran; 108 torr, 3 hrs.

FIGURE 34: Microdensitometer traces of $C_2H_5OC(CH_3)_3$ and tetrahydrofuran band emission spectra.

compounds each exhibit one structureless band which is completely separated from the resonance line. Increasing the size of the alkyl groups causes an increase in the separation of the band maxima from the resonance line. The emission band intensities of these gases vary considerably in the order $(CH_3)_2O > C_2H_5OC(CH_3)_3 > (C_2H_5)_2O \sim$ tetrahydrofuran. A summary of the data obtained from Hg-ether band emission studies is found in Table X.

The band emission intensity and the position of the band maxima of the ethers closely parallels the luminescence efficiency and the band maxima of the alcohols (32). This result substantiates the suggestion that the sensitization of both alcohols and ethers can be interpreted using the same mechanism (see Chapter IV). Since Hg^0 atoms are produced in both systems (42), band emission in the Hg* sensitization of ethers probably originates from an $(Hg\text{-ether})^0$ complex.

The high intensity of band emission (23) and the low quantum yield of decomposition (121) in the Hg^0 sensitization of H_2O can be rationalized in terms of the mechanism proposed for the Hg^0 sensitization of ethers described in Chapter IV. Strong interaction with a remote hydrogen atom, which leads to decomposition, is very unlikely when the Hg^0 atom is bound to the lone pair electrons on the oxygen atom. Therefore, emission from the $(Hg\text{-}OH_2)^0$ complex is likely to

TABLE X

Relative Intensity and Separation of the Emission Band Maxima From the 2536.5Å (39,424 cm^{-1}) Resonance Line for Various Ethers.

Compound	pressure (torr)	$\Delta\omega$ cm^{-1}	intensity relative to $(C_2H_5)_2O$ (a)
CH_3OCH_3	235	-5,410	~18
$C_2H_5OC_2H_5$	240	-5,810	1
	180	-5,980	~ 1
$C_2H_5OC(CH_3)_3$	88	-5,870	~ 5

a. The relative intensities were calculated by linearly extrapolating to equal pressures and exposure times to that of diethylether. This approximation is estimated to have an error of ±15%.

occur from a potential energy surface which describes the >O•••Hg⁰ complex. On the basis of the similarity with (Hg-H_2O)⁰ band emission, it seems that radiative transitions from complexes of Hg⁰ atoms with alcohols and ethers originates from a potential energy surface which describes the Hg⁰-oxygen interaction free from perturbation by a hydrogen atom on the alkane substituent(s). Since the Hg⁰-oxygen bound complex does not decompose via a C-O bond split, this surface must intersect with a Hg⁰-hydrogen potential energy surface that is predissociative to a repulsive surface which correlates with a hydrogen atom (or HgH) and an alkoxy radical.

The band emission intensity will be inversely proportional to the efficiency of the competing non-radiative relaxation process, i.e. crossover to the Hg⁰-H potential energy surface compatible with α-hydrogen abstraction. Although dimethylether has two more α-hydrogens than diethylether, the much lower quenching cross-section of the former suggests that the higher C-H bond energy decreases the rate of the decomposition process and thus band emission competes more favorably. t-Butylethylether would display more intense band emission than diethylether since decomposition is less probable on account of the presence of only two α-hydrogens. On this basis, diethylether and tetrahydrofuran would be expected to show the same band intensity, in agreement with the experimental results.

With the exception of tetrahydrofuran, the trend to wider separation between the band maxima and the resonance line with increasing size of the alkyl groups can be explained in terms of their inductive effect and the electrophilic nature of the Hg^0 atoms. An increase in the inductive effect with increasing size of the alkyl substituents would result in a greater electron donating ability of the oxygen atom and, consequently, stronger interaction with Hg^0 atoms. This would be manifest by a deeper potential well so that the band maxima would lie at progressively longer wavelengths. The deviation from this trend in the case of tetrahydrofuran may be due to its cyclic structure.

(b) $Hg-N_2-Xe$ and $Hg-N_2-C_3H_8$ Systems.

Band emission was obtained from the sensitization of xenon and propane in varying concentration of nitrogen, keeping the total pressure at 200 torr to minimize the effects of pressure broadening on the absorbed light intensity. A reduction of propane concentration from 100 to 11% reduced the emission intensity by about 20% at 2570Å (Figure 35). The spectra obtained with various $Hg-N_2-Xe$ mixtures, displayed in Figure 36, clearly shows that as the nitrogen percentage is increased, the band emission due to the Hg-Xe excimer is decreased. This result, which is contrary to the findings of Phillips and co-workers (25), implies that xenon

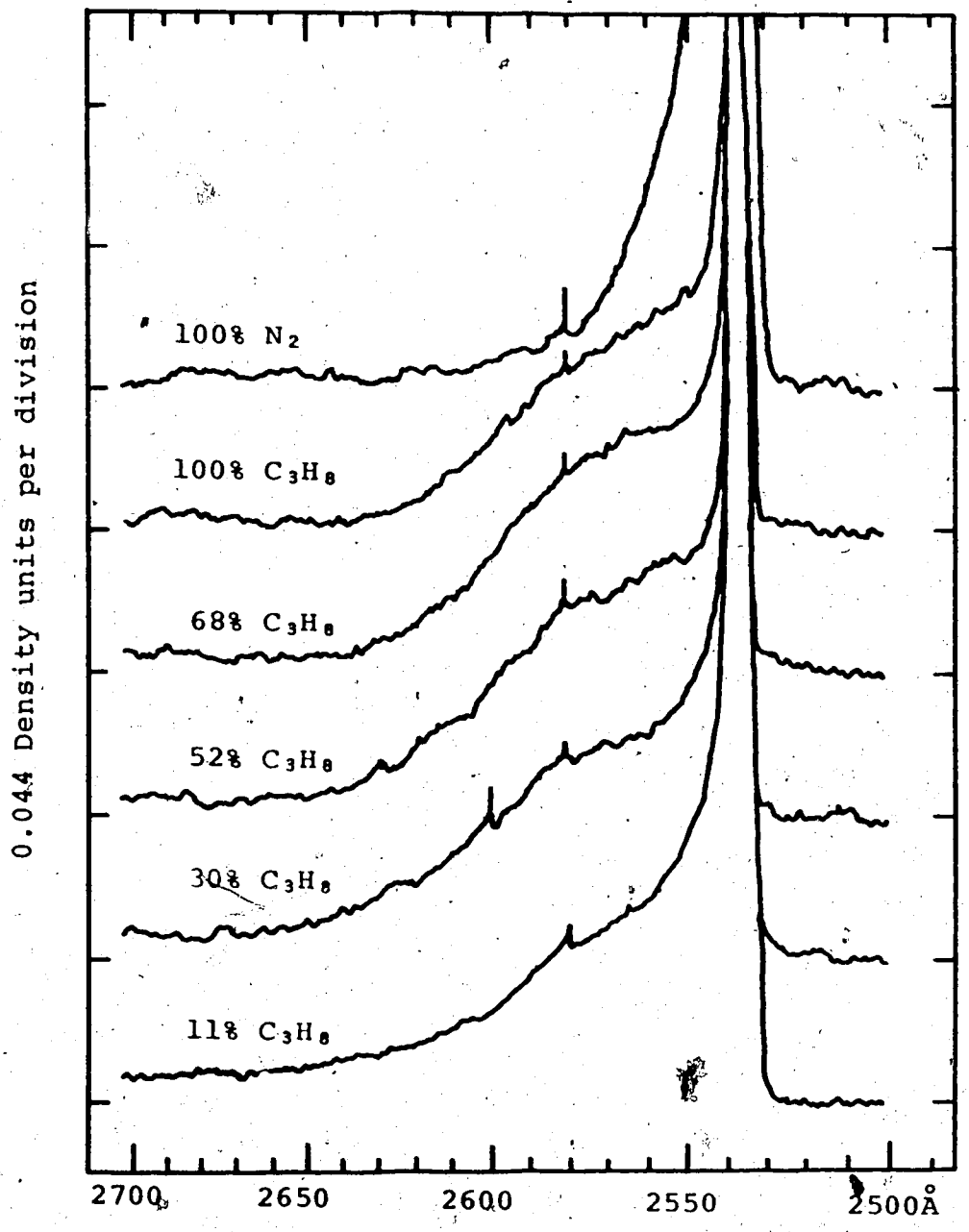

Band spectra of N_2-C_3H_8 mixtures; 200 torr, 3 hrs.

FIGURE 35: Microdensitometer traces of band emission spectra of N_2 + C_3H_8 mixtures.

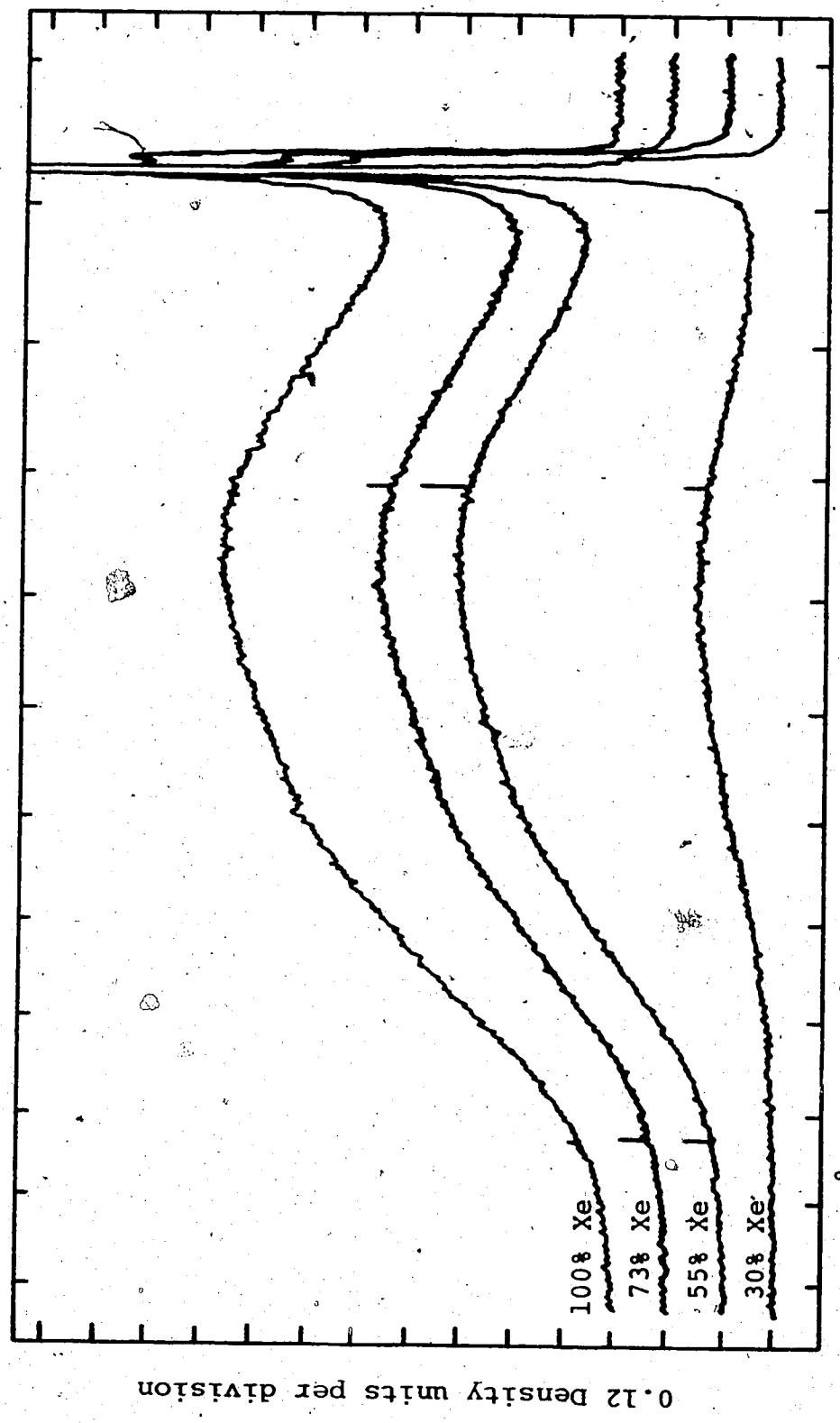

FIGURE 36: Microdensitometer traces of band emission spectra of N_2 + Xe mixtures. B and spectra of N_2-Xe mixtures; 199 torr, 5 min.

forms a complex with Hg* rather than Hg^0 atoms since as the Hg* concentration is decreased by increasing the nitrogen concentration, the observed band emission decreases. The suggestion that Xe, like methane, is a very inefficient quencher of Hg^0 atoms is in line with the band emission results. No definite conclusions can be drawn from the Hg-N_2-C_3H_8 data since the relative populations of Hg* and Hg^0 atoms is affected by the relative quenching by both gases. However, the decrease in the band intensity with increasing nitrogen quenching suggests that most of the emission is due to a $(Hg\text{-}C_3H_8)^*$ complex.

(c) Hg + Various Substrate Gases.

Band emission was not detected in the Hg* sensitization of C_2H_4, C_3H_6, C_2H_3F, $C_2H_2F_2$, C_2F_4, H_2, O_2, CO_2, NO, NO_2, N_2O, CH_3CHO, $CH_3OCH{=}CH_2$, SiD_4, $SiH_2(CH_3)_2$, thiophene, furan or in N_2O-C_3H_6 mixtures. The fluorescence spectra of benzene an erfluorobenzene were observed owing to excitation by direct absorption of 2537Å radiation.

The $(\sigma^*)^2$ values of these gases, where known, are all quite high which suggests that the mercury excimer, if it exists, is ed exclusively by non-radiative processes.

$O(^3P)$ atoms are generated in the Hg* quenching of N_2O (150) and, in the presence of an olefin, add to the double bond to form an unstable epoxide (151). The $O(^3P)$ combina-

tion with propylene evidently does not produce an excited complex of sufficiently long lifetime to allow radiative decay in the 1900-5000Å region.

CHAPTER VI

COMPLEX TIME DEPENDENCE OF 2537Å EMISSION IN $Hg(^3P_1)$-SUBSTRATE MIXTURES.

During the course of the Hg^0 atom quenching experiments, the effect of the pure substrate alone on the 2537Å intensity was investigated. It was found that the decay of the resonance radiation showed more than one intensity maximum in the presence of some substrates. A detailed study of this phenomenon was carried out to obtain more information concerning this unexpected behavior. The results are presented here.

1. Results.

The time dependence of 2537Å radiation intensity was measured in mixtures of mercury with the noble gases, methane, ethane, tetrafluoromethane, nitrogen and dimethylether. A second intensity maximum was observed, which, depending on the nature and pressure of the foreign gas, appeared as two separate peaks, a partially resolved shoulder in the flash decay region or as two superimposed peaks that appeared as a distorted flash profile. Typical examples of these three types of intensity curves are displayed in Figure 37. No irregularity in the 2537Å intensity was observed in the

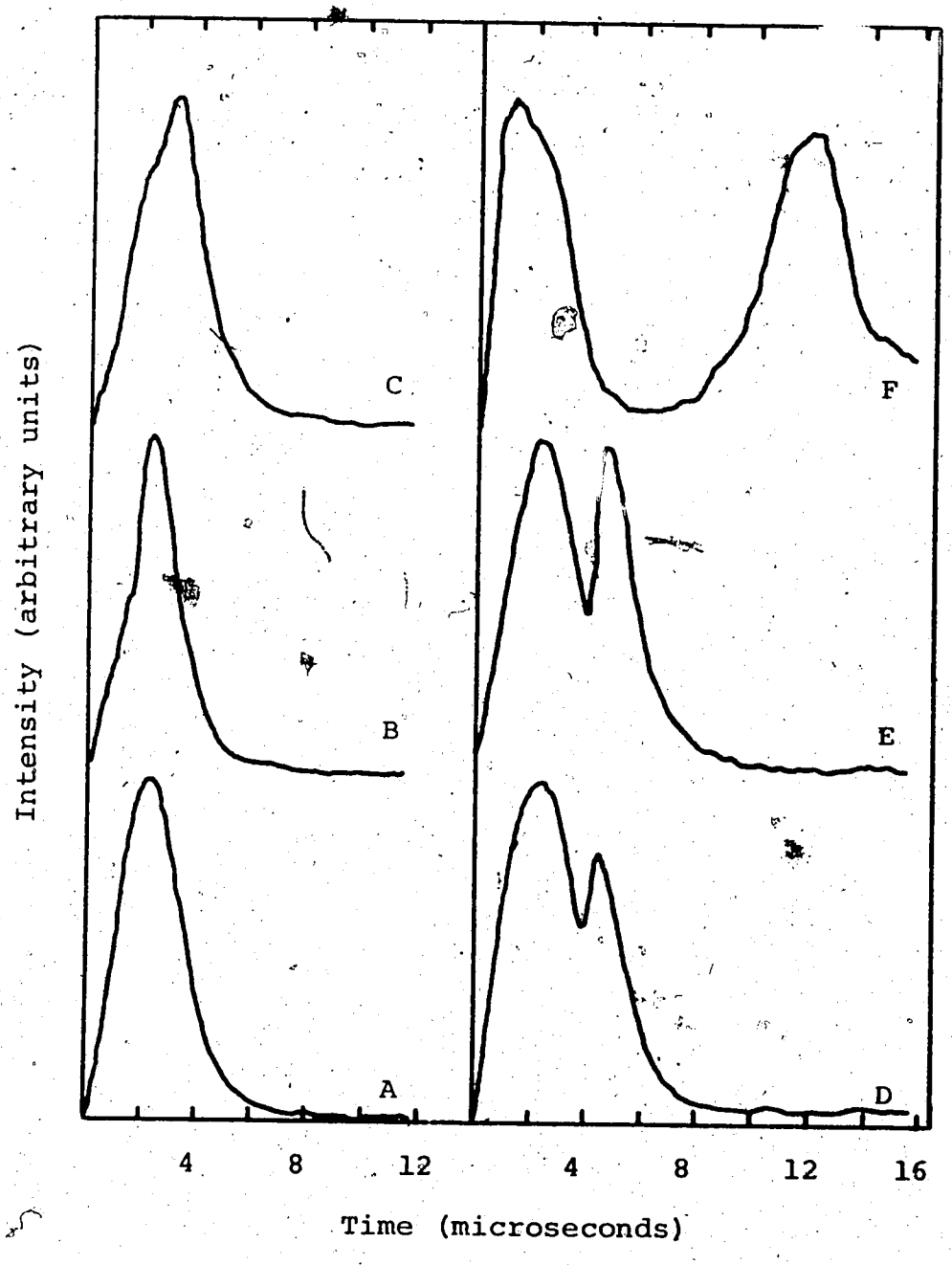

FIGURE 37: Typical time dependence of the 2537Å intensity. A: flash profile, B and C: distorted flash curves, D and E: partially resolved shoulders, F: two separate peaks.

absence of a foreign gas. The time, t', at which the flash reached its maximum without substrate present, occurred between 2.2 and 2.4 microseconds after the lamp was triggered at time t^0. The time of successive intensity maxima, denoted t", t"', etc., ranged from 1.2 to 90 microseconds.

Hg-noble gas mixtures all displayed a second intensity maximum and a third i the Hg-Ar system. t" was measured for these gases as a function of substrate pressure at room temperature (Figures 38-40). In all cases, t" increased as the pressure was increased beyond six torr. t" increases in the order He ~ Ne < Ar < Kr < Xe for a given pressure of gas. The intensity of the peak at t" decreased as the pressure was increased. The third intensity maximum in the Hg-Ar system occurred close to the flash decay curve but was not always observable due to its low intensity or overlapping by the second intensity maximum. No pressure effects on t"' were deduced for this reason.

A distorted flash curve was observed in Hg-He mixtures as the pressure of helium was increased up to 2.0 torr. Abruptly at this pressure, a second intensity maximum appeared at 11.1 microseconds. t" then decreases as the pressure is increased to about six torr and then begins to increase as the pressure is further increased (Figure 39). This is a marked distinction from the behaviour of neon or argon where t" steadily increases with increasing pressure.

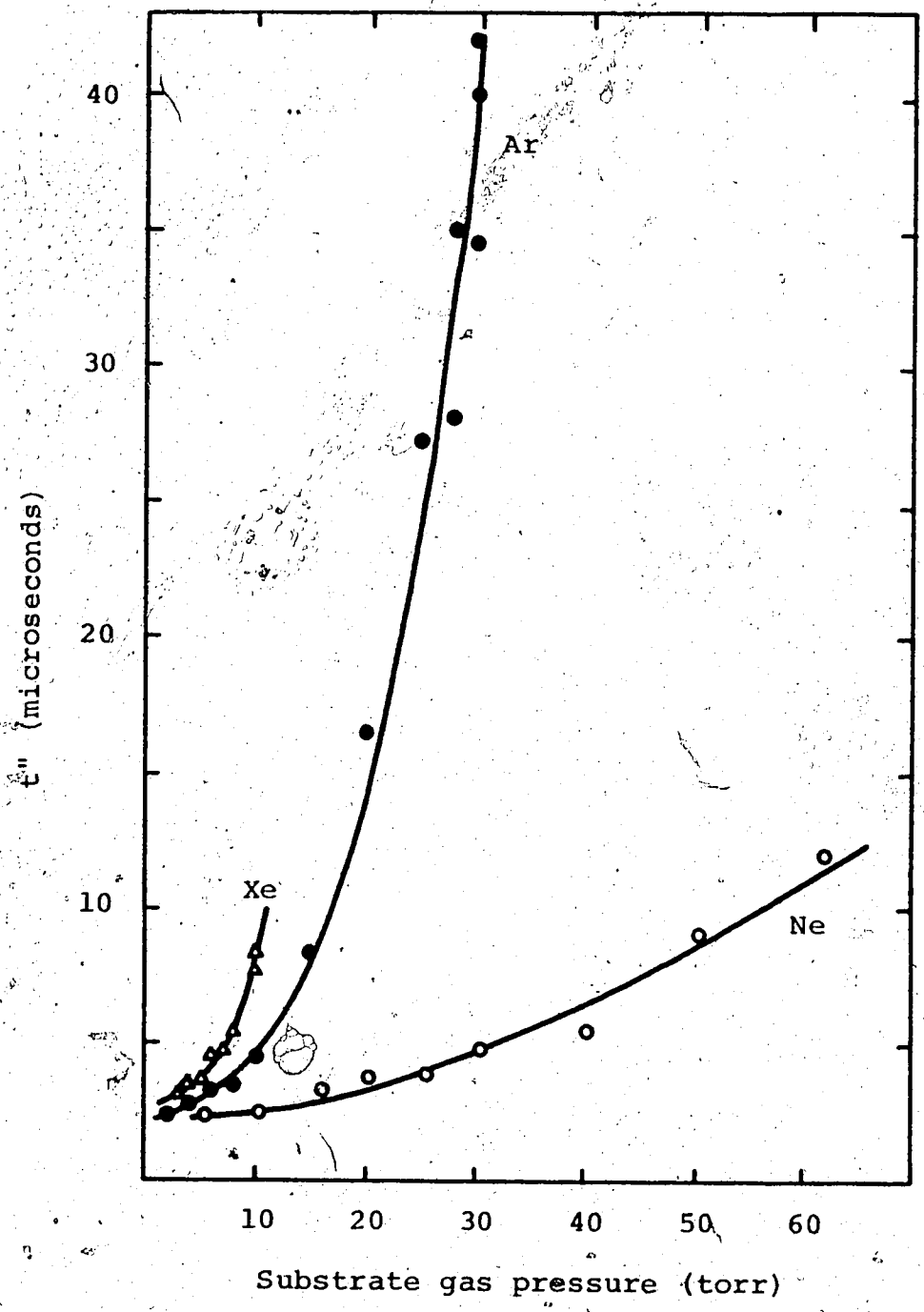

FIGURE 38: t" vs neon, argon and xenon pressure.

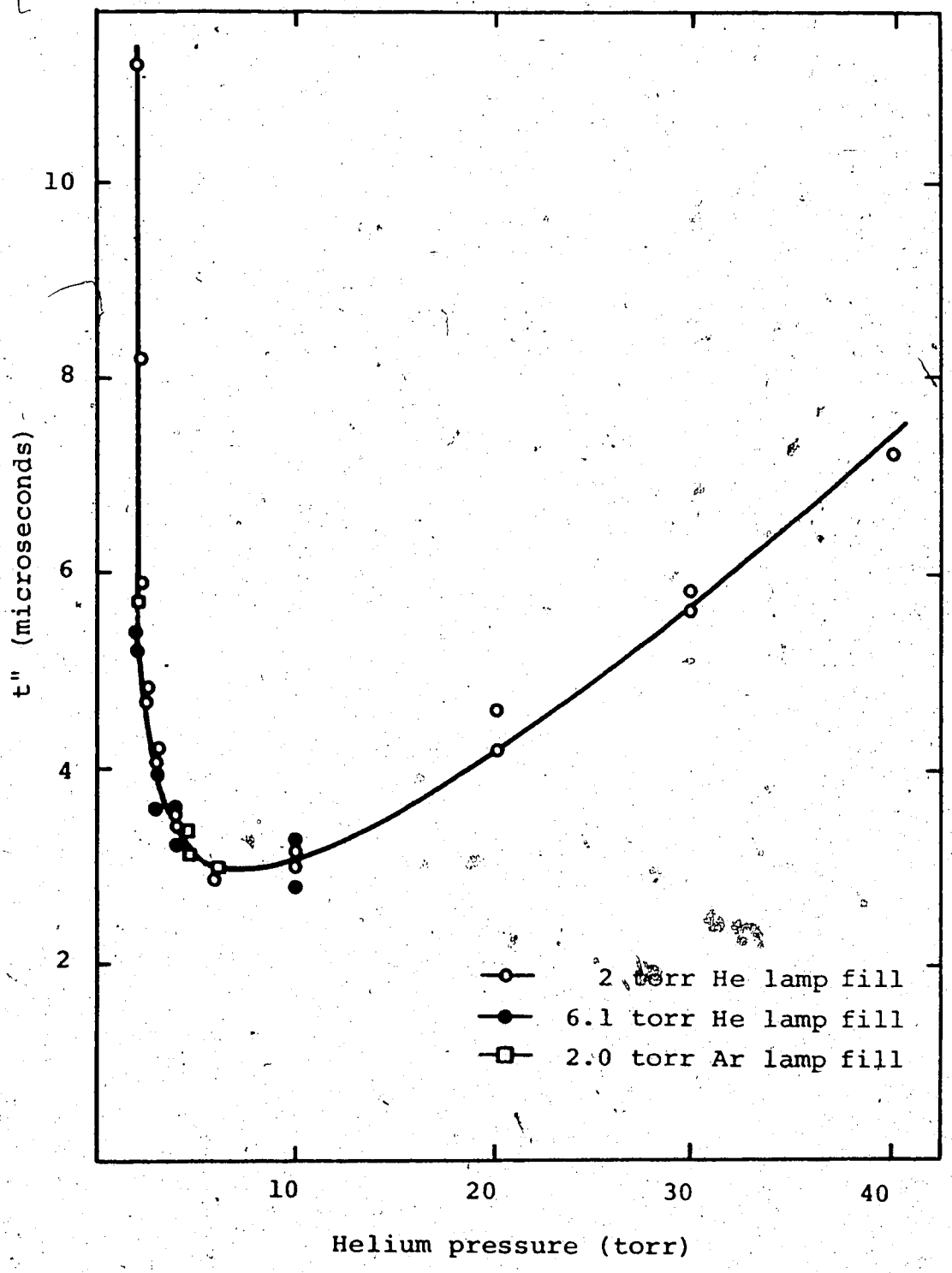

FIGURE 39: t" vs helium pressure.

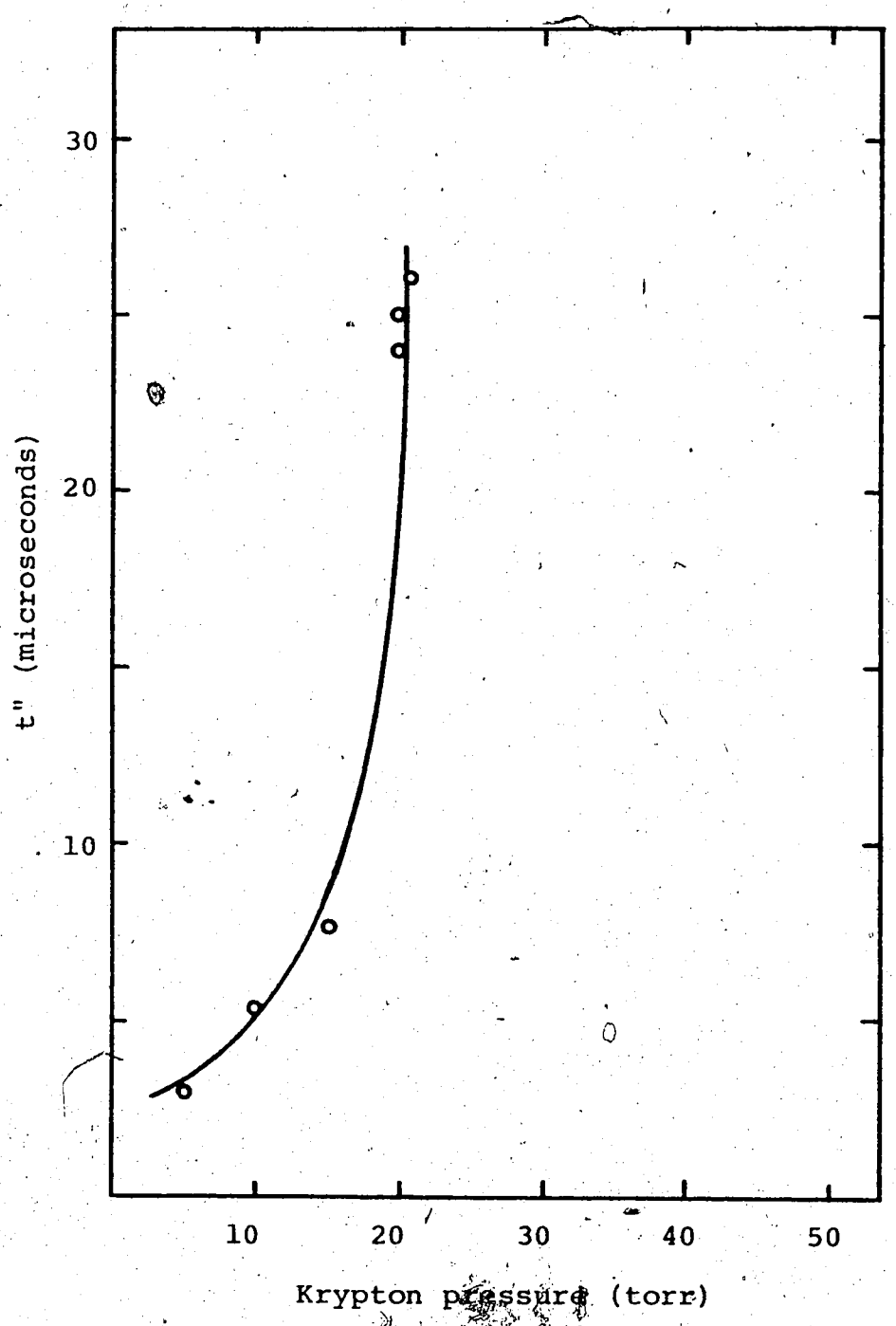

FIGURE 40: t" vs krypton pressure.

A careful search for this effect was not carried out for Kr or Xe below five and two torr, respectively.

The values of t" between two and ten torr He were not affected by increasing the lamp fill from two to six torr He or by changing it to two torr argon (Figure 40).

The mathematical expression which best fits the t" vs pressure curves in Figures 38-40 is most probably an exponential fuction. Plots of ln(t") vs noble gas pressure are shown in Figure 41-42. For comparison, a quadratic pressure dependence, which would be indicated by straight lines in (t"-t')/pressure vs substrate pressure plots, are shown in Figure 43 for argon and xenon.

The effect of temperature on the history of 2537Å light intensity using helium and argon as substrates is shown in Figures 44-45. The concentration of the two gases was 7.0×10^{-4} and 1.51×10^{-5} moles liter^{-1} respectively. An increase in t" and a marked decrease in the intensity of the second maximum as the temperature is increased is apparent from the figures. Plots of t" vs temperature (Figure 46) suggest a linear relationship between these two variables. This is a tenuous conclusion, however, due to the lack of a sufficient number of data points. The time delay of the third intensity maximum is temperature independent at approximately six microseconds but its intensity is enhanced by rising temperature.

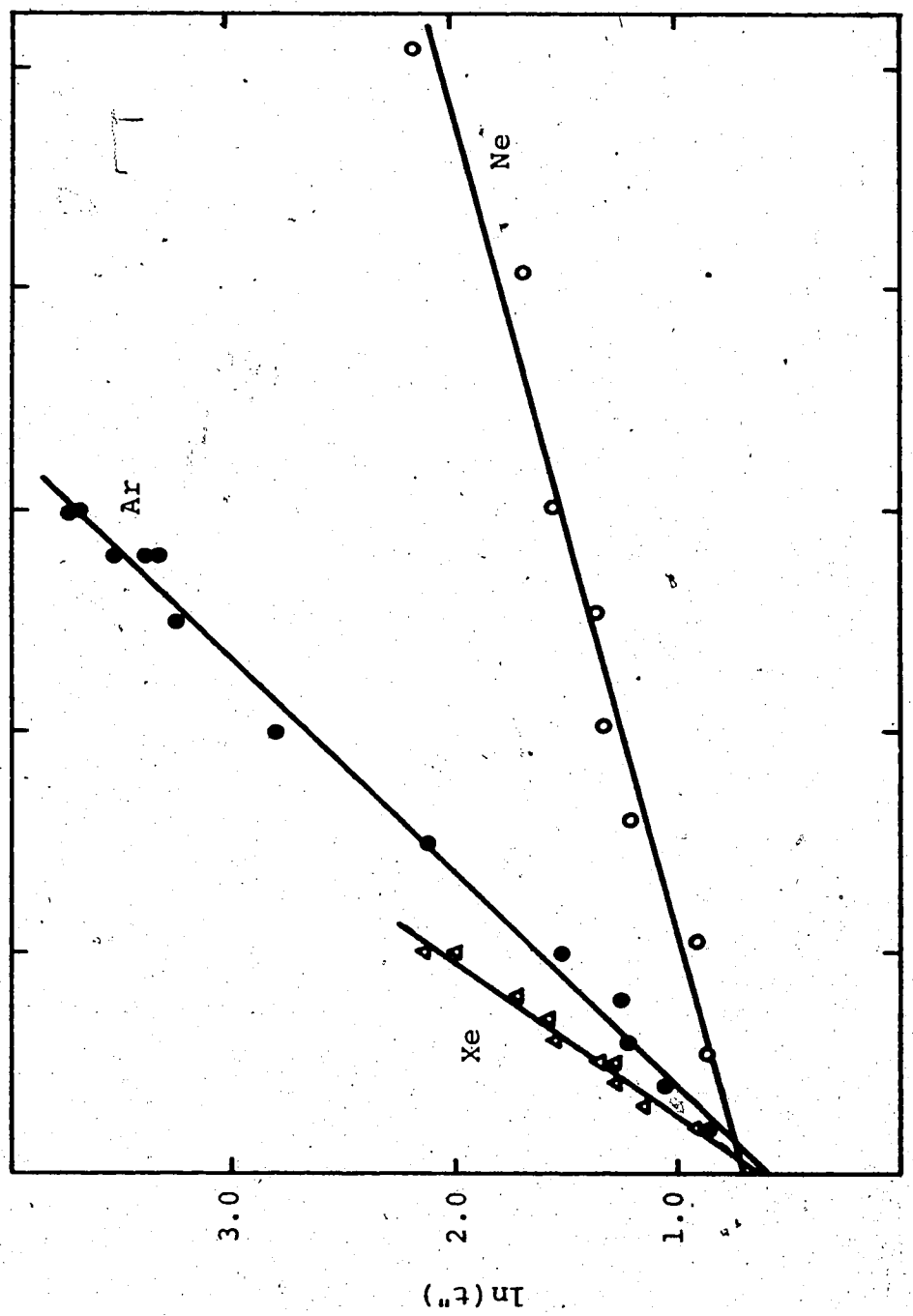

FIGURE 41: ln(t") vs neon, argon and xenon pressure.

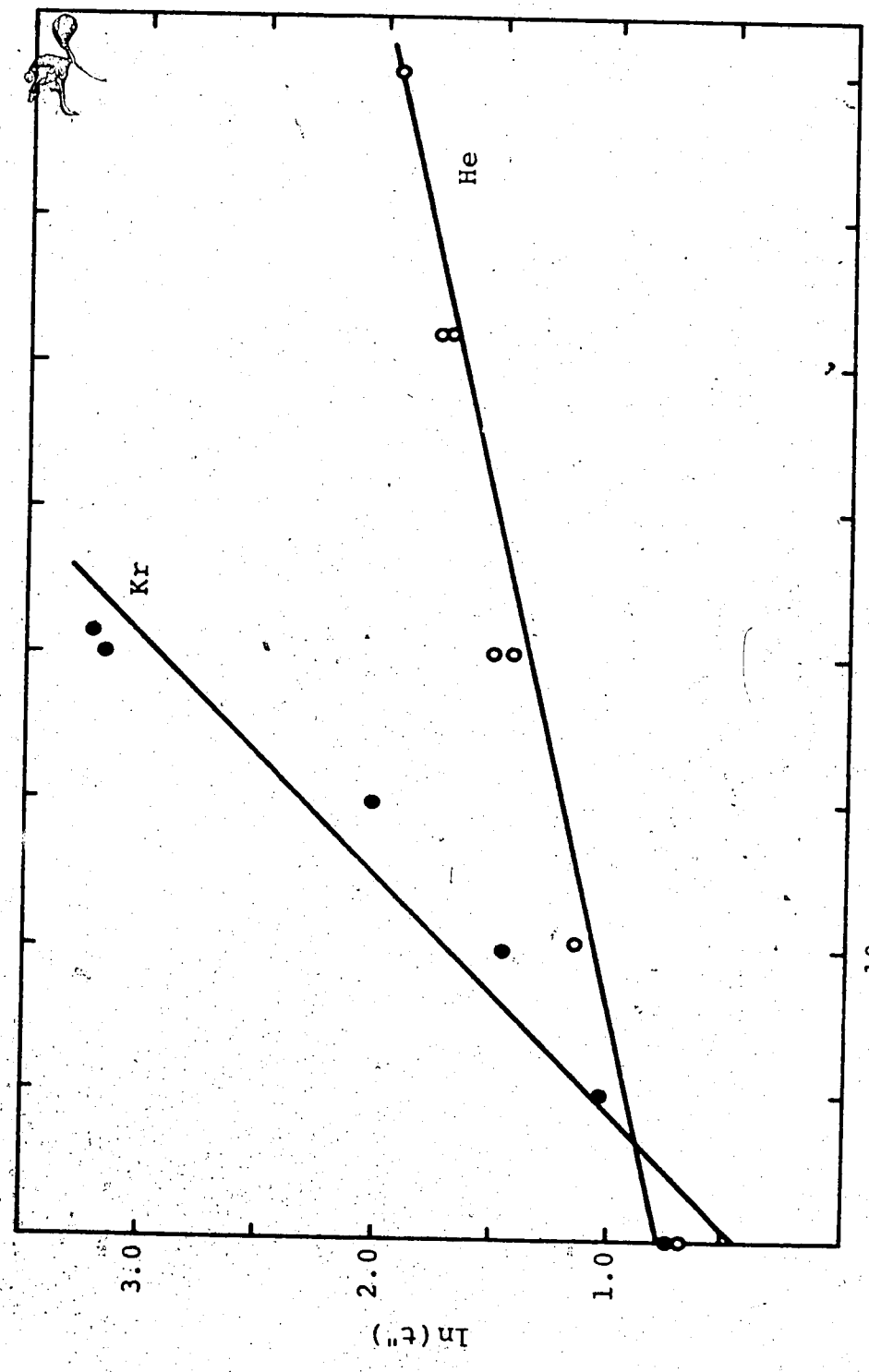

FIGURE 42: ln(t") vs helium and krypton pressure.

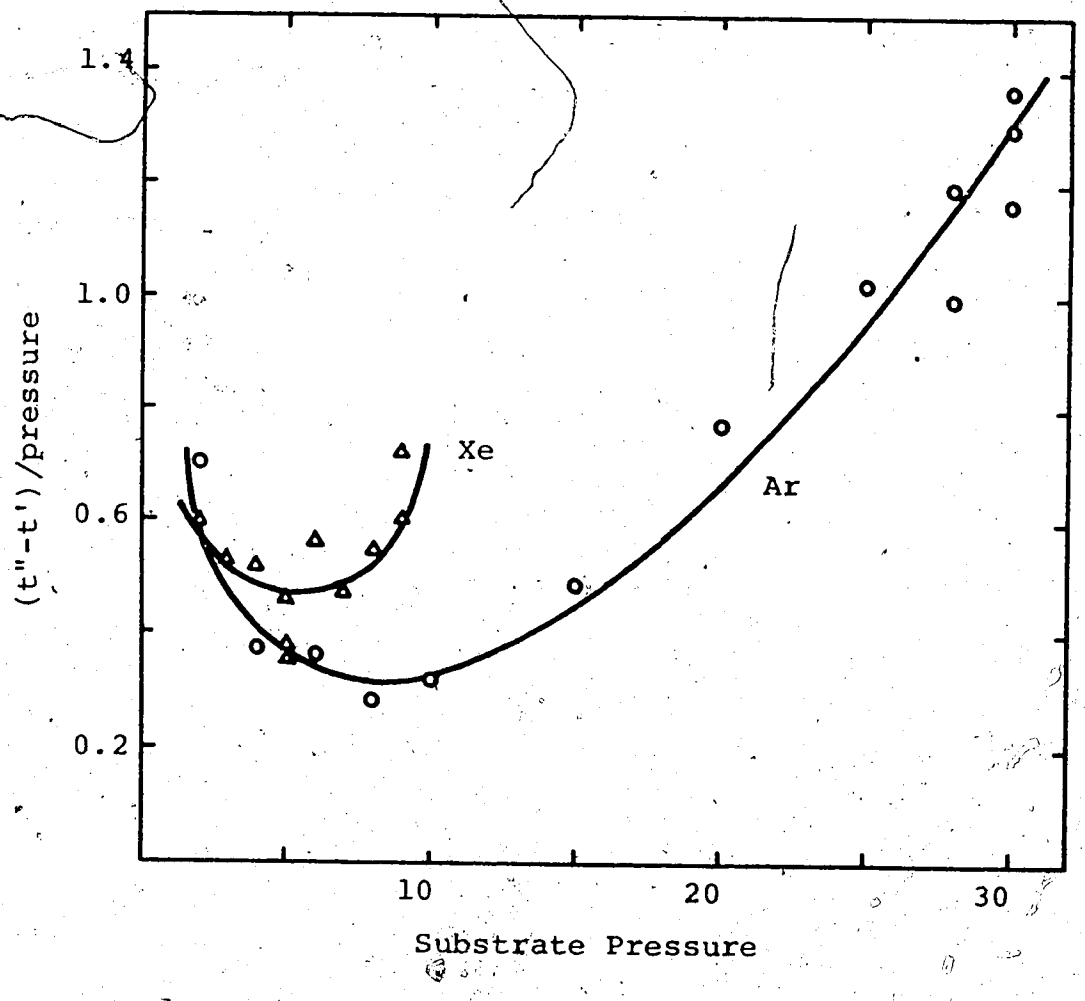

FIGURE 43: (t"-t')/substrate pressure vs substrate pressure for argon and xenon.

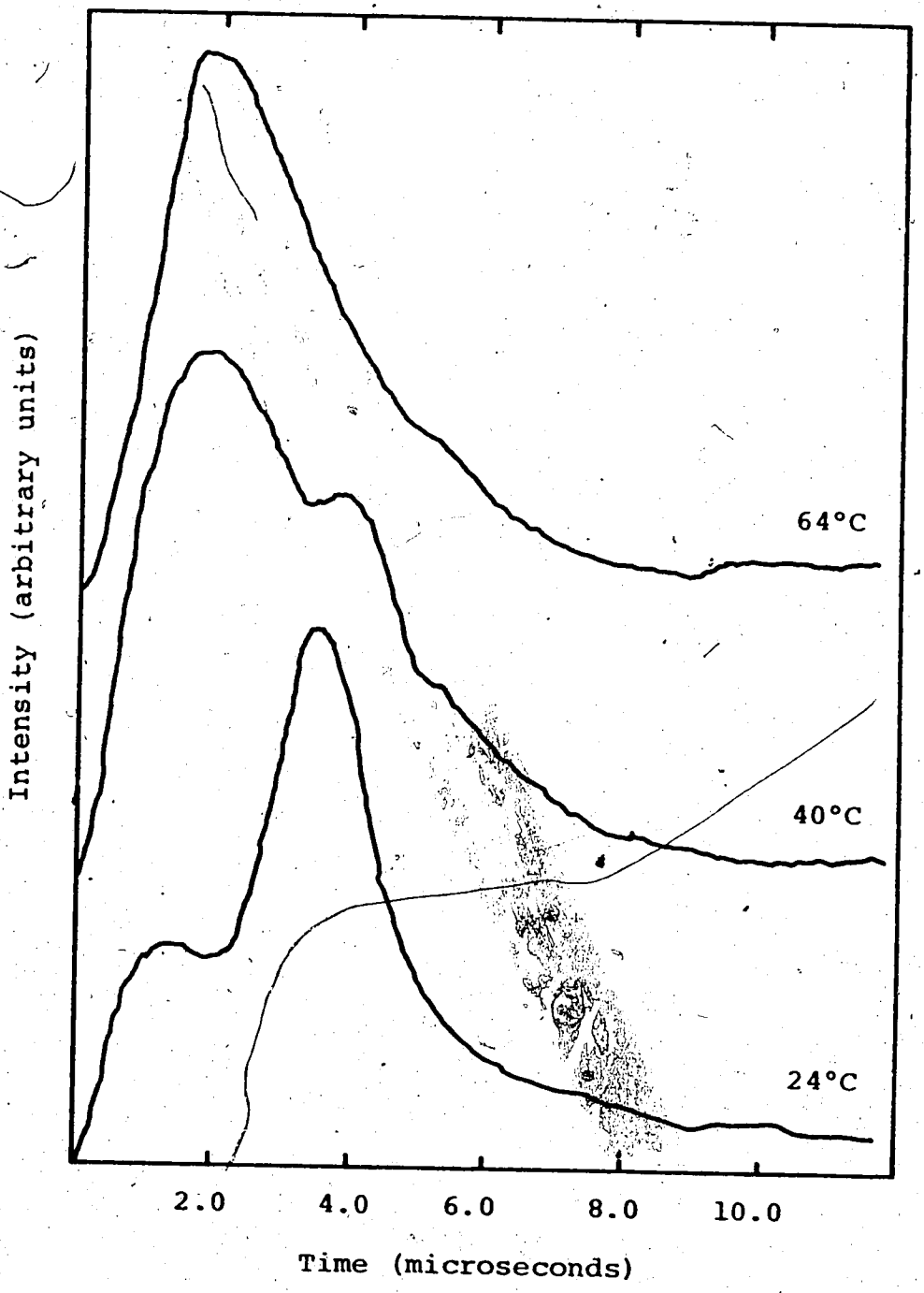

FIGURE 44: Time dependence of 2537Å intensity in the $Hg(^3P_1)$ + He system at various temperatures.

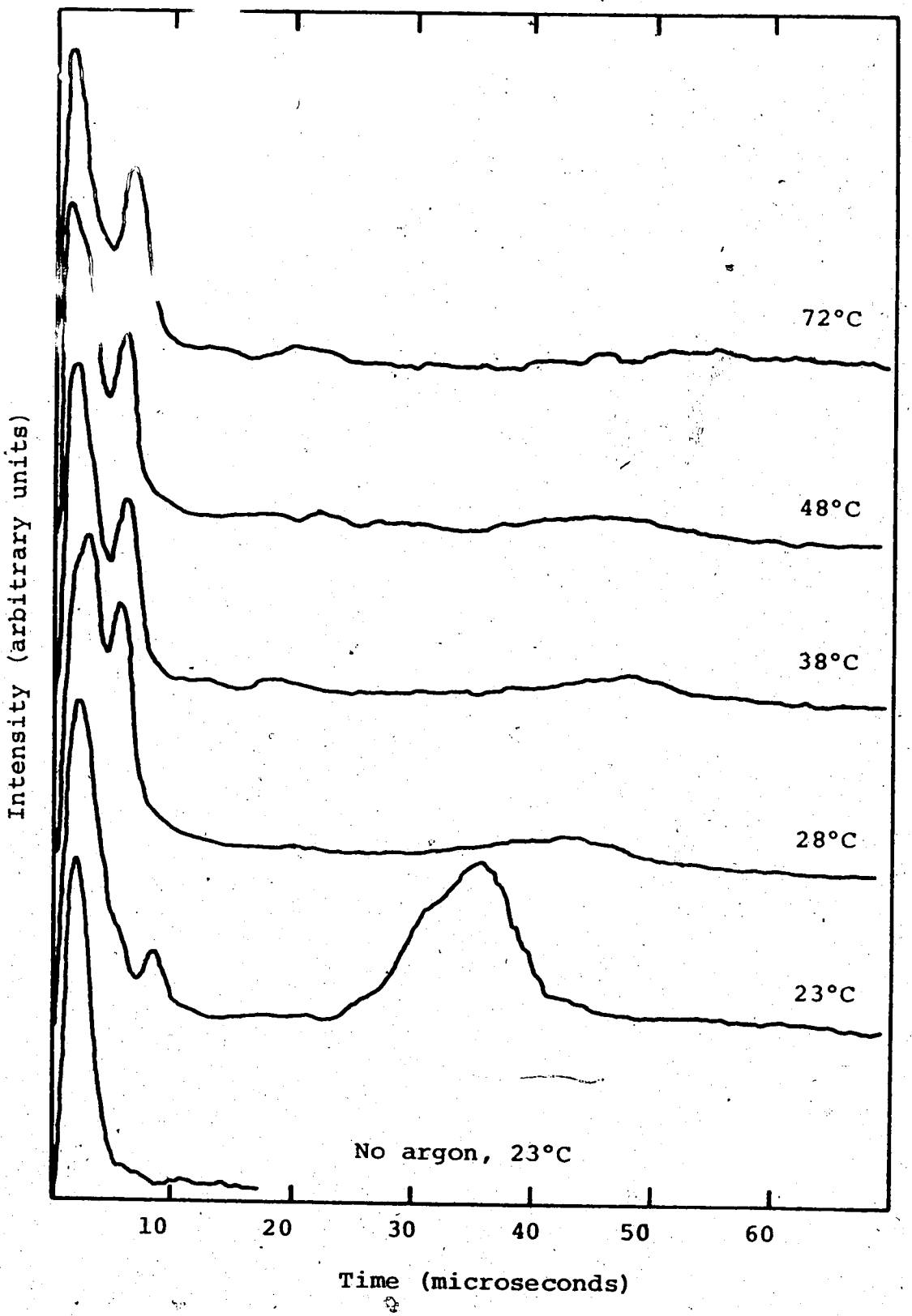

FIGURE 45: Time dependence of 2537Å intensity in the $Hg(^3P_1)$ + Ar system at various temperatures.

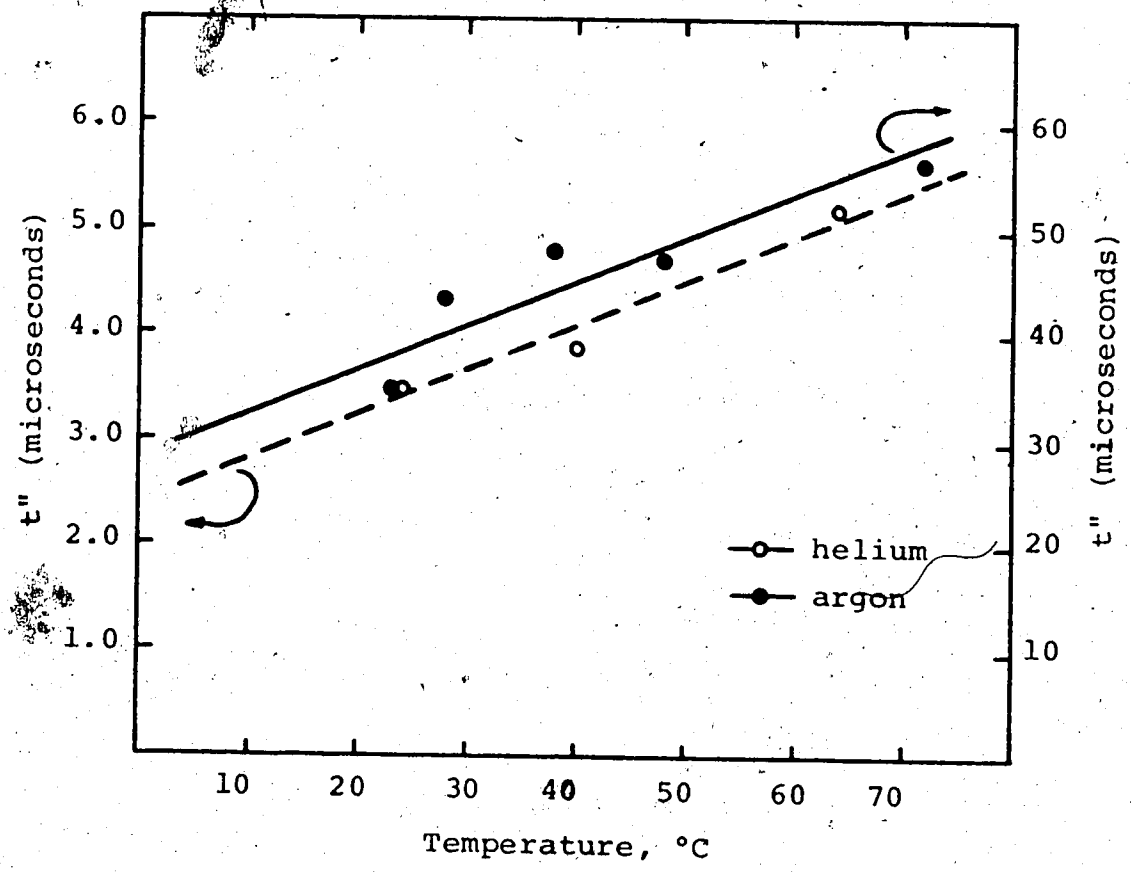

FIGURE 46: t" vs temperature for helium and argon.

The relationship between substrate pressure and t" for nitrogen and dimethylether was investigated at room temperature and at 75°C (Figures 47 and 48). Both of these gases exhibit a pressure dependence similar to that of helium below six torr. The second intensity maximum first appears at six microseconds at pressures of 0.15 and 0.060 torr, respectively, in the room temperature experiments. The second intensity peak then rapidly approaches the first as the pressure is increased, where overlapping with the flash intensity results in a distorted flash curve. Raising the cell temperature to 75°C shifts the pressure at which the second maximum is initially observed to 0.25 and 0.094 torr for N_2 and $(CH_3)_2O$, respectively, and decreases the rate at which t" converges toward t'. The intensity of the second peak was somewhat reduced at the higher temperature, but not as severely as in the case of helium or argon.

A series of runs to determine the relationship between t" and nitrogen pressure were done using 16kV firing voltage, rather than the usual 12kV, at 27°C (Figure 47). Under these conditions, the second intensity maximum first appeared at 0.09 torr and it converged towards the first peak as the pressure was increased at a greater rate than at 12kV.

Plots of ln(t") vs N_2 and $(CH_3)_2O$ pressure for the two different temperatures are displayed in Figures 49 and 50. Acceptable straight lines were obtained in all cases. A

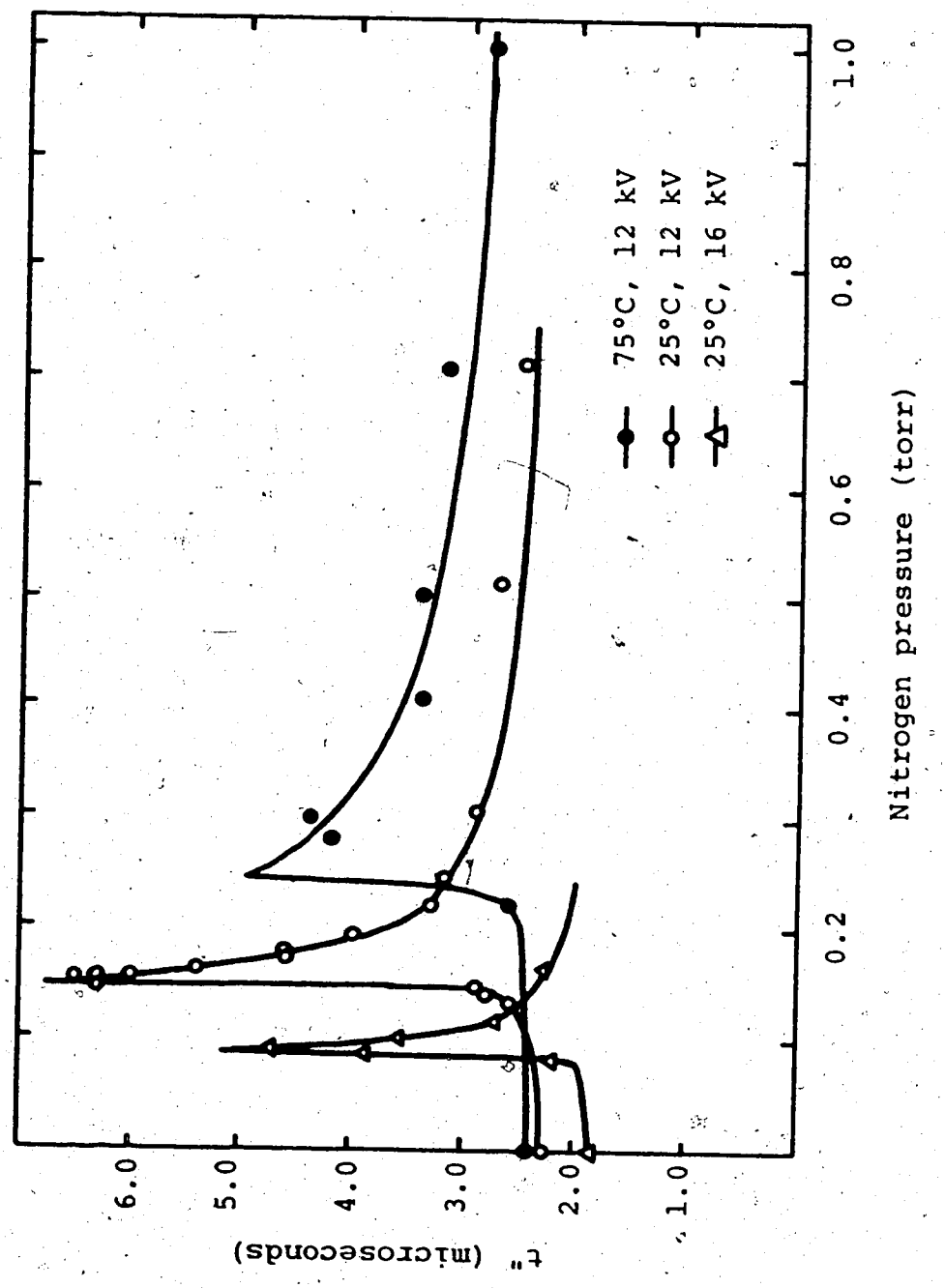

FIGURE 47: t" vs nitrogen pressure.

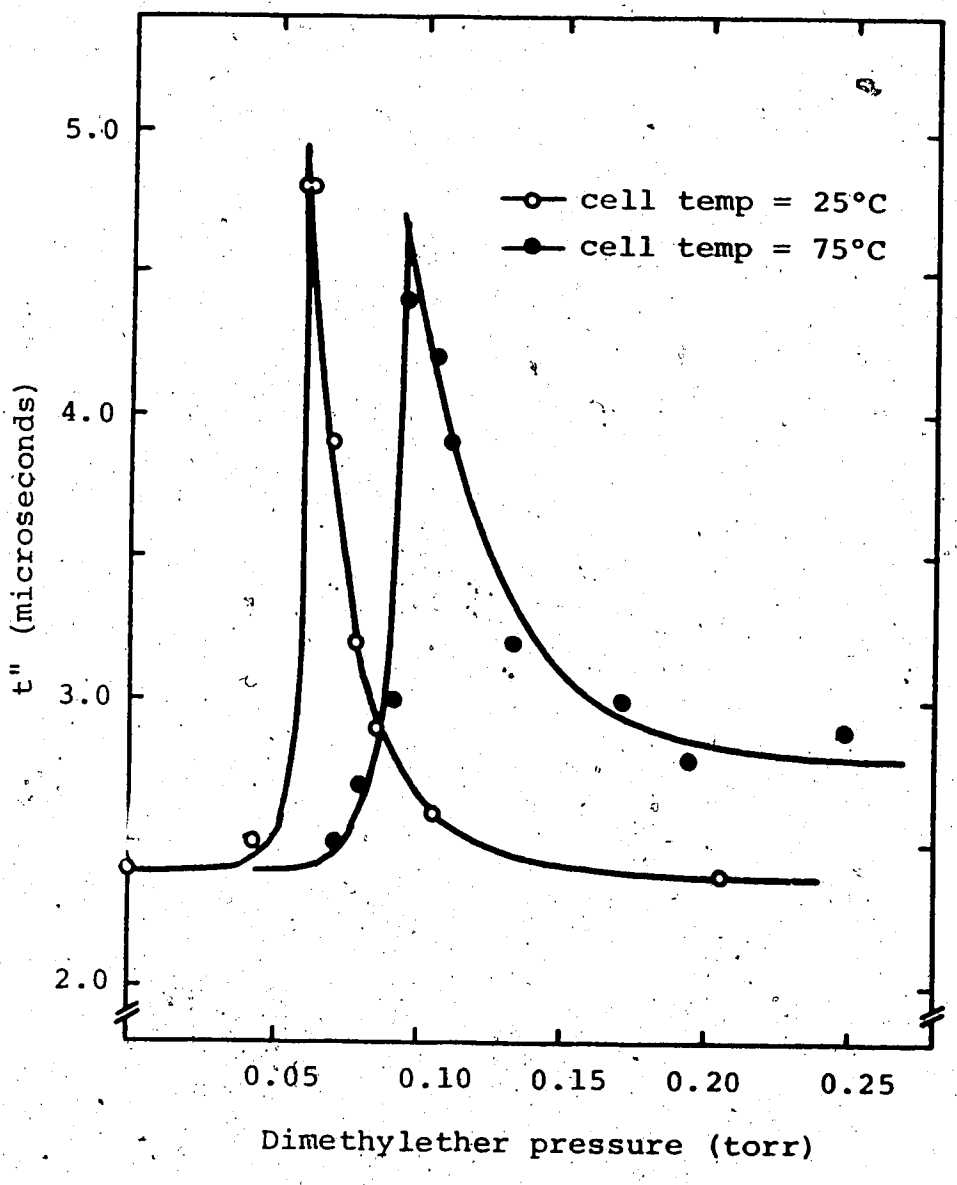

FIGURE 48: t" vs dimethylether pressure.

summary of the results for the noble gases, nitrogen and dimethylether are found in Table XI.

A second intensity maximum appearing as a shoulder on the flash profile was observed in flashed mixtures of Hg with CH_4 and C_2H_6 between 0.5 and 3.0 torr pressure at room temperature. CF_4 in the presence of Hg* showed only a distorted flash curve between 0.2 and 0.5 torr. A detailed pressure study was not carried out with these three gases due to the poor resolution of the two peaks. No auxiliary maxima were detected with hydrogen or ethylene in the region of 0.005 to 2.006 torr at ambient temperature.

Neither t" nor the relative intensity of the two peaks in Hg-He or Hg-Ar mixtures was significantly altered by changing the mercury vapour pressure from 2.1×10^{-4} to 4.9×10^{-3} torr. The cell temperature for these experiments was maintained at 27°C.

Helium and argon were employed as substrate gases in experiments to determine the wavelength distribution of emitted radiation. No intensity was detected except at 2537Å when the photomultiplier was moved to scan beyond a two angstrom region on either side of the resonance line. The slit widths to the spectrograph and photomultiplier were set at 35 microns, which allowed about a two angstrom bandwidth.

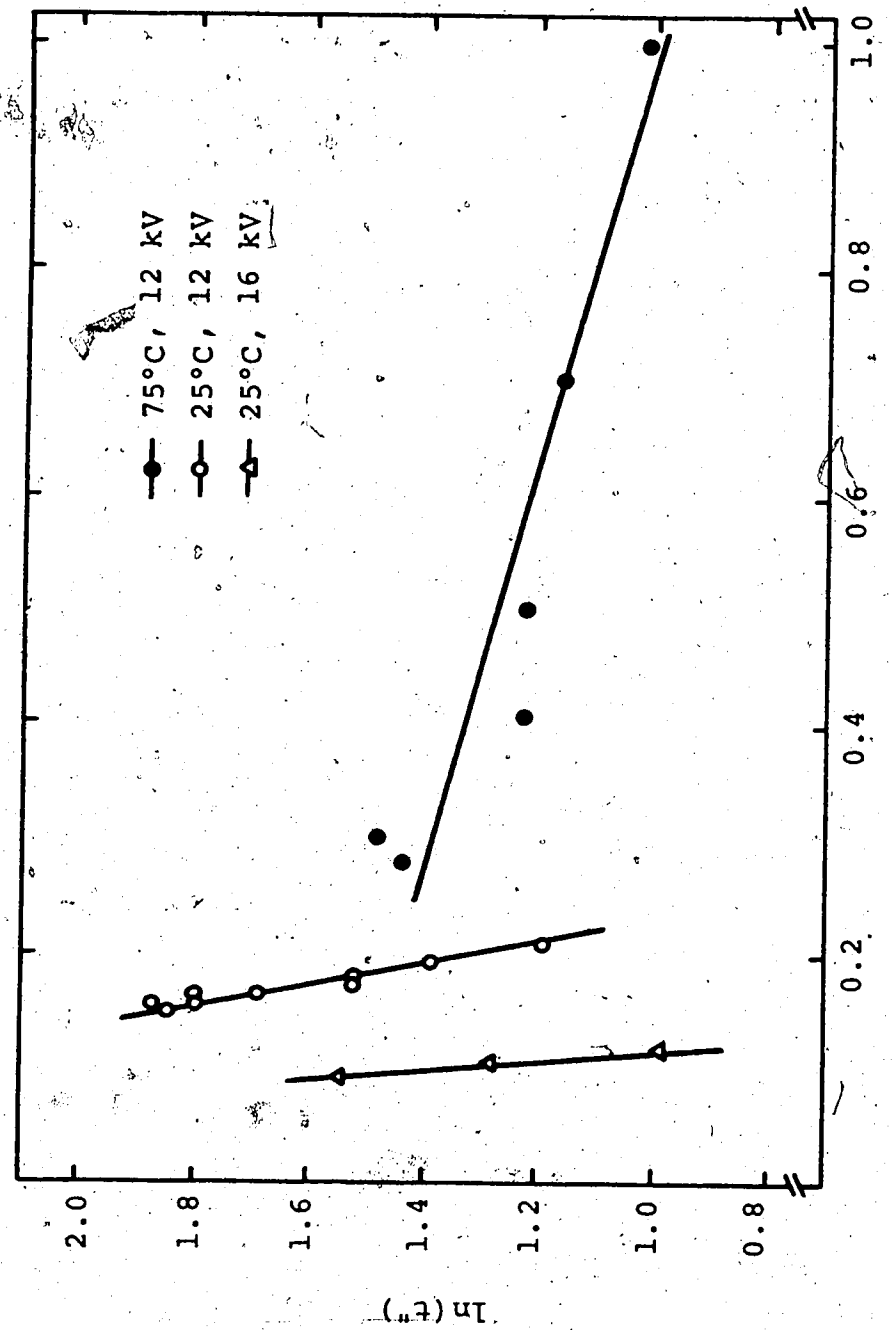

FIGURE 49: ln(t") vs nitrogen pressure.

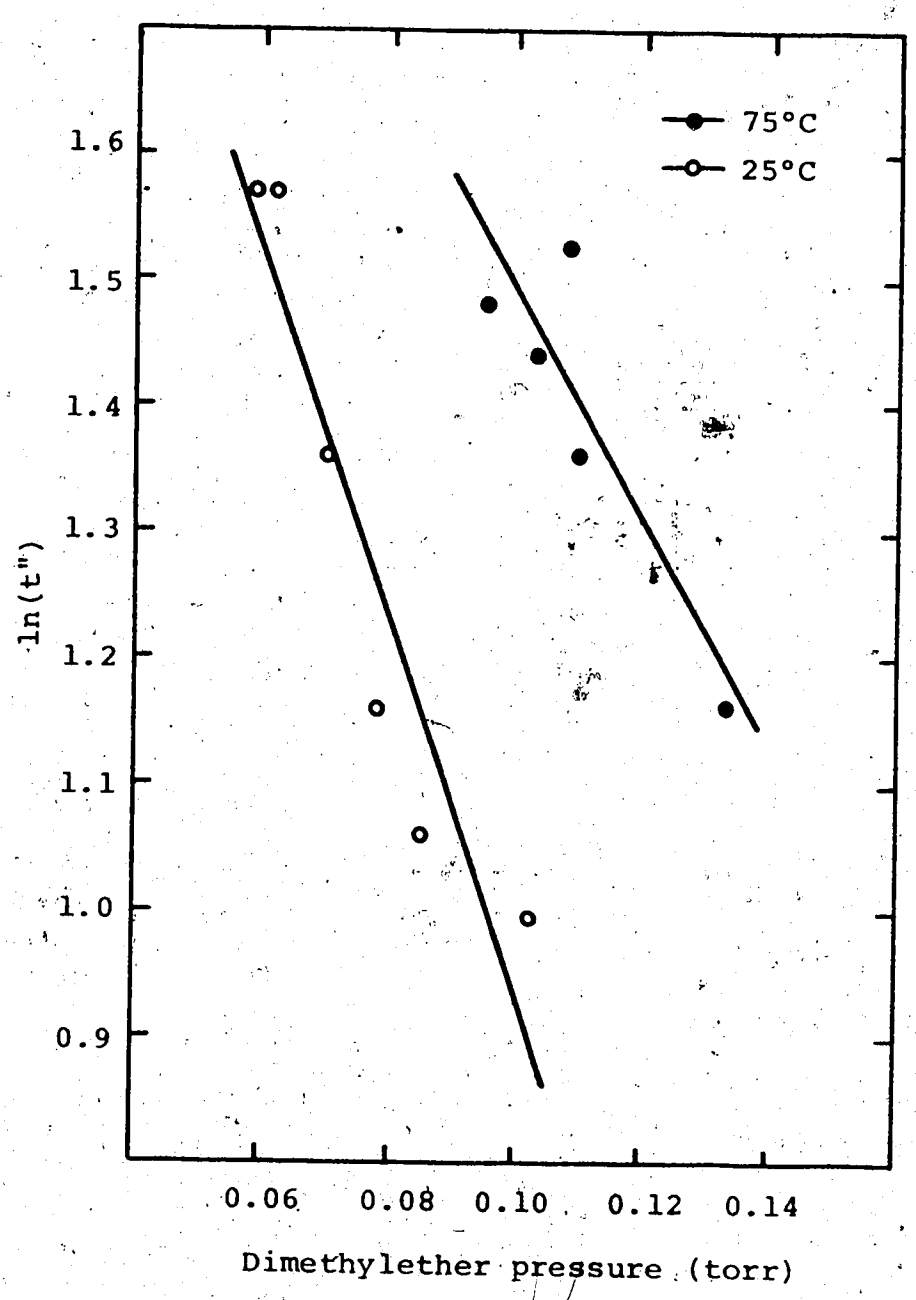

FIGURE 50: ln(t") vs dimethylether pressure.

TABLE XI

Collected Data from Time Dependence of 2537Å Intensity Measurements in Several $Hg(^3P_1)$ + Foreign Gas Systems.

compound	I.P.(a) (ev)	Cell Temp. (°C)	Pressure at largest t" (torr)	Slope of ln(t") vs Pressure Plots ($torr^{-1}$) (b)
He	24.48	26	2.0	- 0.20 ± 0.03 (c) 0.029 ± 0.002(d)
Ne	21.56	26	-	0.027 ± 0.001
Ar	15.75	23	-	0.0103 ± 0.003
Kr	14.00	23	-	0.124 ± 0.010
Xe	12.13	23	-	0.142 ± 0.008
N_2	15.576	27	0.15	-10.0 ± 0.9
		27	0.25	- 0.56 ± 0.13
		28	0.09 (e)	-23.8 ± 2.5 (e)
CH_3OCH_3	9.98	25	0.060	-14.5 ± 2.3
		75	0.094	- 9.1 ± 2.7

a. "Handbook of Chemistry and Physics", 50th ed., Chemical Rubber Publishing Co., Cleveland, Ohio, 1969.

b. Error limits given in standard deviation.

c. Determined between 2 and 6 torr.

d. Determined between 10 and 40 torr.

e. Values obtained at 16kV firing voltage.

2. Discussion.

The detection of more than one flash of 2537Å radiation emitted from some Hg*-foreign gas mixtures has apparently been previously unreported and, therefore, various explanations merit consideration. Several observations, however, suggest a likely approach to a racionalization of the phenomenon.

It is instructive to note that only those gases which exhibit band emission (23) are effective in producing a second flash. Hydrogen and ethylene do not display band emission nor do they show more than one flash. It would appear that the formation of a Hg* complex capable of radiative relaxation is a necessary requirement in order to observe additional flashes. Although band emission originates from Hg^0 complexes in ether sensitization, this does not necessarily rule out complex formation with Hg* atoms.

The intervention of an exciplex is also suggested by related observations in band emission studies (23) and the present work. For the noble gases, band emission studies have demonstrated that, due to the van der Waals nature of the interaction, there exists a trend between the polarizabilities of the reactants and the wavelengths of the band maxima. This trend is paralleled in the present study by a correlation between the ionization potential and the slope

of ln(t") plots (Figure 51). The correlation seems to lose its validity in the case of helium, however. Extrapolation of the line predicts a negative value for the slope of the ln(t") plot for this substrate. Helium does possess a negative value but also a positive value (see Table XI), both of which lie outside of the range allowed by experimental error. Lack of sufficient information about molecular substrates prevents an analysis of the results obtained with nitrogen and dimethylether.

This phenomenon displays properties in common with lasers. The auxiliary maximum is reminiscent of the spiking which is often observed, such as in the chemical lasers produced from $O(^3P)$ atom reactions in the gas phase (152) or rare earth ion chelate lasers (153). It is interesting to note that in some cases, spiking occurs before the flash intensity maximum was reached, as occurred in some of the present experiments. It has been known for some time (154) that laser emission can be detected without mirrors if the laser medium is excited by an intense electrical discharge, in which case the laser is said to be superradiative. Lempiki and Heller (155) detected laser emission using a flash apparatus from a Nd^{+3} ion in $SeOCl_2$ solution contained in a tube that was roughly sealed off at each end. These observations provides evidence that under certain conditions, laser emission may be detected in simple systems like the present apparatus. Recent publications (156-162) have

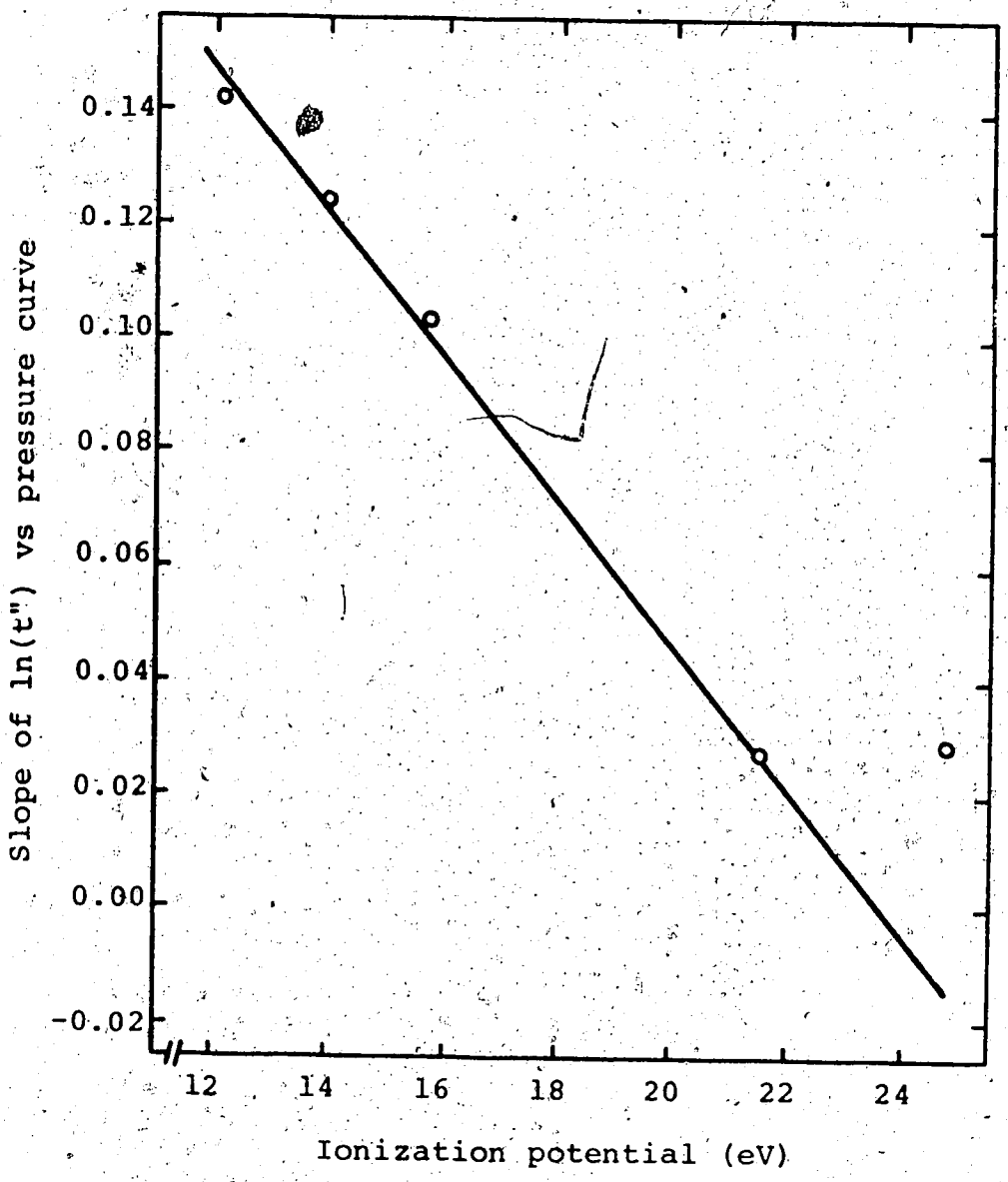

FIGURE 51: Slopes of ln(t") curves as a function of the ionization potential of the noble gases.

reported laser emission in the vacuum ultraviolet from Xe_2* molecules. The delay time for laser initiation (162) and for peak output (157) decreases as the pressure is increased. Premature termination of laser emission was attributed to heating of the xenon gas (162). The effect of pressure and temperature on the temporal behavior of the second emission flash in the present study may be due to the influence of these variables on the populations of the two states involved in laser emission. The changes in the time dependence of the 2537Å radiation in Hg-N_2 mixtures as a result of increasing the firing voltage points to the fact that laser output depends on the intensity of optical pumping (163).

On the basis of the foregoing discussion, it would seem that a laser is possible in Hg*-foreign gas systems where complex formation occurs. It is obvious that the production of (Hg-substrate)* exciplexes immediately creates a population inversion owing to the practically non-existent ground state population of these molecules. The fact that the emitted radiation is in the region around 2537Å is not inconsistent with this suggestion since the band spectra exhibit appreciable pressure broadening of the resonance line. The second flash intensity may simply be due to the band emission radiation in this wavelength region. A reason why band emission could not be detected except around 2537Å may be that only a small fraction of the total band radiation is emitted at these other wavelengths. The observable intensity

would be further reduced on account of the narrow slit widths used in the measurements.

The comparatively high intensity of the second flash implies that efficient production of (Hg-substrate)* complexes takes place. This does not disagree with low $(\sigma^*)^2$ values reported for some of the foreign gases studied, since a large portion of the quenching act would result in re-emission of radiation arcund 2537Å that would be ascribed to unquenched Hg* atoms.

The proposed model suggests that the complexes have radiative lifetimes at least as great as the longest observed delay times for the second flash. This would mean that Hg* complexes with the molecular substrates studied have radiative lifetimes of a few microseconds but that complexes with the noble gases have radiative lifetimes between 10 and 100 microseconds.

A schematic reconstruction of the events which give rise to the intensity profiles shown in Figure 37 may be formulated. As Hg* atcms are generated by the primary excitation a certain fraction will undergo radiative relaxation, evidenced by the first intensity peak, while some will form (Hg-substrate)* exciplexes. A laser burst from these exciplexes may be emitted after a period of time determined by various process, some of which depend on the pressure of the foreign gas. In Hg*-noble gas systems, however, the

laser emission may be preceded by a long period of time in which low intensity spontaneous radiation depletes the upper state population. This accounts for the decreasing intensity of the second flash as the delay time for laser initiation is increased. More than one laser flash is possible if the first occurs prior to extinction of the exciting light or if some exciplex population remains after the first laser burst.

Owing to the unsuitability of the apparatus used, appropriate spectral studies of the emission flashes could not be accomplished. For this reason, the mechanism responsible for the appearance of the second and third emission flashes could not be conclusively established.

This phenomenon would not affect the results obtained in the Hg^0 quenching by molecular substrates described in Chapter IV since it cannot be seen at the high pressures used in the experiments. Moreover, the data points used to determine $1/\tau$ were taken approximately 50 microseconds after the flash. This is beyond the limits at which auxiliary maxima were observed for the molecular substrates.

Brief mention is made here of observation of weak flashes of visible light emitted from the capillary tube of a McLeod gauge, seen when certain gases were being prepared for the present study. A closer investigation disclosed that the flashes are produced by an electrical discharge which

usually attends the separation of electrical charge brought about by the movement of a body of liquid mercury in contact with a glass surface. Because of this origin, the flashes are unrelated to optical phenomena involving gaseous mercury and substrate in the vapour phase only, such as band emission (Chapter V) or the time dependence of radiation at 2537Å noted above. For this reason, a detailed account of the study investigating the phenomenon responsible for the visible flashes would be out of place here, but is presented in Appendix D.

CHAPTER VII

SUMMARY AND CONCLUSIONS

The interaction of Hg^* and Hg^0 atoms with various substrates has been examined in detail. Particular emphasis was placed on elucidating the involvement and reactivity of Hg^0 atoms since this point has been the subject of much debate in the literature.

The results of Hg^0 atom quenching for alkanes demonstrate that the Hg^* initiated reactions of these substrates can be interpreted in terms of the energetics involved. Qualitative potential energy surfaces, displayed in Figure 17, explain a number of observations made in these systems:

(i) the quenching of Hg^0 atoms proceeds via formation of an excited complex which may relax via
   (a) redissociation to reactants
   (b) fragmentation of the substrate to yield ground state mercury atoms, and
   (c) thermal re-excitation back to the Hg^* level.

(ii) quenching cross-sections for Hg^0 atoms are all less than the corresponding $(\sigma^*)^2$ values due to a shallower potential well which results in a higher probability for redissociation of the $(HgHR)^0$ than

the $(HgHR)^*$ complex.

(iii) the trends observed for Hg^0 atom quenching by 1^0, 2^0 or 3^0 C-H bonds and the effect of deuterium substitution implies that quenching efficiency is a sensitive function of the activation energy involved in the abstraction of a hydrogen or deuterium atom.

(iv) the effect of temperature on the quenching cross-sections depends on the particular alkane. Strong quenchers of Hg^0 atoms exhibit a negative temperature effect which may be attributed to the intersection of a potential energy surface, which correlates with decomposition products, within the potential well of the $(HgHR)^0$ complex. In this case, increasing the temperature would favor redissociation of the complex over the decomposition process, which may be assumed to be temperature independent. Therefore, the quenching rate would be reduced. Weak quenchers, on the other hand, show little variation in $(\sigma^0)^2$ values with an increase in temperature. For these alkanes it is suggested that, despite a possible increase in the rate of decomposition, another relaxation process (probably intersystem crossing to the ground state of the complex (108)) decreases to such an extent that little little or no net change in the

quenching rate results.

It was shown that emission from Hg* atoms, formed from thermal re-excitation of Hg^0 atoms to the $^3P_1$ level, is the principle mode by which Hg^0 atoms are relaxed in the Hg-N_2 system. This fact has a profound effect on the measurement of $(\sigma^0)^2$ values for very weak quenchers of Hg^0 atoms such as CH_4 and Xe. It was demonstrated that these two gases interact primarily with Hg* atoms. Further evidence to support this view in the case of Xe was obtained from observations of band emission in various Hg-N_2-Xe mixtures.

Band emission in the mercury sensitization of ethers was photographed for the first time. The emission was attributed to radiative transitions from $(Hg\text{-ether})^0$ complexes from comparision with $(Hg\text{-alcohol})^0$ spectra and the similarity of their reactivity towards Hg^0 atoms. The intensity of the band emission depends on the degree to which emission from the complex can compete with decomposition. On the basis of H/D kinetic isotope effects in the quenching of Hg^0 atoms, decomposition of the ethers proceeds via α-hydrogen abstraction. The trend in the position of the band intensity maxima is due to the varying ability of the alkane substituents to donate electrons to the oxygen atom by the inductive effect.

The spectroscopic and kinetic data presented demonstrate that Hg^0 atoms play an important role in Hg-ether

photosensitized systems. Consequently, the interpretation of experimental results based solely on reaction of Hg* atoms (126-129) is not entirely complete.

A detailed quenching mechanism for Hg^0 atoms by ethers and alcohols has been proposed, based on data obtained from quenching measurements, band emission and photosensitized decomposition kinetic studies (125-129) of these systems. It would appear that Hg* atoms are quenched primarily to the metastable state. Hg^0 atoms form complexes with ether molecules which possess greater stability than the alkane exciplexes owing to the greater nucleophilicity of the oxygen atom. Band emission arises from radiative decay of the complex while the Hg^0 is held to the oxygen atom and free from perturbation by hydrogens on the alkane substituent. The configuration of the Hg^0-oxygen bound complex may become distorted in such a way as to allow a change to a configuration where the Hg^0 atom interacts strongly with a nearby hydrogen atom. Decomposition of the ether may then result. This model accounts for

(i) the observed deuterium isotope effect in the α-position to the oxygen,

(ii) the decrease in the $(\sigma^0)^2$ values with increasing temperature due to the lower probability of attaining the configuration suitable for decomposition and

(iii) the lower reactivity of Hg^0 than Hg* atoms, because of the different mechanisms by which these two atoms are quenched.

Sulphur-containing organic compounds appear to quench Hg* atoms predominantly via spin-orbit relaxation. Hg^0 atoms form complexes with these substrates which may redissociate or decompose via C-S bond rupture. The different quenching mechanisms involved are compatible with $(\sigma^0)^2$ values being lower than the $(\sigma^*)^2$ values for the same substrate. Unlike the case for the oxygen-containing compounds, a transfer of the Hg^0 interaction site from the sulphur to a hydrogen atom is not required in the decomposition process. The crossover leading to fragmentation of the substrate lies below the energy of the separated particles, since increasing the temperature results in a decrease in the quenching rate. Radiative relaxation of $(HgSR_2)^0$ complexes can be expected have a very low probability due to the high efficiency of he decomposition reaction.

Relaxation of Hg^0 atoms in the presence of ammonia proceeds by second and third order kinetics at room temperature but by second order kinetics alone at 70°C. The fact that the quenching of Hg^0 atoms decreases as the temperature is raised can be attributed to the decreasing contribution to the decay rate by the third order process. In order to account for the increasing quantum yield of decomposition as

the temperature is increased (101), the inclusion of a decomposition reaction involving Hg^0 atoms is required.

$(HgQ)^0$ complexes, where Q = Hg, alkane, alcohol, NH_3 or a mercaptan, are remarkably stable to collisional deactivation. This was indicated by the lack of a measurable effect on the $(\sigma^0)^2$ values due to varying the concentration of N_2, or by the fact that ammonia did not affect the radiative lifetime of the $(HgNH_3)^0$ complex at higher NH_3 pressures.

Aromatic molecules quench both Hg^* and Hg^0 atoms with high efficiency. A deuterium isotope effect observed for C_6H_6 and C_6D_6 implies that quenching proceeds by the formation of a complex which undergoes intersystem crossing prior to decomposing tc a ground state mercury atom and an excited aromatic molecule. Apparently the rate of intersystem crossing is decreased by deuterium substitution (116, 117).

A complex time dependence of the 2537Å radiation has been observed in flashed mixtures of mercury and the noble gases, nitrogen and dimethylether. Several intensity maxima may be present, the number, position and relative intensities of which depend on the nature and pressure of the foreign gas, cell temperature and intensity of the incident radiation. Auxiliary maxima were noted only for those gases which display band emission. A correlation exists between the dependence of the position of the second maximum as a

function of noble gas pressure and their ionization potential. Since the noble gases and nitrogen both produce this effect, the presence of Hg^0 atoms does not seem to be involved. These and other characteristics of the time dependence of the 2537Å intensity indicate that (Hg-foreign gas)* exciplexes are involved, possibly in a laser mechanism. Further experimental work is required to elucidate the processes responsible for this unusual behavior of the 2537Å intensity.

BIBLIOGRAPHY

1. J.G. Calvert and J.N. Pitts, "Photochemistry", John Wiley and Sons, Inc., 1966, ch. 2.
2. G. Cario and J. Franck, Zeits. Physik, 11, 161(1922).
3. H.E. Gunning and O.P. Strausz, Adv. in Photochem., 1, 209(1963).
4. R.J. Cvetanovic, Prog. in Reac. Kin., 2, 39(1964).
5. A. Lurio, Phys. Rev., 140, 1505(1965).
6. M.C. Bigeon, J. Physique, 28, 51(1967).
7. J.V. Michael and C. Yeh, J. Chem. Phys., 53, 59(1970).
8. E.A. Milne, J. London Math. Soc., 1, 40(1926).
9. E.W. Samson, Phys. Rev., 40, 940(1932).
10. T. Holstein, Phys. Rev., 72, 1212(1947); 83, 1159(1951).
11. D. Alpert, A.O. McCoubrey and T. Holstein, Phys. Rev., 76, 1259(1949).
12. B.V. Waddell and G.S. Hurst, J. Chem. Phys., 53, 3892 (1970).
13. L.M. Biberman, Zh. Eksperim. i Teor. Fiz., 17, 416(1947); 19, 584(1949).
14. P.J. Walsh, Phys. Rev., 116, 511(1959).
15. K. Yang, J. Am. Chem. Soc., 88, 4575(1966).
16. S. Mrozowski, Rev. Mod. Phys., 16, 153(1944).
17. O. Oldenberg, Zeits. Physik, 47, 184(1927); 49, 609(1928); 50, 580(1928); 51, 40, 605(1928); 55, 1(1929).
18. H. Kuhn and O. Oldenberg, Phys. Rev., 41, 72(1932).

19. R.W. Wood, Proc. Roy. Soc., A106, 679 (1924).

20. E. Gaviola and R.W. Wood, Phil. Mag., 6, 1191 (1928).

21. G. Glockler and F.W. Martin, J. Chem. Phys., 2, 46 (1934).

22. S. Penzes, O.P. Strausz and H.E. Gunning, J. Chem. Phys., 45, 2232 (1966).

23. J.M. Campbell, Ph.D. Thesis, University of Alberta, 1972.

24. H.E. Gunning, S. Penzes, H.S. Sandhu and O.P. Strausz, J. Am. Chem. Soc., 91, 7684 (1969).

25. C.G. Freeman, M.J. McEwan, R.F.C. Claridge and L.F. Phillips, Chem. Phys. Letters, 6, 482 (1970).

26. R.H. Newman, C.G. Freeman, M.J. McEwan, R.F.C. Claridge and L.F. Phillips, Trans. Faraday Soc., 66, 2827 (1970).

27. C.G. Freeman, M.J. McEwan, R.F.C. Claridge and L.F. Phillips, Chem. Phys. Letters, 5, 555 (1970).

28. C.G. Freeman, M.J. McEwan, R.F.C. Claridge and L.F. Phillips, Chem. Phys. Letters, 8, 266 (1971).

29. C.G. Freeman, M.J. McEwan, R.F.C. Claridge and L.F. Phillips, Chem. Phys. Letters, 9, 578 (1971).

30. J. Koskikallio, A.E. Callear, and J.H. Connor, Chem. Phys. Letters, 8, 467 (1971).

31. C.G. Freeman, M.J. McEwan, R.F.C. Claridge and L.F. Phillips, Trans. Faraday Soc., 66, 2974 (1970).

32. C.G. Freeman, M.J. McEwan, R.F.C. Claridge and L.F. Phillips, Trans. Faraday Soc., 67, 67 (1971).

33. C.G. Freeman, M.J. McEwan, R.F.C. Claridge and L.F. Phillips, Trans. Faraday Soc., 67, 2567 (1971).

34. R.H. Newman, C.G. Freeman, M.J. McEwan, R.F.C. Claridge and L.F. Phillips, Trans. Faraday Soc., 67, 1360 (1971).

35. C.G. Freeman, M.J. McEwan, R.F.C. Claridge and L.F. Phillips, Trans. Faraday Soc., 67, 3247 (1971).

36. C.G. Freeman, M.J. McEwan, R.F.C. Claridge and L.F. Phillips, Trans. Faraday Soc., 67, 2004 (1971).

37. R.W. Wood, Zeits. Physik, 13, 353 (1912).

38. A.J. Yarwood, O.P. Strausz and H.E. Gunning, J. Chem. Phys., 41, 1705 (1964).

39. A.C.G. Mitchell and M.W. Zemansky, "Resonance Radiation and Excited Atoms", The Macmillan Co., New York, 1934.

40. M.W. Zemansky, Phys. Rev., 36, 919 (1930).

41. K. Yang, J. Am. Chem. Soc., 87, 5294 (1965).

42. M.G. Bellas, Y. Rousseau, O.P. Strausz and H.E. Gunning, J. Chem. Phys., 41, 768 (1964).

43. R. Payette, M. Bertrand and Y. Rousseau, J. Am. Chem. Soc., 90, 5341 (1968).

44. C.G. Matland, Phys. Rev., 92, 637 (1953).

45. S. Penzes, Ph.D. Thesis, University of Alberta, 1968

46. Y.K. Bykhovskii and E.E. Nikitin, Opt. and Spectrosc., 16, 111 (1964).

47. G. Karl, P. Kruus and J.C. Polanyi, J. Chem. Phys., 46, 224 (1967).

48. G. Karl, P. [illegible], J.C. Polanyi and W.M. Smith, J. Chem. Phys., 48, [illegible] (1967).

49. P. Pringsheim, "Fluorescence and Phosphorescence", Interscience Publishers Inc. New York, 1949, p.224.

50. E. Gaviola, Phil. Mag. 6, 1167 (1928).

51. M.L. Pool, Phys. Rev., 33, 22 (1929); 38, 955 (1931).

52. S. Penzes, A.J. Yarwood, O.P. Strausz and H.E. Gunning, J. Chem. Phys., 43, 1524 (1965).

53. J.A. Berberet and J.C. Clark, Phys. Rev., 100, 506 (1955).

54. G.H. Kimbell and D.J. Le Roy, Can. J. Chem., 38, 1714 (1960).

55. J.M. Campbell, S. Penzes, H.S. Sandhu and O.P. Strausz, Int. J. Chem. Kin., III, 175 (1971).

56. H. Horiguchi and S. Tsuchiya, Bull. Chem. Soc. Japan, 44, 1213 (1971).

57. A.B. Callear and R.G.W. Norrish, Proc. Roy. Soc., A259, 304 (1960); A266, 299 (1962).

58. A.B. Callear and G.J. Williams, Trans Faraday Soc., 60, 2158 (1964).

59. A.B. Callear and R.E.M. Hedges, Trans. Faraday Soc., 66, 605 (1970).

60. A.B. Callear and R.E.M. Hedges, Nature, 218, 163, (1968).

61. A.B. Callear and R.E.M. Hedges, Trans. Faraday Soc., 6, 615 (1970).

62. A.B. Callear and J. McGurk, Chem. Phys. Letters, 7, 491 (1970).

63. A.B. Callear and J.C. McGurk, Chem. Phys. Letters, 6, 417(1970).

64. A.B. Callear and J.C. McGurk, Nature,266,844(1970).

65. A.C. Vikis, G. Torrie and D.J. Le Roy, Can. J. Chem., 48,3771(1970).

66. A.C. Vikis, G. Torrie and D.J. Le Roy, Can. J. Chem., 50,176(1972).

67. H. Horiguchi and S. Tsuchiya, Bull. Chem. Soc. Japan, 44,3221(1971).

68. T. Asada, R. Ladenberg and W. Tietze, Zeits. Physik,29, 549(1928).

69. I. Asyrbichanu, I. Kukurezyanu, V. Vasiliu and I. Popesku, Opt. and Spectrosc.,11,155(1961).

70. J.H. Couliette, Phys. Rev.,32,639(1928).

71. B.deB. Darwent and F.G. Hurturbise, J. Chem Phys.,20, 1684(1952).

72. M.D. Scheer and J. Fine, J. Chem. Phys.,36,1264(1964).

73. A.C. Vikis and F.C. Moser, J. Chem. Phys.,53,1491 (1970).

74. J. Pitre, K. Hammond and L. Krause, Phys. Rev. A,6,2101 (1972).

75. A.B. Callear, [illegible] Opt. Supp.,2,145(1965).

76. H.W. Webb and H.A. Messenger, Phys. Rev.,40,466(1932).

77. R.W. Wood and E. Gaviola, Phil. Mag.,6,271(1928).

78. W. Orechowski, Zeits. Physik,109,485(1938).

79. G.H. Kimbell and D.J. Le Roy, Can. J. Chem., 40, 1229 (1962).

80. J.L. Spier, Physica, 7, 381 (1940).

81. S. Penzes, H.S. Sandhu and O.P. Strausz, Int. J. Chem. Kin., IV, 449 (1972).

82. Y. Rousseau, O.P. Strausz and H.E. Gunning, J. Chem. Phys., 39, 962 (1963).

83. M. Stupavsky, G.W.F. Drake and L. Krause, Phys. Letters, 39A, 349 (1972).

84. Lord Rayleigh, Proc. Roy. Soc. (London), A137, 101 (1932).

85. A.O. McCoubrey, Phys. Rev., 93, 1249 (1954).

86. A.G. Ladd, G.G. Freeman, M.J. McEwan, R.F.C. Claridge and L.F. Phillips, J. Chem. Soc., Faraday II, 69, 849 (1973).

87. R.W. Wood, Phil. Mag., 50, 774 (1925).

88. J.E. McAlduff and D.J. Le Roy, Can. J. Chem., 43, 2279 (1965).

89. J.E. McAlduff, D.D. Drysdale and D.J. Le Roy, Can. J. Chem., 46, 199 (1968).

90. S. Penzes, H.E. Gunning and O.P. Strausz, J. Chem. Phys., 47, 4869 (1967).

91. B.deB. Darwent, J. Chem. Phys., 18, 1532 (1950).

92. Y. Rousseau and H.E. Gunning, Can. J. Chem., 41, 465 (1963).

93. Y. Rousseau, G.N.C. Woodall and H.E. Gunning, J. Chem. Phys., 37, 2722 (1962).

94. G.N.C. Woodall and H.E. Gunning, Bull. Soc. Chim. Belg., 71, 725 (1962).

95. E.W.R. Steacie, "Atomic and Free Radical Reactions. Vol. II", The Macmillan Co., New York, 1964.

96. M.M. Papic and K.J. Laidler, Can. J. Chem., 49, 535, 549 (1971).

97. R.A. Holroyd and G.W. Klein, J. Phys. Chem., 67, 2273 (1963).

98. J.P. Chesick, J. Am. Chem. Soc., 86, 3597 (1964).

99. E. Jakubowski, P. Kebarle, O.P. Strausz and H.E. Gunning, Can. J. Chem., 45, 2287 (1967).

100. R.A. Back and van der Auwera, Can. J. Chem., 40, 2339 (1962).

101. S. Takamuku and R.A. Back, Can. J. Chem., 42, 1462 (1964).

102. J.M. Campbell, H.E. Gunning and O.P. Strausz, Can. J. Chem., 47, 3763 (1969).

103. J.M. Campbell, O.P. Strausz and H.E. Gunning, J. Am. Chem. Soc., 95, 740 (1973).

104. A.C. Vikis and D.J. Le Roy, 50, 595 (1972); 51, 1207 (1973).

105. K. Yang, J. Am. Chem. Soc., 89, 5344 (1967).

106. I. Melander, "Isotope Effects on Reaction Rates", Ronald Press Co., New York, 1960.

107. A.C. Vikis and H.C. Moser, J. Chem. Phys., 53, 2333 (1970).

108. H.E. Gunning, J.M. Campbell, H.S. Sandhu and O.P. Strausz, J. Am. Chem. Soc., 95, 746 (1973).

109. H.S. Johnstone, "Gas Phase Reaction Rate Theory", Ronald Press Co., New York, 1966, p 176.

110. K. Yang, J.D. Paden and C.L. Hassell, J. Chem. Phys., 47, 3824 (1964).

111. J.C. Light, J. Chem. Phys., 40, 3211 (1964).

112. T. Pollock, E. Jakubowski, H.E. Gunning and O.P. Strausz, Can. J. Chem., 47, 3474 (1969).

113. A.B. Callear and J.C. McGurk, J. Chem. Soc., Faraday II, 68, 289 (1972).

114. D.J. Le Roy, and E.W.R. Steacie, J. Chem. Phys., 9, 829 (1941).

115. R.J. Cvetanovic, H.E. Gunning and E.W.R. Steacie, J. Chem. Phys., 31, 573 (1959).

116. G.J. Mains and M. Trachtman, J. Phys. Chem., 74, 1647 (1970).

117. G. Mains and M. Trachtman, J. Phys. Chem., 76, 2665 (1972).

118. M.Z. Hoffman, M. Goldwasser and P.L. Damour, J. Chem. Phys., 47, 2195 (1955).

119. C.C. McDonald and H.E. Gunning, J. Chem. Phys., 23, 532 (1955).

120. A.B. Callear and J.H. Connor, Chem. Phys. Letters, 13, 245 (1972).

121. H.W. Melville, Proc. Roy. Soc. (London), A157, 621 (1936).

122. A.R. Knight and H.E. Gunning, Can. J. Chem., 39, 1231 (1961).

123. A.R. Knight and H.E. Gunning, Can. J. Chem., 39, 2466 (1961).

124. A.R. Knight and H.E. Gunning, Can. J. Chem., 40, 1134 (1962).

125. A. Kato and R.J. Cvetanovic, Can. J. Chem., 45, 1845 (1967).

126. R.A. Marcus, B.deB. Darwent and E.W.R. Steacie, J. Chem. Phys., 16, 987 (1948).

127. I.F. Loucks and K.J. Laidler, Can. J. Chem., 45, 2763 (1967).

128. S.V. Filseth, J. Phys. Chem., 73, 793 (1969).

129. R. Payette, M. Bertrand and Y. Rousseau, Can. J. Chem., 46, 2693 (1958).

130. A.B. Callear and J.C. McGurk, J. Chem. Soc., Faraday II, 97, 97 (1973).

131. W.M. Preston, Phys. Rev., 51, 298 (1936).

132. A. Micheals, H. de Kluiver and C.A. Ten Saldam, Physica, 25, 1321 (1959).

133. I. Kline and H. Margeneau, J. Chem. Phys., 30, 1556 (1959).

134. L. Mahan and M. Lapp, Phys. Rev., 179, 19 (1969).

135. J. Szudy, Acta Phys. Pol., A38, 779 (1970); Bull. Acad. Pol. Sci. Ser., Sci., Math., Astron., Phys., 17, 315 (1969).

136. J. Fiutak and M. Frackowiak, Bull. Acad. Pol. Sci. Ser., Sci., Math., Astron., Phys., 11, 175 (1963).

137. C. Jefimenko, J. Chem. Phys., 37, 2125 (1962); 42, 205 (1965).

138. J. Kieffer, J. Chem. Phys., 51, 1852 (1969).

139. J.M. Farr and W.R. Hindmarsh, Phys. Letters, A27, 512 (1968).

140. R.G. Breene, Jr., Acta Phys. Pol., A37, 447 (1970).

141. D.E. Cunningham and L.O. Olsen, Phys. Rev., 119, 681 (1960).

142. A. blonski, Zeits. Physik, 70, 723 (1931).

143. G.S Schwarzenback and K. Lutz, Helv. Chim. Acta, 23, 1139 (1940).

144. A. Jones, S. Yamashita and F.P. Lossing, Can. J. Chem., 46, 833 (1968).

145. D.R. Tyholiz and A.R. Knight, J. Am. Chem. Soc., 95, 1726 (1973).

146. G. London, A.C. Vikis and D.J. Le Roy, Can. J. Chem., 48, 1420 (1970).

147. O.P. Strausz, J.M. Cambell, S. De Paoli, H.S. Sandhu and H.E. Gunning, J. Am. Chem. Soc., 95, 732 (1973).

148. R.A. Svehla, NASA Technical Report R132, 1962.

149. J.N. Demas and W.A. Adamson, J. Phys. Chem., 75, 2463 (1971).

150. R.J. Cvetanovic, J. Chem. Phys., 23, 1203 (1955).

151. R. Atkinson and R.J. Cvetanovic, J. Chem. Phys., 56, 432 (1972).

152. M.C. Lin, Int. J. Chem. Kin., V, 173 (1973).

153. A. Lempicki and H. Samuelson, Phys. Letters,4,133 (1963).

154. K.G. E[illegible]son and L.R. Lindholt, IEEE J. Quant. Elect., QE-3,94 (1967).

155. A. Lempicki and A. Heller, App. Phys. Letters,9,108 (1966).

156. H.A. Koehler, L.J. Ferderber, D.L. Redhead and P.J. Ebert, App. Phys. Letters,21,198(1972).

157. J.B. Gerardo and A.W. Johnson, IEEE J. Quant Electr., QE-9,748(1973).

158. E.V. George and C.K. Rhodes, App. Phys. Letters,23,139 (1973).

159. J.B. Gerardo and A.W. Johnson, J. App. Phys.,44,4120 (1973).

160. A.R. Ault, M.L. Bhaumik, W.M. Hughes, R.J. Jensen, C.P. Robinson, A.C. Kolb and J. Shanon, IEEE J. Quant. Electr.,QE-9,1031(1973).

161. P.W. Hoff, J.C. Swingle and C.K. Rhodes, App. Phys. Letters,2[illegible] 245(1973).

162. W.M. Hughes, J. Shannon, A. Kolb, E., Ault and M. Bhaumik, App. Phys. Letters,23,385(1973).

163. B.A. Lengyel, "Lasers", John Wiley and Sons, Inc., 1971.

164. P.S.H. Henry, Brit. J. App. Phys. Supp.,2,6(1953).

165. J.A. Medley, Brit. J. App. Phys. Supp.,2,28(1953).

166. W.R. Harper, Adv. in Phys.,6,365(1957).

167. I.J. Schoen, Can. J. Phys., 38, 697 (1960).

168. K. Ikenoue and Y. Sasada, Mem. Defense Acad. Japan, II, 49, 57 (1962).

169. J.L. Sherman, C.E. Cardwell, D.Q. Lamb, Jr. and C.E. Mandeville, Bull. Am. Phys. Soc., 11, 77 (1966).

170. G.L. Dybwad and C.E. Mandeville, Phys. Rev., 161, 527 (1967).

171. G.L. Dybwad, J. App. Phys., 40, 4977 (1969).

172. A. Wolf, "A History of Science, Technology and Philoscphy in the 16th and 17th Centuries". The Macmillan Co., New York, 1935. p. 303.

173. Fra. Hauksbee, Phil. Trans. Roy. Soc. (London), 24, 2130 (1705).

APPENDIX A

DERIVATION OF THE RATE EQUATION IN THE $Hg(^3P_1) + N_2$ SYSTEM

The elementary chemical reactions which describe the Hg^*-N_2 system after the termination of the flash are:

$$Hg^* \rightarrow Hg + h\nu(2537\text{Å}) \qquad [2]$$

$$Hg^* + N_2 \rightarrow Hg^0 + N_2(v=1) \qquad [11]$$

$$Hg^0 + N_2 \rightarrow Hg^* + N_2 \qquad [12]$$

$$Hg^0 + Hg + N_2 \rightarrow Hg_2^* A(^3\Sigma_u) + N_2. \qquad [13]$$

The rate of change of Hg^* and Hg^0 atom concentrations is given by

$$d[Hg^*]/dt = k_{12}[N_2][Hg^0] - (k_{11}[N_2] + k_2)[Hg^*] \qquad [46]$$

and

$$d[Hg^0]/dt = k_{11}[N_2][Hg^*] - (k_{12}[N_2] + k_{13}[Hg][N_2])[Hg^0], \qquad [47]$$

respectively. A solution of these two simultaneous differential equations can be derived using the method of differentiation and elimination. Making the substitutions

$$x = [Hg^*]$$

$$y = [Hg^0]$$

$$a = k_{12}[N_2]$$

$$b = k_{11}[N_2] + k_2$$

$$g = k_{11}[N_2] \text{ and}$$

$$h = k_{12}[N_2] + k_{13}[Hg][N_2],$$

equations [46] and [47] become

$$dx/dt = ay - bx \qquad [48]$$

$$dy/dt = gx - hy. \qquad [49]$$

Differentiating equation [48] yields

$$d^2x/dt^2 = a(dy/dt) - b(dx/dt) \qquad [50]$$

Equation [49] is substituted into equation [50] to give

$$d^2x/dt^2 = agx - ahy - b(dx/dt). \qquad [51]$$

By re-arranging equation [48] into the form

$$y = \{(dx/dt) + bx\}/a \qquad [52]$$

and substituting into equation [51] offers

$$d^2x/dt^2 + (b+h)(dx/dt) + (bh-ag)x = 0. \qquad [53]$$

Equation [53] has a solution of the form

$$x = [Hg^*] = C_1\exp(r_1t) + C_2\exp(r_2t) \qquad [54]$$

where r_1 and r_2 are the roots of the complimentary equation given by

$$r_1 = -(U + \{U^2 - 4V\}^{1/2})/2 \text{ and} \qquad [55]$$

$$r_2 = -(U - \{U^2 - 4V\}^{1/2})/2, \qquad [56]$$

where $U = b + h$ and $V = bh - ag$. The square root terms in equations [55] and [56] can be put in the form

$$(U^2 - 4V)^{1/2} = U(1 - 4V/U^2)^{1/2} \qquad [57]$$

so that a binomial expansion of the right hand side may be carried out. Equation [57] reduces to

$$(U^2 - 4V)^{1/2} = U(1 - 2V/U), \qquad [58]$$

since all terms except the first are negligibly small. Substitution of equation [58] back into [55] and [56] gives

$$r_1 = (-U^2 + V)/U \text{ and}$$

$$r_2 = -V/U.$$

$U >> V$ under the experimental conditions so that $r_1 = -U$ and $\exp(r_1 t) << \exp(r_2 t)$. Thus equation [54] reduces to

$$x = [Hg^*] = C_2 \exp(-\{V/U\}t). \qquad [59]$$

Now, after expanding and collecting terms,

$$V = bh - ag = k_2[N_2](k_{12} + k_{13}[Hg]) + k_{11}k_{13}[Hg][N_2]^2 \text{ and}$$

$$U = b + h = k_{11}[N_2] + k_2 + k_{12}[N_2] + k_{13}[Hg][N_2].$$

Since the 2537Å radiation is proportional to the Hg^* atom concentration, the rate of decay of the resonance line and the $[Hg^*]$ are identical and is defined by the rate constant $k_{N_2} = V/U$.

At low mercury concentrations,

$$k_{13}[Hg][N_2] + k_{12}[N_2] \ll k_2 + k_{11}[N_2]$$

so that U may be expressed simply as

$$U = k_{11}[N_2] + k_2$$

and

$$k_{N_2} = \frac{k_2[N_2](k_{12} + k_{13}[Hg]) + k_{11}k_{13}[Hg][N_2]^2}{k_2 + k_{11}[N_2]} \quad [14]$$

At high nitrogen pressure where nearly complete quenching results, $k_2 \ll k_{11}[N_2]$ and equation [14] may be expressed, after re-arranging terms, by the formula

$$k_{N_2} = k_2 k_{12}/k_{11} + k_{13}[Hg][N_2]. \quad [60]$$

Using the relationship between k_{12} and k_{11}

$$k_{12}/k_{11} = 3.0 \exp(-5.0 \times 10^3/RT)$$

given in reference 88, equation [60] can be written as

$$k_{N_2} = 3.0 \exp(-5.0 \times 10^3/RT) k_2 + k_{13}[Hg][N_2], \quad [15]$$

If the simultaneous differential equations [46] and [47] are solved for the Hg^0 atom concentrations, a solution identical to [59] can be derived except for a different constant in place of C_2. Thus, the decay rates of Hg^0 atoms and the delayed fluorescence intensity are the same.

APPENDIX B

DERIVATION OF THE Hg A($^3O_u^-$) CONCENTRATION AS A FUNCTION OF TIME

The following reaction mechanism has been used to interpret the kinetics involving the mercury excimers:

$$Hg^0 + Hg + N_2 \rightarrow Hg_2^* \ (^3\Pi_u) + N_2 \qquad [13]$$

$$Hg_2^* \rightarrow 2Hg + h\nu(3350\text{Å}) \qquad [16]$$

$$Hg_2^* + N_2 \rightarrow Hg_2^{**} \ (^3O_u^-) + N_2 \qquad [17]$$

$$Hg_2^* + N_2 \rightarrow 2Hg + N_2 \qquad [18]$$

$$Hg_2^{**} \rightarrow 2Hg + h\nu(4850\text{Å}) \qquad [19]$$

$$Hg_2^{**} + N_2 \rightarrow 2Hg + N_2. \qquad [20]$$

It is assumed that the time dependence of the Hg^0 atom concentration is known from the decay rate constant, k_{N_2}, of the delayed fluorescence intensity at 2537Å, i.e.

$$[Hg^0] = A \exp(-k_{N_2} t) = A \exp(-mt)$$

The rate equation for Hg_2^* is

$$d[Hg_2^*]/dt = k_{13}[Hg][N_2][Hg^0] - (k_{16} + \{k_{17} + k_{18}\}[N_2])[Hg_2^*] \qquad [61]$$

Applying the substitutions

$$n = [Hg_2^*]$$

$$p = k_{16} + \{k_{17} + k_{18}\}[N_2] \text{ and}$$

$$q = Ak_{13}[Hg][N_2],$$

equation [61] takes the form

$$dn/dt + pn = q \exp(-mt)$$

and has the solution

$$n = [Hg_2^*] = q/(p-m)\ \{\exp(-mt) - \exp(-pt)\} \qquad [62]$$

using exp(pt) as an integration factor and the condition that $[Hg_2^*] = 0$ at $t = 0$.

The rate equation for Hg_2^{**} is

$$d[Hg_2^{**}]/dt = k_{17}[N_2][Hg_2^*] - (k_{19} + k_{20}[N_2])[Hg_2^{**}] \qquad [63]$$

which can be put in the form

$$du/dt + vu = wq/(p-m)\ \{\exp(-mt) - \exp(-pt)\} \qquad [64]$$

by making the following substitutions

$$u = [Hg_2^{**}]$$

$$v = k_{19} + k_{20}[N_2] \text{ and}$$

$$w = k_{17}[N_2].$$

Equation [64] has the solution

$$u = [Hg_2^{**}]$$

$$= \frac{wq[(v-p)\exp(-mt) - (v-m)\exp(-pt) + (p-m)\exp(-vt)]}{(p-m)(v-m)(v-p)} \qquad [65]$$

using the boundary condition that $[Hg_2^{**}] = 0$ at $t = 0$. Since

$$I_{4850} = d(h\nu)/dt = k_{19}[Hg_2^{**}],$$

the time dependence of the 4850Å band intensity is expressed by

$$I_{4850} = \frac{A' k_{13} k_{17} k_{19} [Hg][N_2]^2 \{X - Y + Z\}}{(p-m)(v-m)(v-p)}, \qquad [21]$$

where $m = k_{N_2}$

$p = k_{16} + \{k_{17} + k_{18}\}[N_2]$

$v = k_{19} + k_{20}[N_2]$

$X = (v-p)\exp(-mt)$

$Y = (v-m)\exp(-pt)$

$Z = (p-m)\exp(-vt)$ and

A' is a constant.

APPENDIX C

DERIVATION OF THE RATE EQUATIONS IN $Hg(^3P_0)$-N_2-FOREIGN GAS SYSTEMS

The following mechanism describes the important reactions taking place in a Hg*-N_2-foreign gas mixture after flash excitation has ceased:

$$Hg^* \rightarrow Hg + h\nu(2537\text{Å}) \qquad [2]$$

$$Hg^* + N_2 \rightarrow Hg^0 + N_2(v=1) \qquad [11]$$

$$Hg^0 + N_2 \rightarrow Hg^* + N_2 \qquad [12]$$

$$Hg^0 + Hg + N_2 \rightarrow Hg_2^*, A(^3\Sigma_u^+) + N_2 \qquad [13]$$

$$Hg^* + Q \rightarrow Hg + \text{products} \qquad [24]$$

$$Hg^* + Q \rightarrow Hg^0 + Q \qquad [25]$$

$$Hg^0 + Q \rightarrow Hg + \text{products} \qquad [26]$$

where Q signifies the quencher molecule and "products" indicate electronic excitation, decomposition, band emission, etc.

The rate of change of Hg* and Hg^0 atom concentration are, respectively,

$$d[Hg^*]/dt = k_{12}[N_2][Hg^0] - \{k_2+k_{11}[N_2]+(k_{24}+k_{25})[Q]\}[Hg^*] \qquad [66]$$

$$d[Hg^0]/dt = \{k_{11}[N_2] + k_{25}[Q]\}[Hg^*] - \{k_{12}[N_2] + k_{26}[Q] + k_{13}[Hg][N_2]\}[Hg^0]. \qquad [67]$$

The method of differentiation and elimination described in Appendix A can be used to solve the simultaneous differential equations [66] and [67]. The Hg* atom concentration as a function of time is given by:

$$[Hg^*] = K \exp(-k_T t)$$

where k_T is the reciprocal of the decay lifetime of the 2537Å delayed fluorescence, $1/\tau$, given by:

$$1/\tau = k_T = \frac{\left[\{k_2+k_{11}[N_2]+(k_{24}+k_{25})[Q]\}\{k_{12}[N_2]+k_{26}[Q]+k_{13}[Hg][N_2]\} - k_{12}[N_2](k_{11}[N_2]+k_{25}[Q])\right]}{k_2+k_{11}[N_2]+(k_{24}+k_{25})[Q]+k_{13}[Hg][N_2]+k_{12}[N_2]+k_{26}[Q]} \qquad [68]$$

If the quencher concentration is kept small and the pressure of nitrogen is ≥ 100 torr, then

$$k_{11}[N_2] >> k_2+(k_{24}+k_{25})[Q]+k_{26}[Q]+k_{13}[Hg][N_2]+k_{12}[N_2]$$

and the denominator of equation [68] becomes simply $k_{11}[N_2]$. By expanding the numerator and collecting terms, equation [68] can be reduced to the form:

$$k_T = k_2k_{12}/k_{11} + k_{13}[Hg][N_2] + k_{26}[Q] + k_{24}k_{12}/k_{11}[Q] + \{\{k_2+(k_{24}+k_{25})[Q]\}/k_{11}[N_2]\}\, k_{26}[Q] \qquad [69]$$

since $k_{11}[N_2] >> k_2+(k_{24}+k_{25})[Q]$. The coefficient of $k_{26}[Q]$ in the last term of equation [69] expresses the ratio

of the relaxation rate of Hg* atoms by emission and quenching by the foreign gas to the rate of spin-orbit relaxation by nitrogen. This ratio is << 1 and

$$\{ \{k_2 + (k_{24}+k_{25})[Q]\}/k_{11}[N_2] \}\ k_{26}[Q] \ll k_{26}[Q]$$

and can be neglected. Thus, equation [69] can be re-written as:

$$k_T = k_2 k_{12}/k_{11} + k_{13}[Hg][N_2] + (k_{24}k_{12}/k_{11} + k_{26})[Q]. \quad [32]$$

APPENDIX D

CHEMICAL REACTIONS AND TRIBOLUMINESCENCE INITIATED BY TRIBOELECTRICITY

In the course of the present work, it was noticed that a red flash of light was emitted from the capillary of a McLeod gauge, containing neon gas, while the mercury was being drained. This observation prompted a close study of the phenomenon involved, the results of which are reported here.

The optical display has its origin in the familiar phenomenon of a charge separation induced by the rubbing together of two dissimilar substances. This electrification, commonly referred to as triboelectrification, is believed to arise from the contact potential difference of the two substances (164). Rubbing is not a necessary requirement but serves only to bring about intimate surface contact over larger areas. Since the majority of the research concerning static electricity has usually been carried out in connection with its relevance to industrial processes, a detailed survey of the work is beyond the scope of the present study. The term triboluminescence is applied to the optical phenomena which often accompanies triboelectrification.

Triboelectricity and triboluminescence generated by

mercury in contact with an insulator has only recently attracted study (165-171), although it was discovered centuries ago (172,173). Medley (165) demonstrated that mere contact between mercury and a plastic sheet was sufficient to produce a static charge of up to 500 e.s.u./cm^2. Dybwad and Mandeville (170) attributed the electrification of mercury on a quartz surface to the migration of electrons from the mercury to the quartz. They estimated an electron density on the quartz of about 6 x 10^{12} electrons/cm^2 as compared to a surface density of 2.4 x 10^{15} atoms/cm^2. A large total charge may be produced by sliding the mercury over the glass and depends on the rate at which the mercury is agitated, the surface areas in contact, the pressure between the two surfaces and the electrical conductivity of the insulator.

An electrical discharge will result if the mercury is slid along the surface exposing the charge on the insulator to the vapour above. This produces triboluminescence in the form of flashes of light which occur as electrons jump back to the mercury from the surface of the glass and a continuous discharge or glow, usually the dominant form, arising from the slow leakage of electrons from deeper electron traps (170). The flashes preceed the glow but, depending on the cleanliness of the surface and its conductivity, these flashes may be absent. The spectra (167,170) include lines from mercury, any foreign gas which may be present and atoms

of the glass material in both neutral and ionized states. The lines assigned to the atoms of the wall material such as silicon and boron indicate that these are on the surface and not part of the internal crystalline structure (170).

The present investigation was undertaken to examine the effect on the emission of varying the nature and pressure of a foreign gas, the nature and condition of the wall material subjected to different cleaning treatments and temperature. The chemical changes brought about in the foreign gas, which may be anticipated from an electrical discharge, were also investigated since no previous study of this aspect of the phenomenon appeared to have been made.

Three tube materials, pyrex glass, vycor 7910 and fused quartz were examined. Various treatments of surface conditioning were applied before the tubes were filled with about thirty torr neon and five grams of mercury. The results are tabulated in Table XII. The relative intensities of emission were determined by visual observation as the tube was shaken in a laboratory shaker. The most intense emission is denoted by the number 1. Such observations are subject to large errors due to the inability of the eye to distinguish between differences in intensities when such differences become small. There appeared to be no significant difference in intensity between the brightest emissions from the three kinds of tube material.

TABLE XII

Effect of Wall Material and Surface Treatment on the Relative Intensity of Triboluminescence from Ampules Containing Mercury and Neon (a).

Wall Material	HF (b)	Chromic Acid (c)	KOH (d)	Untreated (e)
quartz	-	3	1	2
vycor	2	1	3	4
pyrex	3	2	1	4

a. Cardinal numbers refer to the brightness of the emission where 1 is the brightest.

b. The tubes were washed with 25% HF and rinsed with water.

c. The tubes were washed with a saturated solution of potassium dichromate in concentrated sulphuric acid and then rinsed with water.

d. The tubes were washed with 10% aqueous KOH and rinsed with 95% ethanol.

e. The tubes were not treated.

It appears that the diameter of the tube has little effect on the emission intensity. Pyrex tubes, washed with KOH and rinsed with ethancl, were filled with 31.3 torr neon and 5 grams of mercury. The tubes were 7, 9, 10 and 13 mm (o.d.) and about 12 cm in length. No difference in emission intensity could be discerned.

Several gases were used for filling and checked for visible light. All were found to yield an emission, the intensity of which is a function of pressure. The relative emission intensities were determined and denoted by cardinal numbers as explained abcve. Pyrex tubes (9 mm by 120 mm) were used, without any previous treatment. Each tube contained approximately five grams of mercury. The results are summarized in Table XIII.

The tubes having the brightest intensity of each different gas were compared with each other. A wide variation in intensity was noted, as indicated in Table XIV. The brightness was evaluated by degree to which the eye required dark adaptation in order to see the emission.

A small amount of biacetyl in the neon and hydrogen tubes decreased the intensity of the emission greatly. A tube containing mercury, neon and biacetyl (5 gms., 26.6 and 1.4 torr respectively) emitted a bluish red color of weaker intensity than the tube containing biacetyl and mercury only

TABLE XIII

Variation in Triboluminescence Intensity With Pressure of Several Foreign Gases.

Foreign Gas	Relative Intensity With Gas Pressure (torr) 1	2	3	4	5	6
He	39.6	19.1	11.9	29.2	55.0	0.7
Ne	39.2	29.1	20.9	1.9	9.4	49.2
Ar	2.8	14.2	36.6	60.1	-	-
Kr	33.1	52.1	12.6	83.8	-	-
Xe	23.1	35.5	11.3	60.9	-	-
H_2	21.1	2.7	10.8	-	-	-
N_2	2.8	10.0	20.5	52.5	114.2	-
CO	3.0	16.4	34.5	59.5		-
CH_4	4.3	11.5	36.8	59.5	-	-
C_2H_4	1.5	9.9	22.3	44.1	-	-

a. Cardinal numbers refer to the brightness of the emission where 1 is the brightest.

Table XIV

Comparison of Maximum Emission Intensities of Various Foreign Gases.

Gas Fill	Color of Emission	Degree of Brightness
Ne	orange red	The emission can be seen in dim room light.
CO	greenish blue	
H_2	light blue	
Xe	light blue	
CH_4	light blue	The emission can be seen after 5 to 10 seconds of dark adaptation of the eyes.
Ar	light blue	
He	light blue	
N_2	violet blue	
Kr	light blue	
biacetyl (24.3 torr)	light blue	
C_2H_4	light blue	The emission can be seen after about 30 seconds of dark adaptation of the eyes.
air (24.4 torr)	light blue	
Hg (no gas fill)	light blue	

(cf. Table XIV). A tube with mercury, hydrogen and biacetyl (5 gms., 16.7 and 1.0 torr respectively) was found to emit a light blue radiation which again is less intense than the tube containing only hydrogen and mercury.

The use of a sodium amalgam instead of pure mercury as the liquid metal in the tubes seemed to suppress the emission almost entirely as well as changing the color. The tubes used in this experiment contained approximately 10 grams of amalgam composed of 442 grams of Hg and 0.24 grams of Na. The tubes were of pyrex, 13 mm o.d. and 120 mm long. Table XV gives the results of the experiment. Difficulty in preventing the formation of oxidation products on the inside wall of the tubes decreases the reliability of the observations. In this connection, Harper (167) has shown that the presence of oxides may have a profound effect on the triboelectrical properties of a metal in contact with an insulator, including the reversal of the sign of the electrical charges on the two materials.

A Wood's alloy metal melting at 70°C was used instead of mercury in a tube containing neon. When shaken, the tube emitted the characteristic orange-red color of the neon fill. The metal was composed of the elements Bi, Pb, Sn and Cd in the proportions 50 : 26.7 : 13.3 : 10.0 respectively.

When cesium or bromine was used instead of mercury along with added neon, no emission could be seen.

TABLE XV

Emission Characteristics from Sodium Amalgam.

Gas Fill	Color
30.6 torr helium	very weak reddish color
26.5 torr neon	very weak blue color
10.2 torr hydrogen	no visible emission

A pyrex tube was joined to a plexiglass tube containing three grams of mercury and 29.0 torr of neon. The red glow from the neon was about the same intensity when the mercury was agitated inside the glass section or the plastic section.

A brief investigation into the effect of temperature on the emission was also carried out. A tube containing only mercury showed flashes of whitish-blue light at room temperature but when immersed in boiling water the emission intensity is greatly increased and becomes very diffuse. With 39.2 torr neon at room temperature the major color is orange-red with a trace of blue. When immersed in boiling water the red light seems to retain the same intensity but the intensity of blue light, which appears near the mercury surface, is very much increased to the point where the intensity of the two colors become about equal.

The intensity of emission could be increased by increasing the area of contact surface between the mercury and the glass. This was achieved by placing one or two glass spirals axially in the tube. A pyrex tube, 40 mm by 120 mm, containing two glass spirals and 40 torr neon pressure gave the strongest emission which could be readily seen from a distance of about fifty yards in the dark.

The chemical reactions which take place in the gas

atmosphere during the electrical discharge and triboluminescence represent an interesting possible application of the phenomenon. For these experiments the reaction tubes were made of pyrex, 30 mm by 120 mm, encasing a pyrex coil to increase the contact surface area. The tubes were treated with 10% KOH, rinsed with distilled water and ethanol prior to use. To each tube, approximately 70 grams of mercury was added and then filled with the reactant gas(es). The filled tube was then mildly shaken for a period of time in a laboratory shaker. The results are presented in Table XVI with the product yields expressed in relative g.c. peak areas. An interesting product in hydrocarbon systems is the formation of alkyl mercurials in relatively high yields. Similar products could be brought about by bubbling the gases through a pool of mercury.

The implication that spurious products may arise from gas phase experiments performed with apparatus in which mercury moves in contact with a glass material was tested out. Non-condensable gases were produced from hydrocarbons and acetone on extensive manipulation by a Toepler pump.

The mechanisms of these reactions are obviously complex and are expected to involve ionic as well as photochemical processes.

TABLE XVI

Product Yields from the Triboelectrical Discharge Decomposition of Hydrocarbons and Acetone.

	Decomposition product yield (a) (for initial substrate pressure and reaction time)		
	11.0 torr CH_4	9.5 torr C_3H_8	11.8 torr CH_3COCH_3
Products	24 hours	24 hours	12 hours
CH_3HgCH_3	128	55	621
C_2H_2	60	60	
C_2H_4	52	32	
C_2H_6	45	112	137
H_2	29	12	
C_3H_8	17		23
C_3H_6	2	50	27
CH_4			107
C_4 (b)		35	45
$CH_3HgC_2H_5$		11	
CO			814

a. Measured in relative g.c. peak areas.

b. Denotes an unidentified four carbon compound.

TABLE XVI (cont'd)

Product Yields from the Triboelectrical Discharge Decomposition of Hydrocarbons and Acetone.

	Decomposition Product Yield (a) (for initial substrate pressure and reaction time)	
	11.3 torr C_2H_4	8.3 torr H_2 + 6.6 torr C_2H_4
products	13.5 hours	24 hours
CH_3HgCH_3	171	40
C_2H_2	2014	396
C_2H_6	208	130
H_2	62	
C_3H_8	72	42
C_3H_6	147	21
CH_4	333	not measured
C_4(b)		17
$CH_3HgC_2H_5$	191	
$HC{\equiv}CCH_3$	366	
Yellow polymer	✓	✓

a. Measured in relative g.c. peak areas.

b. Denotes an unidentified four carbon compound.